Institutional Repository - Research Portal
Dépôt Institutionnel - Portail de la Recherche
researchportal.unamur.be
University of Namur

THESIS / THÈSE

MASTER IN CHEMISTRY PROFESSIONAL FOCUS

Etude de la structure et de l'inhibition de la phosphosérine phosphatase de Mycobacterium avium

Callaerts, Nephtali

Award date:
2019

Awarding institution:
University of Namur

Link to publication

General rights
Copyright and moral rights for the publications made accessible in the public portal are retained by the authors and/or other copyright owners and it is a condition of accessing publications that users recognise and abide by the legal requirements associated with these rights.

- Users may download and print one copy of any publication from the public portal for the purpose of private study or research.
- You may not further distribute the material or use it for any profit-making activity or commercial gain
- You may freely distribute the URL identifying the publication in the public portal ?

Take down policy
If you believe that this document breaches copyright please contact us providing details, and we will remove access to the work immediately and investigate your claim.

Download date: 04. May. 2023

UNIVERSITE DE NAMUR
Faculté des Sciences
Secrétariat du Département de Chimie
Rue de Bruxelles 61 – 5000 NAMUR
Téléphone : +32(0)81 72.54.44 – Téléfax : +32(0)81 72.54.40
E-mail : enseignement.chimie@unamur.be - www.unamur.be/sciences

Etude de la structure et de l'inhibition de la phosphosérine phosphatase de *Mycobacterium avium*

CALLAERTS Nephtali

Résumé

La tuberculose est actuellement l'une des 10 premières causes de mortalité dans le monde. En effet, *Mycobacterium tuberculosis* (*M.tb*), l'agent pathogène responsable de cette maladie, est capable de facilement se propager via les gouttelettes de salive en suspension dans l'air. En outre, cette mycobactérie présente une résistance croissante aux médicaments actuels. Il est de ce fait primordial de développer de nouvelles cibles thérapeutiques afin de concevoir une nouvelle génération de médicaments contre *M.tb*.

De nombreuses expériences au sein de notre groupe de recherche se sont centrées sur la phosphosérine phosphatase de *M.tb* (SerB2) comme nouvelle cible thérapeutique intéressante, et ce pour trois raisons principales. Premièrement, l'enzyme est vitale pour la survie du pathogène : son inhibition entrave la voie métabolique de la L-sérine menant à la mort bactérienne. De plus, SerB2 possède un effet pathogène intrinsèque facilitant l'infection. Enfin, la séquence primaire de la phosphosérine phosphatase est conservée parmi de nombreux pathogènes. L'étude de son inhibition pourrait ainsi mener à un médicament utilisé comme panacée, principalement contre la tuberculose.

Suite au criblage de la chimiothèque NAMEDIC, nos recherches ont mené à la découverte de certains inhibiteurs très efficaces. Cependant, le mécanisme d'action de ces inhibiteurs reste nébuleux car la structure cristallographique de SerB2 n'a jamais été obtenue à ce jour. L'objectif principal de ce projet de recherche correspond à l'étude du plus proche homologue de SerB2 (83,5% d'identité) qui peut être cristallisé : la phosphosérine phosphatase de *Mycobacterium avium* (SerB). En effet, cette enzyme peut à priori être surexprimée et cristallisée après purification optimisée. Les résultats obtenus indiquent que les inhibiteurs de SerB2 restent efficaces contre SerB et gardent une cinétique enzymatique similaire. En outre, des tests de co-cristallisation de SerB avec ces inhibiteurs et certains acides aminés ont été réalisés et de nouvelles structures expérimentales de SerB complexé avec divers ligands ont été obtenues. Les interactions entre enzyme et ligands sont étudiées afin de fournir davantage d'informations concernant la structure et l'inhibition de SerB2.

Mémoire de master en Sciences Chimiques (Orientation Chimie du Vivant et des Nanomatériaux) : Finalité Spécialisée

Janvier 2019

Promoteur: Prof. J. Wouters
Encadrante: M. Haufroid

UNIVERSITE DE NAMUR
Faculté des Sciences
Secrétariat du Département de Chimie
Rue de Bruxelles 61 – 5000 NAMUR
Téléphone : +32(0)81 72.54.44 – Téléfax : +32(0)81 72.54.40
E-mail : enseignement.chimie@unamur.be - www.unamur.be/sciences

Study of the structure and inhibition of *Mycobacterium avium* phosphoserine phosphatase

CALLAERTS Nephtali

Summary

Tuberculosis remains currently one of the top ten causes of death worldwide. As a matter of fact, *Mycobacterium tuberculosis* (*M.tb*), which is the pathogen responsible for this disease, spreads easily and quickly through saliva droplets in air. Moreover, this bacterium is becoming more and more multidrug-resistant. Hence, new therapeutic targets need to be found in order to design new efficient drugs against *M.tb*.

Multiple previous experiments in our research group focus on *M.tb* phosphoserine phosphatase (SerB2) as new perfect therapeutic target, for three main reasons. Firstly, the enzyme is vital for the pathogen: SerB2 inhibition stops the biosynthetic pathway of L-serine and leads to bacterial death. In addition, SerB2 possesses an intrinsic pathogenic effect and expedites the infection. Finally, the primary sequence of phosphoserine phosphatase is highly conserved among pathogens. The study of its inhibition could therefore lead to the design of a drug, used as *panacea*, especially against tuberculosis.

As a result of our research, some efficient inhibitors have been discovered, thanks to the screening of NAMEDIC's chemo-library. However, the precise mechanism of action of the aforementioned inhibitors remains unclear because the crystallographic structure of SerB2 was never obtained. The main goal of this research project is the study of the closest counterpart of SerB2 (83.7% of identity) that can be crystallized: the *Mycobacterium avium* phosphoserine phosphatase (SerB). Indeed, this enzyme can be overexpressed, and crystallized after an optimized purification. Our results show that SerB2 inhibitors follow similar enzymatic kinetics and remain effective against SerB. In addition, some crystallographic assays of SerB complexed with the inhibitors and some amino acids have led to new experimental structures of SerB complexed with selected ligands. Interactions between the enzyme and these compounds are studied to provide more information about the structure and the inhibition of SerB2.

Master's thesis in Chemical Sciences (Field of Life Chemistry and Nanomaterials): Specialized Orientation

January 2019

Supervisor: Prof. J. Wouters
Tutor: M. Haufroid

« *Improvise. Adapt. Overcome.* »

Clint Eastwood, Heartbreak Ridge (1986)

Acknowledgments/Remerciements

Je me permets de laisser temporairement de côté l'anglais afin d'aborder plus sereinement la partie la plus importante (et certainement la plus consultée) de mon mémoire. Et cela est tout à fait naturel, au vu du nombre de personnes intervenant dans ma vie, et influençant de manière plus ou moins directe le résultat d'une année d'introduction à la recherche scientifique et de cinq ans d'étude (résultat que vous tenez actuellement entre vos mains). La science de la nature est un champ de connaissance exceptionnel pour d'innombrables raisons. Mais il n'en reste cependant pas moins profondément humain et il me semble important de mettre en avant les différentes personnes qui permettent de se sentir bien dans ce que l'on fait, là où l'on est.

Je souhaite remercier en premier lieu Johan Wouters qui a été un professeur passionné et passionnant tout au long de mes cinq années d'étude, mais aussi mon promoteur durant cette année de mémoire. Merci de m'avoir accepté au sein du laboratoire. Merci pour votre ouverture d'esprit, votre modestie non feinte, votre disponibilité et votre pertinence dans les diverses remarques et autres conseils.

J'aimerais ensuite remercier sincèrement mon encadrante Marie Haufroid qui a eu le courage de me supporter durant un an. Merci pour ta complicité, ta disponibilité et ta positivité sans faille ! Tu m'as permis d'apprendre tout en restant indépendant, et je pouvais toujours compter sur toi pour me guider dans le monde cruel et surprenant de la biochimie des protéines. Tu m'as aussi permis d'évoluer en Nephtaloss mais je suis sûr que le Nephtenfer n'est plus très loin !

Dans la continuité, je souhaite remercier les membres du CBS pour l'ambiance toujours propice au travail mais aussi pour l'entre-aide et la bonne atmosphère permanente au bureau ou au laboratoire. Merci également pour les kilos de pâtisseries immédiatement convertis en kilos tout court, avec un rendement de ~100%.

Je remercie aussi tous les membres des laboratoires qui m'ont vu passer le temps de midi chez eux, de manière ponctuelle. Merci à nos très chers collègues de l'UCPTS d'en face et plus particulièrement à Pierre Beaujean pour sa critique externe, ses conseils et pour nos conversations-pause au milieu de la journée. Merci aux organiciens du troisième pour leur spontanéité géniale et surtout à Loïc Jeanmart pour m'avoir permis d'obtenir glace et azote liquide à profusion. Merci au quatrième étage pour les immanquables rendez-vous belote du midi. Le goût du papier reste amer en bouche mais cela valait bien la peine, au vu de nos nombreuses parties jouées. Je remercie aussi plus spécialement tous les membres de la cellule didactique de m'avoir permis d'utiliser le lecteur UV-Visible multi-puits. Merci au cinquième pour leur sympathie toujours présente. Merci également aux différents membres de l'URBM pour l'utilisation de leur matériel et aussi pour leur aide et conseils sur place.

Evidemment, je remercie aussi mes collègues et amis de Master 2 : une promotion géniale et toujours soudée au fil des cinq années. J'aimerai remercier notre groupe, officieusement baptisé « les irréductibles », pour tous les moments partagés ensemble, à l'université ou ailleurs, et pour notre réelle complicité qui perdurera, je l'espère, encore longtemps. Merci également à Manon pour m'avoir aidé avec la partie cristallographique de mon mémoire, pour notre panique partagée en voyant des fautes juste avant l'impression finale du (mi-)mémoire, et aussi pour m'avoir poussé à une consommation abusive de cupcakes.

Mes remerciements vont également à mes amis de Master 1 pour leur contribution dans la détermination des courbes d'IC_{50}, dans le cadre des travaux pratiques au sein du laboratoire. Bienvenue à ceux et celles qui voudront rejoindre le CBS !

Après une longue journée de cours, il est important de rejoindre un cadre de vie où l'on se sent bien. Je remercie pour cela Valentin et Thibault, mes deux physiciens colocataires. J'ai réellement l'impression d'avoir tout vécu avec vous deux, vu les cas extrêmes que vous êtes, mais aussi à la fois très différents l'un de l'autre. Merci pour notre bonne entente permanente au kot.

Je remercie aussi notre groupe d'amis qui perdure depuis les secondaires et compte beaucoup pour moi, malgré le faible nombre d'occasions de se retrouver. Mais quand on se retrouve rien n'a changé et c'est ça le plus important ! Je remercie en particulier les sœurs Lemaitre pour leur aide en anglais et surtout à Perrine pour l'ensemble de notre relation, qui est l'essence même de ma motivation et joie de vivre quotidienne.

Pour terminer, je remercie ma famille qui a toujours cru en moi et qui m'a poussé toujours plus loin. Merci à mes parents pour leur soutien et amour, sous toutes les formes que ce soit : la finance de mes études, les petits plats, les boîtes surprises du dimanche mais aussi la joie de me voir revenir tous les week-ends.

A vous tous, et à vous qui lisez ces quelques lignes, (encore) merci !

Table of contents

List of abbreviations

ACT	Aspartate kinase, Chorismate mutase and Tyr A.
APS	Ammonium persulfate
BSA	Bovine Serum Albumin
CMPSA	p-chloromercuriphenylsulfonic acid
DMSO	Dimethyl sulfoxide
DTT	DL-dithiothreitol
EC number	Enzyme Commission number
EDTA	Ethylenediaminetetraacetic acid
FT	Flow Through
HAD	Haloacid Dehalogenase
HIGK	Human Immortalized Gingival Keratinocytes
His_6-Tag	Hexahistidine tail
HIV	Human Immunodeficiency Virus
hPSP	Human Phosphoserine Phosphatase
HRV-3C	Human Rhinovirus 3C
IC_{50}	Median Inhibition Concentration
IL-8	Interleukin 8
IMAC	Immobilized Metal Affinity Chromatography
IPTG	Isopropyl β-D-1-thiogalactopyranoside
IUPAC	International Union of Pure and Applied Chemistry
IWGMT	International Working Group on Mycobacterial Taxonomy
Ki	Inhibition constant
Km	Michaelis constant
$Km_{app.}$	Apparent Michaelis constant
LB	Lysogenic Broth
LIC	Ligation Independent Cloning
MAC	*Mycobacterium avium* Complex
MAPK	Mitogen-Activated Protein Kinase
MB	Multibacillary
MDR	Multidrug-resistant
MES	2-(N-morpholino)ethanesulfonic acid
MIC	Minimum Inhibitory Concentration
M.tb	*Mycobacterium tuberculosis*
MW	Molecular Weight
NAMEDIC	Namur Medicine & Drug Innovation Center
NARILIS	Namur Research Institute for Life Sciences
NCIDTP	National Cancer Institute Developmental Therapeutic Program
NF-κB	Nuclear Factor-κB
NTA	Nitriloacetic acid
OD_{600nm}	Optical Density at 600 nm
PAGE	Polyacrylamide Gel Electrophoresis
PB	Paucibacillary
PCR	Polymerase Chain Reaction
PDB	Protein Data Bank
PDXP	Pyridoxal Phosphate Phosphatase
PEG	Polyethylene glycol
PHOSPHO1	Phosphoethanolamine/phosphocholine Phosphatase

Pi	Inorganic phosphate (aka. orthophosphate)
P-serine	*O*-phospho-L-serine
PSP	Phosphoserine Phosphatase
RNA	Ribonucleic acid
SDS	Sodium Dodecyl Sulfate
SEC	Size-Exclusion Chromatography
SEM	Scanning Electron Microscopy
SerA	D-3-phosphoglycerate dehydrogenase
SerB	*Mycobacterium avium* phosphoserine phosphatase
SerB2	*Mycobacterium tuberculosis* phosphoserine phosphatase
SerC	Phosphoserine Aminotransferase
SSGCID	Seattle Structural Genomics Center for Infectious Diseases
TB	Tuberculosis
TEMED	Tetramethylethylenediamine
THP-1	Tamm-Horsfall Protein 1
Tris	Tris(hydroxymethyl)aminomethane
UV-VIS	Ultraviolet-Visible
Vmax	Maximum rate
WHO	World Health Organization
XDR	Extensively/extremely drug-resistant
ε	Enzyme

List of amino acids

Amino acid	Three letters code	IUPAC code	Formula	Side chain feature
L-alanine	Ala	A	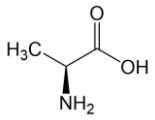	Nonpolar
L-arginine	Arg	R	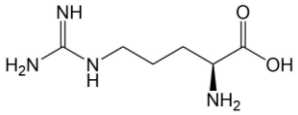	Positive (neutral pH)
L-asparagine	Asn	N	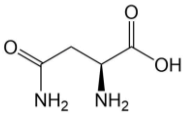	Polar
L-aspartic acid	Asp	D	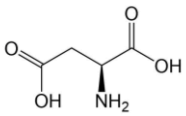	Negative (neutral pH)
L-cysteine	Cys	C	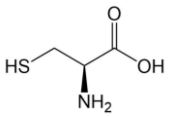	Nonpolar
L-glutamic acid	Glu	E	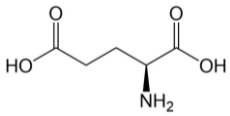	Negative (neutral pH)
L-glutamine	Gln	Q	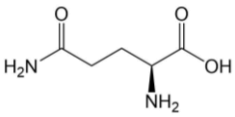	Polar
L-glycine	Gly	G	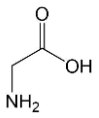	Nonpolar
L-histidine	His	H	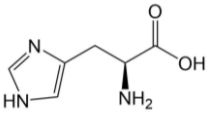	Polar
L-isoleucine	Ile	I	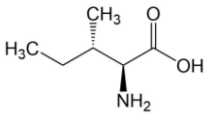	Nonpolar
L-leucine	Leu	L	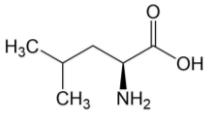	Nonpolar
L-lysine	Lys	K	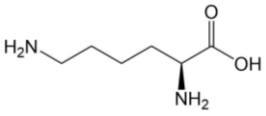	Positive (neutral pH)

Amino acid	Three letters code	IUPAC code	Formula	Side chain feature
L-methionine	Met	M	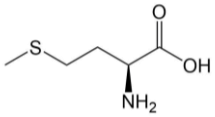	Nonpolar
L-phenylalanine	Phe	F	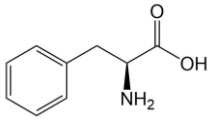	Aromatic/ nonpolar
L-proline	Pro	P	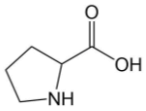	Nonpolar
L-serine	Ser	S	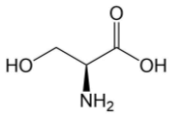	Polar
L-threonine	Thr	T	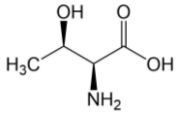	Polar
L-tryptophan	Trp	W	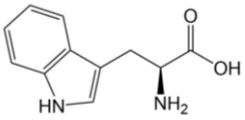	Aromatic/ nonpolar
L-tyrosine	Tyr	Y	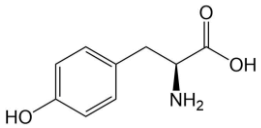	Aromatic/ polar
L-valine	Val	V	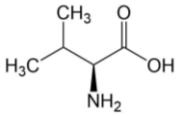	Nonpolar

Introduction

Introduction

1. The global pathogenic effect of mycobacteria

Mycobacteria are aerobic, nonmobile and rod-shaped bacteria, as shown in Figure 1. The latter are widespread in nature and most of them have a pathogenic effect on humans and animals[1,2]. As a matter of fact, pathogenic mycobacteria are intracellular parasites, which multiply within the host macrophage and cause tuberculosis, leprosy (aka. Hansen's disease) or other miscellaneous infections[3].

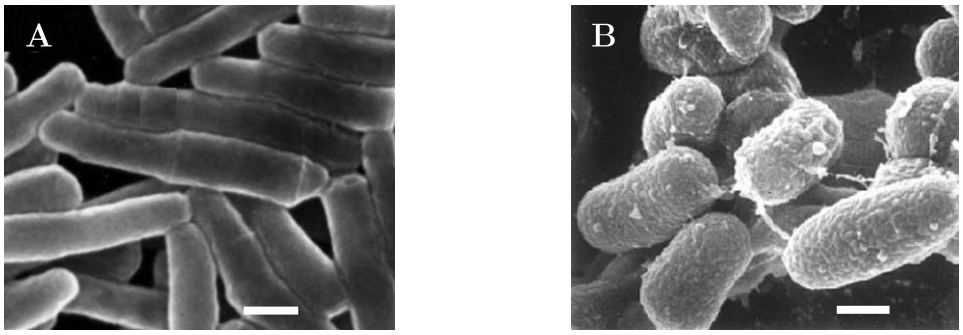

Figure 1 – Scanning Electron Microscopy (SEM) picture of *M. tuberculosis* (A)[4] and *M. avium* ss. *paratuberculosis* (B)[5]. These mycobacteria belong to the two most frequently encountered complex of human pathogenic mycobacteria. Bar = 300 nm.

1.1 Mycobacterial taxonomy

Mycobacteria were firstly described in the late 1800s with the discovery of the tubercle and leprosy bacillus. In 1896, Lehmann and Neumann introduced the first classification of mycobacteria: the latter are included in the genus *Mycobacterium* within the *Mycobacteriaceae* family[6]. Subsequently, mycobacteria species were differentiated depending on the growth rate and the pigmentation of strains: this first phenotypic classification is the root of the Runyon classification, proposed in 1959[7] and summarized in Figure 2-A. Species recognition was thereafter improved with numerous phenotypic, chemotaxonomic and serotaxonomic tests[1], performed on strains cultivated *in vitro*. In order to facilitate analysis, many researchers (38 investigators representing 13 countries) were reunited into an International Working Group on Mycobacterial Taxonomy (IWGMT), established in 1971[8]. Thanks to the huge number of cooperative taxonomic study executed from 1971 to the late 1990s[9-20], *Mycobacterium* has become one of the best described genera and important advances in the clinical diagnosis have been generated. However, numerical taxonomy measures phenotypic similarities that do not necessarily correspond to phylogenetic relatedness[21]. Nowadays, the genus *Mycobacterium* contains 188 species and further comparative genomic analysis highlight

[1] Species are biologically classified through tests, based on a comparison of apparent features (phenotypic tests), a comparison of similarities in the chemical structure of compounds found in the organism (chemotaxonomic tests) or a comparison of protein reaction with a given serum (serotaxonomic tests).

five distinct monophyletic groups within the genus: the "*Tuberculosis-Simiae*", "*Terrae*", "*Triviale*", "*Fortuitum-Vaccae*" and "*Abscessus-Chelonae*" clades, as shown in Figure 2-B[22].

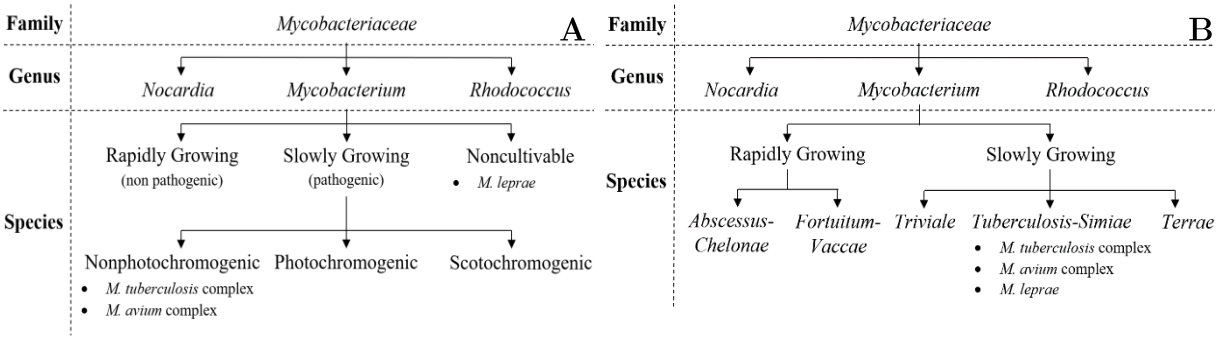

Figure 2 – Mycobacteriaceae taxonomy based on phenotypic features (A, adapted from T.M. Shinnick and R.C. Good[6]) and based on phylogenetic relatedness (B, adapted from R.S. Gupta et al.[22]).

1.2 Mycobacterial features

1.2.1 Acid-alcohol fastness

Although classified as gram-positive organisms, mycobacteria share notable features with Gram-negative cell walls, such as a low permeability barrier acting as a pseudo-outer membrane[23]. As a matter of fact, mycobacteria are characteristically acid-fast: once stained, mycobacteria retain dyes even after exposition to strong decolorizing solutions, such as acids and alcohols[24]. Because Gram stain is often ineffective on them, an acid-fast stain has been thenceforth developed: the Ziehl–Neelsen stain[25].

1.2.2 Mycolic acids as pseudo-outer membrane

Mycobacteria are encompassed by an elaborate cell wall with remarkably low permeability, containing the inner plasma membrane, the peptidoglycan-arabinogalactan complex and the pseudo-outer membrane, as shown in Figure 3. The inner membrane is unusually rich in diacyl phosphatidylinositol dimannosides (represented in Figure 3-B). Because this molecule contains many fatty acids chains, the bilayer is surrounded by an exceptionally low fluidity environment[26]. Arabinogalactan, a highly branched polysaccharide, serves to covalently connect peptidoglycan with the outer mycolic acid layer[23]. The latter is essentially composed of mycolates (known as wax esters), which contain desaturation or a cyclopropane and an internal ester group, as shown in Figure 3-A[27]. Mycolic acids can also be found in other genera (*Culynebacterium*, *Gordona*, *Nocardia*, *Rhodococcus*, and *Tsukamurella*) but only mycobacterial mycolic acids are cleaved to C_{22} to C_{26} fatty acid methyl esters by pyrolysis[24]. An example is shown in the chemical Equation 1: the pyrolysis (at 300°C in vacuum) of a mycolic acid found in a strain of *M. tuberculosis* gives volatile *n*-hexacosanoic acid[28].

$$C_{88}H_{176}O_4 \xrightarrow{\Delta} nC_{26}H_{52}O_2 + subproducts \quad (1)$$

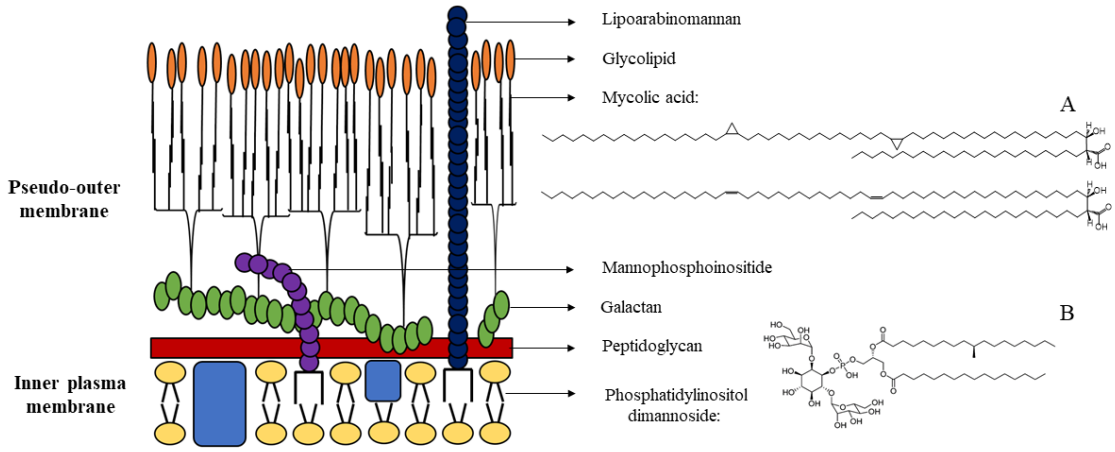

Figure 3 – Schematic representation of mycobacterial cell wall[29] with representative structures of α mycolic acids (A)[27] and of phosphatidylinositol dimannoside (B)[30].

1.2.3 High Guanine and Cytosine content

The generally accepted G+C content of the DNA for the genus *Mycobacterium* is comprised between 61 to 71 mol%. This range encompasses the values for other mycolic acid-producing genera. However, a lower range of G+C content has been reported for *M. leprae* (54 to 57 mol%)[24].

1.2.4 Intrinsic drugs resistance

An intrinsic resistance can be defined as the resistance of any bacterial species that has not been acquired as a result of exposure to antibiotics. In mycobacteria, numerous mechanisms that contribute to drug resistance exist. Those mechanisms include a low cell wall permeability, the production of drug-modifying and drug-inactivating enzymes and efflux-related mechanisms, as illustrated in Figure 4[31].

- **Low cell wall permeability**: the low fluidity and permeability of cell wall slow the influx of drugs and present a significant barrier to the penetration of antimicrobials. Relatively hydrophobic antibiotics (like rifampicin and fluoroquinolones) are able to cross the cell wall whereas hydrophilic and nutrients can diffuse only *via* porins. However, porin channels are very specific and scarcely present on the membrane[32].
- **Drug-modifying enzymes**: mycobacteria produce enzymes that degrade or modify certain antibiotics leading to their inactivation. For instance, β-lactamases are produced by most mycobacterial species (except for *M. avium* complex) and provide multi-resistance to β-lactam antibiotics[33,34].
- **Efflux pumps**: multidrug resistance efflux pumps reduce the intracellular concentration of several antibiotic to subinhibitory levels. Multidrug resistance transporters are grouped into two main classes: secondary multidrug transporters which use the transmembrane electrochemical gradient of protons or sodium ions to pump drugs out of the cell, and ABC-type multidrug transporters which use the free energy of ATP hydrolysis to extrude drugs from the cell[31].

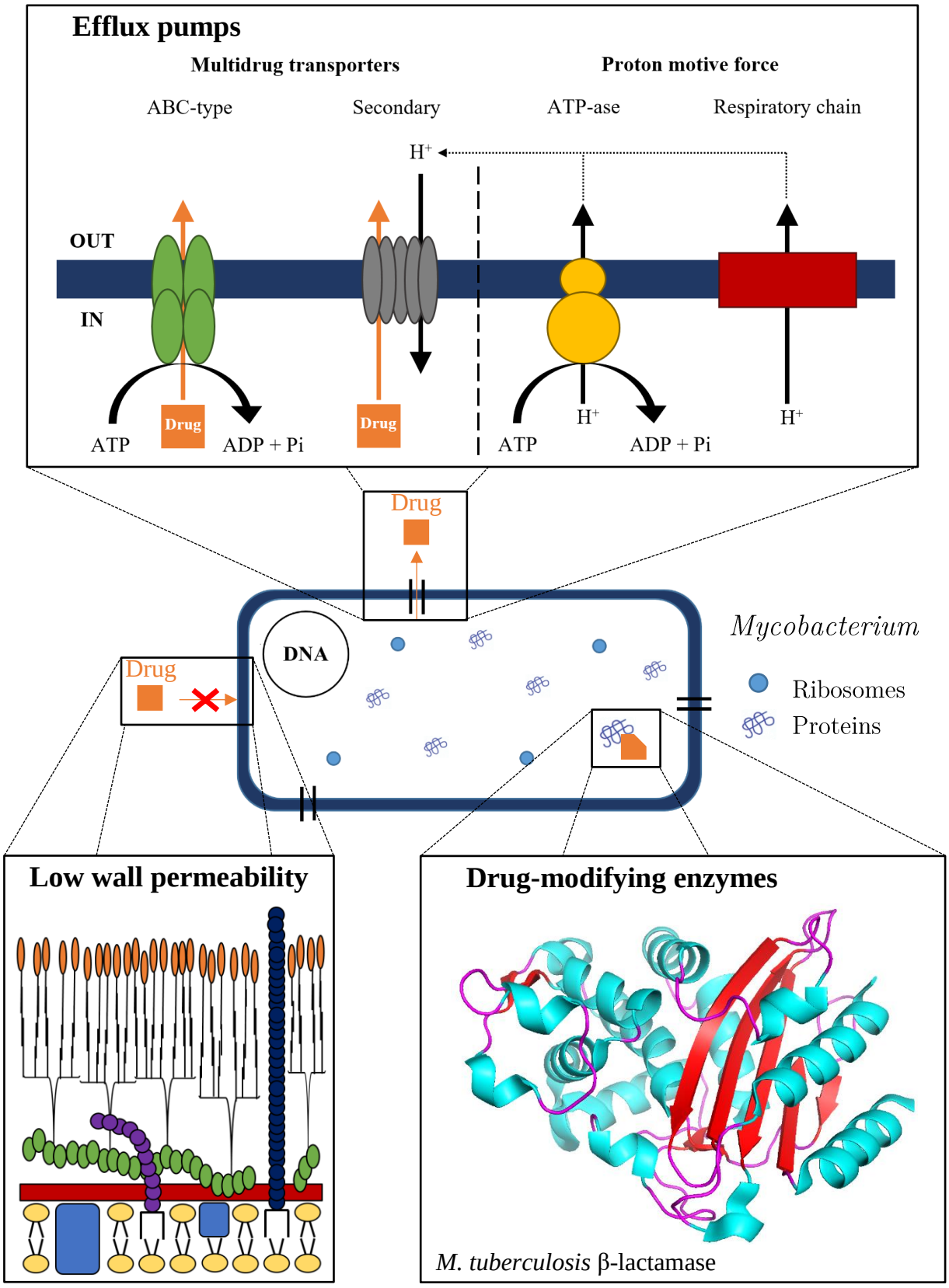

Figure 4 – The three roads of intrinsic resistance in mycobacteria: presence of efflux pumps within the mycobacterial membrane (adapted from H.W. van Veen et al.[35]), a low cell wall permeability (adapted from S. Akira et al.[29]) and presence of drug-modifying enzymes (structure of *M.tb* β-lactamase as example, adapted from F. Wang et al.[36], PDB: 2GDN).

This intrinsic drugs resistance is generally described for mycobacteria, but each species has its own specificities. As a matter of fact, differences in mycolic acid structure affect the membrane permeability and fluidity[37]. In addition, different mycobacterial species possess different set of drug-modifying enzymes and multidrug transporters. These differences may explain the different sensitivity levels among mycobacterial species to lipophilic or hydrophilic inhibitors.

1.3 Mycobacterial pathogenic effect

Beyond rigorous phylogenetic relatedness, the genus *Mycobacterium* can be usefully divided in three groups, depending on diagnosis and treatment of the pathogen: the *M. tuberculosis* (*M.tb*) complex, *M. leprae* (complex) and environmental mycobacteria (also referred to atypical or nontuberculous mycobacteria). A "complex" is defined as a set of species leading to the same pathogenic effect and whose requires similar medical treatment[6]. However, species within a same complex can exhibit distinct phenotypic properties, host range and/or drugs sensitivity. Therefore, a correct identification of the species is sometimes essential to ensure appropriate and accurate patient treatment.

1.3.1 *M. tuberculosis* complex

The *M.tb* complex comprises 8 species: *M. tuberculosis*, *M. africanum*, *M. canettii*, *M. bovis*, *M. caprae*, *M. pinnipedii*, *M. microti* and *M. mungi*. *M.tb* remain the predominant cause of human tuberculosis but *M. africanum* and *M. bovis* are important agents in certain geographical regions[38,39]. Globally, tuberculosis remains a big health issue, especially in South Africa and in Indonesia, as shown in Figure 5.

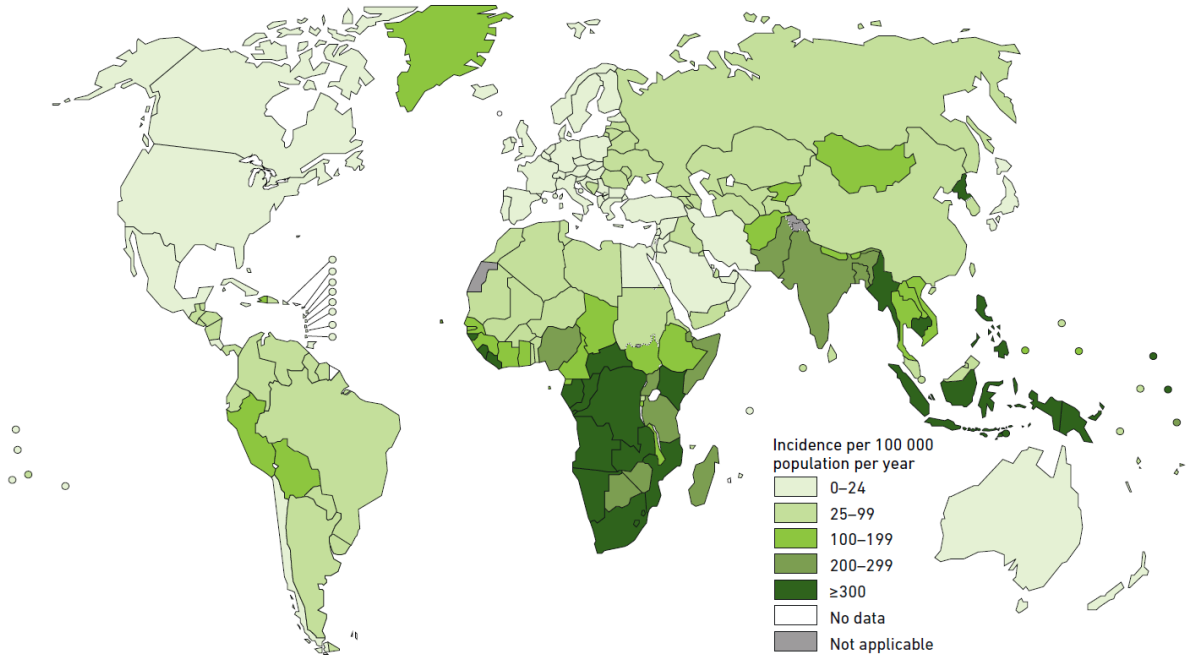

Figure 5 – Estimated TB incidence rates in 2017[40].

Tuberculosis (TB) is currently one of the top 10 causes of death worldwide and the leading cause from a single infectious agent (above HIV). In 2017, TB caused approximately 1.3 million deaths among HIV-negative people and additionally 300 000 deaths among HIV-positive people. Furthermore, 10 million people developed the disease during this single year[40]. In fact, the pathogen spreads very easily and quickly through inhalation of droplet nuclei. The latter are particles of 1-5 µm in diameter containing *M.tb*, which can remain suspended in the air for several minutes to hours. Although the immune response can stop the disease progression, the pathogen is able to persist with some bacilli in a nonreplicating state in the host, without any clinical symptoms: this phase is called the latent infection. The process of *M.tb* infection is summarized in Figure 6. When the immune response is compromised, the latent infection is then reactivated[41], especially for immunodeficient people (co-infection with TB and HIV synergistically influence each other's progress, rendering the host vulnerable to death)[42]. TB typically affects the lungs (pulmonary TB) or, for 14% of incident case, other infection sites like lymph nodes, pleura and osteoarticular areas (extrapulmonary TB)[43].

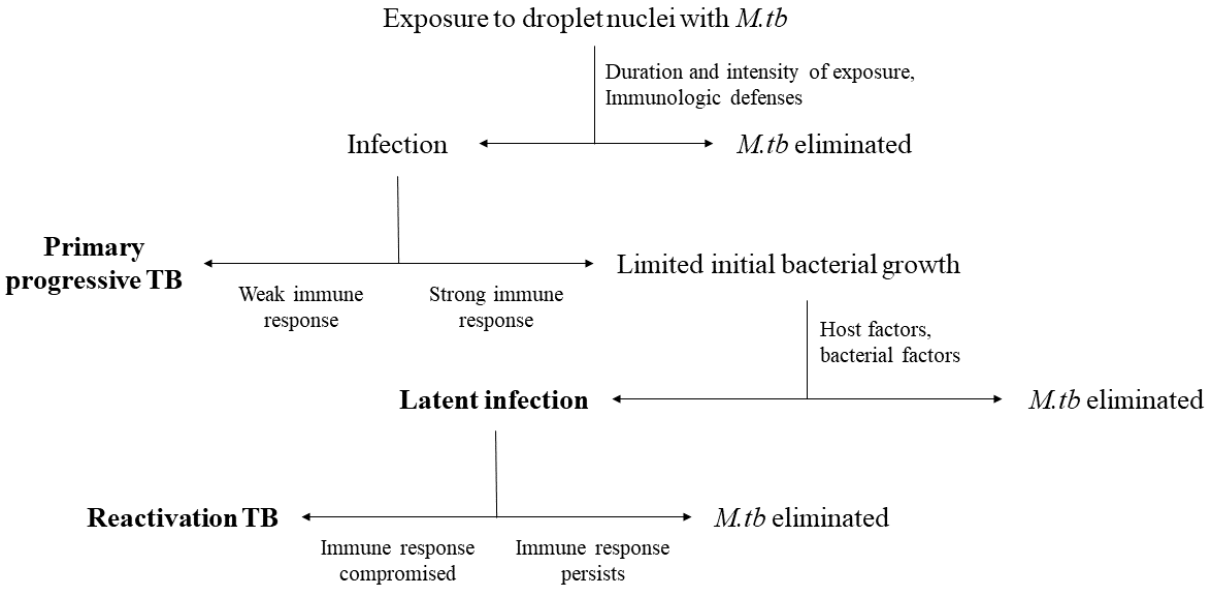

Figure 6 – General process of *M.tb* infection (adapted from S. Ahmad[41]).

The discovery of streptomycin brought about several drugs development programs that lasted from the 1940s through the 1960s. The war against TB was considered winnable. Decreased attention to tuberculosis control worldwide led to a resurgence of the pathogen in the late 1980s[44]. The growing emergence of multidrug-resistant (MDR) TB (resistance to at least the first-line drugs isoniazid and rifampin) and extensively/extremely drug-resistant (XDR) TB (additional resistance to fluoroquinolone and kanamycin, amikacin or capreomycin) has become a global health issue. In addition to intrinsic resistance, an acquired/extrinsic resistance to anti-TB drugs appears by spontaneous mutation and resulting mutants are selected by subsequent bad treatment compliance from patients[31]. It takes usually very long time to treat the disease (6

months), especially if the pathogen is multidrug-resistant one and/or in the latent state (18-20 months). Moreover, the rapid disappearance of clinical symptoms facilitates the premature ending of the treatment[42]. Nowadays, tuberculosis is commonly treated thanks to the four first line curative agents: isoniazid, rifampicin, pyrazinamide and ethambutol (shown in Figure 7).

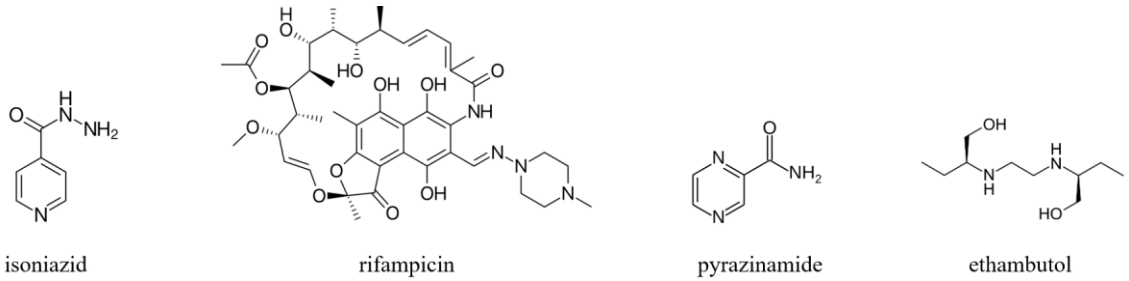

Figure 7 – Structure of first line curative agents used in multidrug therapy against TB.

In order to treat MDR-TB infections, available drugs are reevaluated and divided into three categories based on the balance of effectiveness to safety. Regimens against MDR-TB include at least five medicines to be effective[45]:

- Group A includes three firstly prioritized drugs: levofloxacin or moxifloxacin, bedaquiline and linezolid (shown in Figure 8).
- Group B is composed of two next added drugs: cycloserine or terizidone and clofazimine (also shown in Figure 8).
- Group C includes drugs added to complete the regimen and when medicines from Group A and B cannot be used: ethambutol, delamanid, pyrazinamide, imipenem-cilastatin, meropenem, amikacin (streptomycin), ethionamide or prothionamide and *p*-aminosalicylic acid.

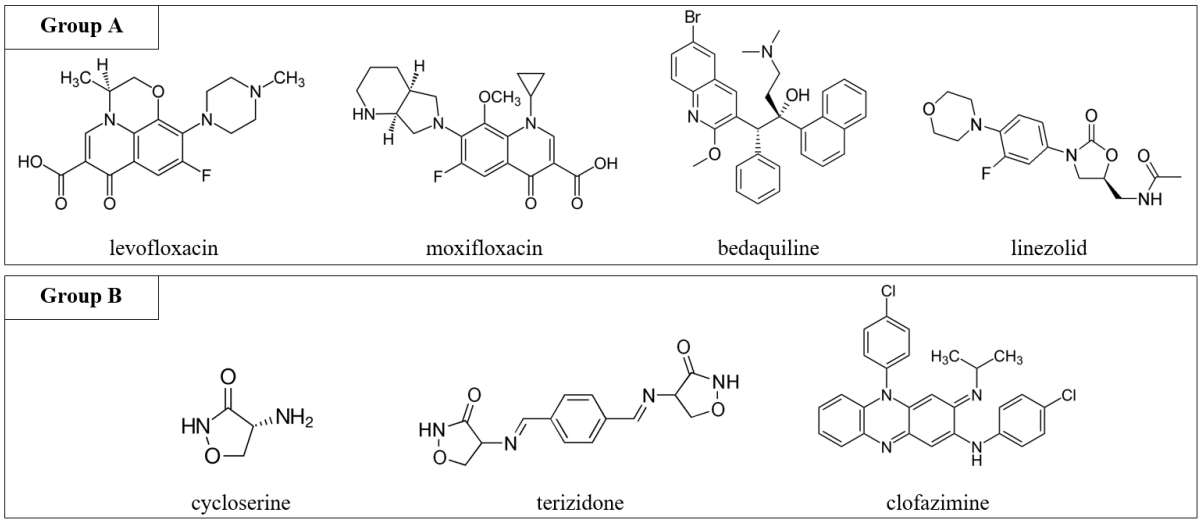

Figure 8 – Structure of curative agents currently used in multidrug therapy against MDR-TB.

Currently, some drugs like isoniazid, rifampin, kanamycin or capreomycin are no longer recommended in order to decrease the risk of treatment failure caused by the development of MDR- and XDR-TB[45]. This multidrug therapy with harsh side effects and the continuous spreading of multidrug-resistant strains highlight the urgent need for new therapeutic targets and associated curative agents, against tuberculosis.

1.3.2 *M. leprae* (complex)

M. leprae has long been recognized as the only pathogen responsible for leprosy. However, *M. lepraemurium* which causes feline leprosy[46] and the recently discovered *M. lepromatosis* (the new human leprosy-causing agent)[47] could be described within a "*M. leprae* complex". All attempts to culture *M. leprae in vitro* have failed because the latter has the longest doubling time of all known bacteria (11 to 13 days)[48,49]. The pathogen remained therefore unclassifiable for a long time according to phenotypic classification.

Leprosy, also known as Hansen's disease, is an ancient and demyelinating disease which affects mainly the skin, peripheral nerves, eyes and mucosa of the upper respiratory tract. As a matter of fact, *M. leprae* infects macrophages as well as dendritic and Schwann cells: leprosy is therefore a chronic dermatological and human neurological disease[49,50]. Although the mode of transmission of the pathogen has not yet been demonstrated, nasals passages are commonly accepted as probable entry-way[51].

The introduction of multidrug therapy to leprosy programs in the mid-1980s resulted in a significant reduction in the prevalence of the disease: a few hundred thousand cases are identified nowadays. The current global leprosy strategy is applied in order to reach a leprosy-free world in 2020[52]. However, because of its severity, leprosy is still considered as a serious public health problem[50].

Treatment regimens were originally based on the Ridley-Jopling classification, which usefully divided leprosy into two forms in function of how they smear the skin: paucibacillary (PB) and multibacillary (MB) leprosy[49,53]. Currently, WHO advocates a 3-drugs regimen of rifampicin, dapsone and clofazimine (shown in Figure 9) for all leprosy patients, with a duration of treatment of 6 months for PB leprosy and 12 months for MB leprosy[54].

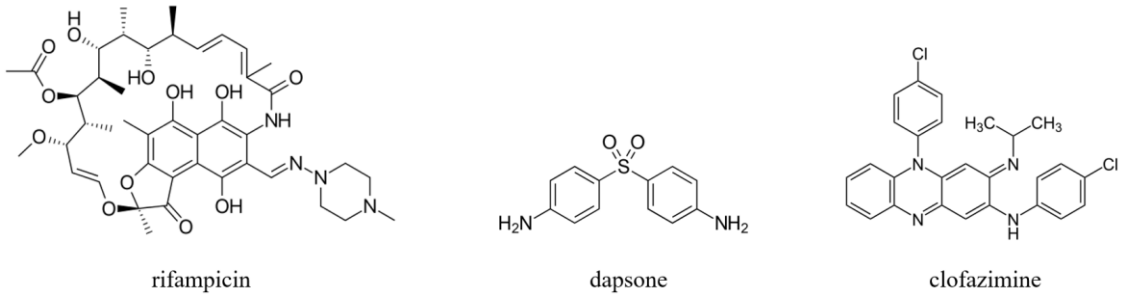

Figure 9 - Structure of therapeutic agents currently used in multidrug therapy against leprosy.

1.3.3 Environmental mycobacteria

Virtually, all other mycobacteria are classified as environmental (atypical or nontuberculous) mycobacteria, which possess other kinds of pathogenic effects, besides tuberculosis and leprosy. Environmental mycobacteria are ubiquitous bacteria that can be found in soil, natural and treated water sources, food or other environmental samples and are considered opportunistic pathogens for numerous animal species mainly birds, pigs and humans[55]. They are less hazardous than tuberculosis or leprosy but much more common in nature and cause colonization, infection and nosocomial outbreaks (namely outbreaks in health care settings)[56].

The most encountered environmental mycobacteria complex (and the second most frequently encountered mycobacterial group, after *M.tb* complex) is the *M. avium* complex (MAC), composed of at least *M. avium* and *M. intracellulare*[6]. In addition, the *M. avium* species is usually divided into four subspecies which correspond to pathogenicity and host range characteristics[57,58]: *M. avium avium* (causes avian tuberculosis in birds), *M. avium paratuberculosis* (causes paratuberculosis aka. Johne's disease in ruminants and is involved in Crohn's disease in humans), *M. avium hominissuis* (affects pigs and humans) and *M. avium silvaticum* (poorly described).

The MAC, mostly encountered among children or immunocompromised patients, leads to pulmonary disease, disseminated disease or lymphadenitis and even (rarely) skin, soft tissues and bones infections. In fact, *M. avium* is the most important pathogen in disseminated disease, whereas *M. intracellulare* is the most common respiratory pathogen[59]. MAC is prevalent worldwide and more especially in the United States: an incidence of 5.6 of MAC lung disease cases per 100 000 persons per year has been estimated in 2009[60]. Although there is no evidence of animal-to-human or human-to-human transmission of environmental mycobacteria[59], the seroprevalence[2] of MAC is still increasing nowadays and suggests that increasing environmental exposure may be in play as well[61]. The treatment depends on the kind of observed symptoms[62]:

- **MAC lung disease**: the treatment is composed of macrolide with rifamycin (a group of antibiotics that includes among others rifampicin and rifabutin) and ethambutol (shown in Figure 10) during at least 12 months.
- **Disseminated MAC disease**: regimen includes macrolide associated with ethambutol and optionally rifabutin (also shown in Figure 10). The treatment remains uninterrupted as long as the immune response is compromised.
- **MAC lymphadenitis**: a surgical treatment is required. An adjunctive drugs regimen is currently being debated.

[2] Seroprevalence is the number of persons who have been in contact with a pathogen and who have developed specific antibodies against the associated disease.

However, like *M. tuberculosis*, *M. avium* resistant-drugs strains have been described and the latter cause macrolide-resistant MAC lung disease. These strains are especially resistant to clarithromycin and azithromycin, two common macrolides (illustrated in Figure 10)[63]. Furthermore, some *M. avium* isolates are resistant to macrolides, quinolones and rifamycins[64]. In the case of multidrug resistant MAC strains, the treatment failure probability is very high (~50%)[65]. In addition, aforementioned multidrug treatments have numerous side effects[62]. That fact highlights once again the need for new therapeutic targets and associated curative agents.

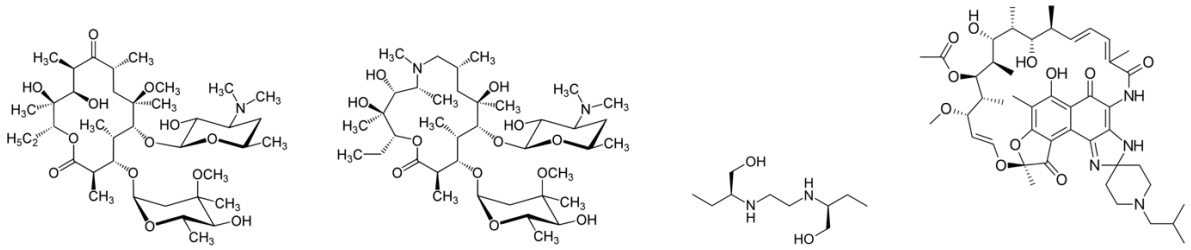

Figure 10 - Structure of therapeutic agents currently used in multidrug therapy against MAC infections. Clarithromycin and azithromycin are two commonly used macrolides and rifabutin is exploited against disseminated MAC disease and MAC lung disease.

2. Need for a new therapeutic target

2.1 Drug design

Drug development can explore numerous avenues of attack, like drug delivery methods, adjunctive immune regulation, therapeutic vaccines, inhibiting efflux pumps or silencing RNA[44]. However, in order to design a new efficient drug, a relevant therapeutic target needs firstly to be identified. Drugs are either bacteriostatic agents (which prevent the growth of bacteria and keep them in the stationary phase of growth) or bactericidal agents (which kill bacteria)[66]. As a matter of fact, a therapeutic target is an essential structure for the homeostasis of the pathogen: the degradation or destruction of this structure (after interaction with curative agents) leads to the inhibition of the bacterial growth or to its lysis. The final outcome of this interaction is an alteration on the pathogenic effect and must lead to the disappearance of the patient's symptoms. The present research work focuses on phosphoserine phosphatase (SerB2) as great therapeutic target for *M.tb*.

2.2 Phosphoserine phosphatase as new therapeutic target

Multiple experiments have highlighted the phosphoserine phosphatase (PSP) as new perfect therapeutic target, for three main reasons:

- PSP is vital for the pathogen: its inhibition stops the main biosynthetic pathway of L-serine and therefore leads to bacterial death.
- In certain pathogens, PSP possesses an intrinsic pathogenic effect and expedites the infection of the host cell.
- The primary sequence of PSP is highly conserved among pathogens. The study of its inhibition could therefore lead to the design of a drug, used as *panacea*, especially against *M. tuberculosis* and *M. avium* complexes.

2.2.1 PSP inhibition leads to bacterial death: the L-serine pathway

Thanks to further study of a pathogen like *M.tb*, some therapeutic targets can be identified though interactome, reactome, genome and/or structural analysis[67]. One common way to identify a therapeutic target utilizes high-throughput screening of mutant libraries coupled with functional genomics. The genome sequence of an organism provides a list of all of the encoded genes. Then, a library of bacterial mutants is generated and strains with growth defects are identified: *M.tb* genes required for intracellular survival are therefore highlighted. The functional genomics is finally used in order to associate selected genes with encoded proteins and their functions in some essential metabolic pathways of the pathogen. This method was used on *M.tb*: the Rv3042c locus, coding for the *M.tb* PSP (SerB2), has been highlighted among others by C.M. Sassetti et al.[68]. This research work sustains previous theoretical metabolic

pathway analysis[69] and is widely referred in further *M.tb* studies[70-72]: SerB2 inhibition leads to dysregulation of serine biosynthesis and growth defect of the pathogen[73].

Numerous therapeutic targets are vital enzymes acting in biosynthetic pathways of cell wall constitutes or of amino-acids. From the genome sequence analysis, it appears likely that mycobacteria have all the amino-acid metabolic pathways common to other bacteria[74]. In this case, *M.tb* PSP (SerB2) is an enzyme which catalyzes the last step of the phosphorylated pathway of L-serine biosynthesis. This phosphorylated pathway, firstly described by A. Ichihara and D.M. Greenberg in 1956[75], occurs in three steps (summarized in Figure 11) and is used in almost all organisms (from bacteria to mammals)[76]. The first step of this pathway is the oxidation (NAD^+ dependent reaction) of L-3-phosphoglycerate into phosphohydroxypyruvate thanks to a D-3-phosphoglycerate dehydrogenase (SerA). Then, the phosphohydroxypyruvate is converted to L-3-phosphoserine with glutamate as an amine donor, thanks to a phosphoserine aminotransferase (SerC). Finally, PSP produces L-serine from L-3-phosphoserine (last enzyme referred to the EC number 3.1.3.3)[74-78].

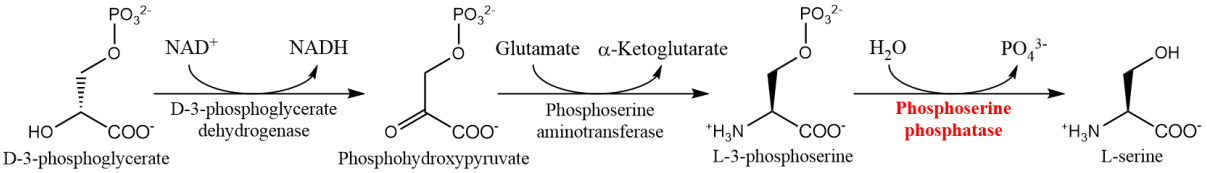

Figure 11 – Phosphorylated pathway of serine biosynthesis (three enzymes: EC 1.1.1.95, EC 2.6.1.52 and EC 3.1.3.3 respectively).

Although the phosphorylated pathway is the most used in order to synthesize L-serine among organisms, this amino acid can be obtained by several other ways: directly by food or through other metabolic pathways like the non-phosphorylated pathway (which occurs in two steps: EC 1.1.1.29/1.1.1.81 and EC 2.6.1.45/2.6.1.51) or the glycine pathway (EC 2.1.2.1). However, the PSP inhibition often leads to death because L-serine is not produced at an adequate rate to satisfy the needs of proliferating cells[74]. As a matter of fact, L-serine is considered to be non-essential (due to the presence of all the enzymes needed for its synthesis in the cell) but this amino acid occupies a pivotal position in metabolism, because of its role as a direct or indirect precursor for many essential metabolites in various metabolic pathways. As shown in Figure 12, L-serine is, *inter alia*, the predominant source of one-carbon units in the biosynthetic pathways of many amino acids (glycine, tryptophan, cysteine,…) and of purines and pyrimidines[79,80]. Furthermore, L-serine is intimately linked with the regulation of D-serine: in humans, ~90% of the L-serine in the nervous system is supplied by PSP and L-serine is the major source for D-serine, which is a co-agonist of a neurotransmitter receptor in the central nervous system. The deficiency of PSP activity is linked to decreased serine levels in the nervous system, leading to neurological abnormalities and diseases[81].

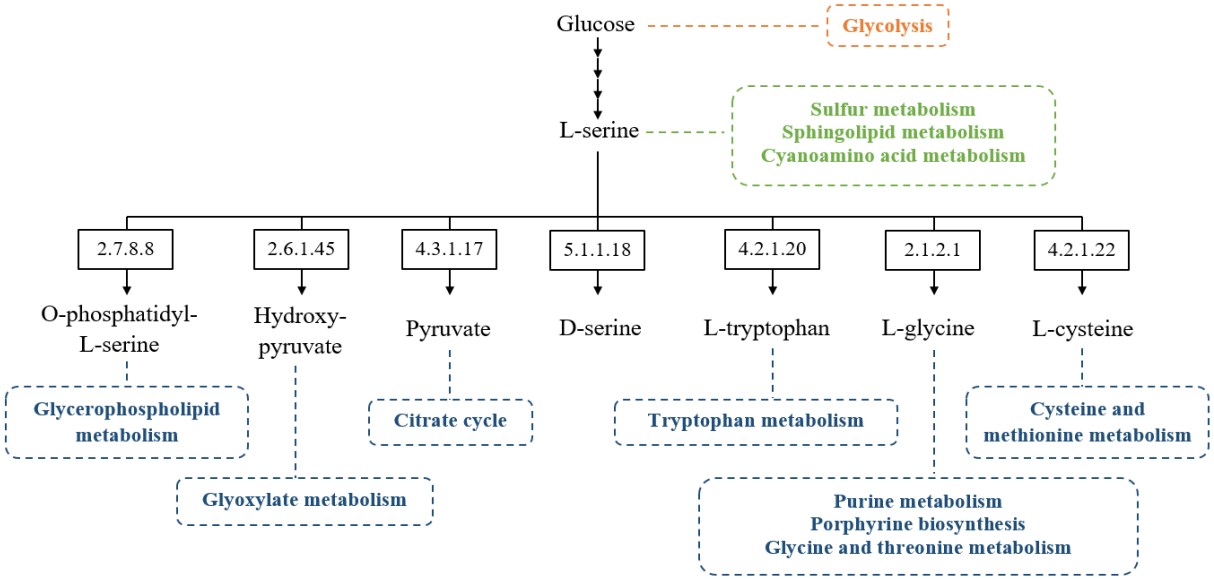

Figure 12 – Overview about the role of L-serine in organisms. Metabolic pathway required for the synthesis of L-serine is highlighted in orange, metabolic pathways directly linked with L-serine are indicated in green and metabolic pathways indirectly associated with L-serine are highlighted in blue (EC number of enzymes associated with each reaction are detailed in frame).

2.2.2 PSP has an intrinsic pathogenic effect

Infection with most mycobacteria like *M.tb* starts with phagocytosis of the pathogen by phagocytic antigen-presenting cells, including macrophages and dendritic cells. Usually, the interaction of the bacterium with host receptors initiates an intracellular signaling cascade which leads to a proinflammatory response. However, the pathogen has also evolved strategies that can trigger signals that modulate this innate immune response[41]. The modulation of host signaling mechanisms is a dynamic process requiring bacterial virulence factors which are molecules that interfere with these pathways and assist the bacterium colonize the host at the cellular level[82].

As a matter of fact, PSP has been identified as an important virulence factor in *Porphyromonas gingivalis*[83-87] and in *M.tb*[88-91], with a similar mechanism of action for both bacteria. During the phagocytosis of the pathogen, PSP is secreted in the cytosol of the macrophages. Although the enzyme possessed exclusive metabolic functions, it gained new functions which help the pathogen in immune evasion and invasion of host cell (summarized in Figure 13):

- **Suppression of IL-8 production**: firstly, PSP facilitates immune evasion through suppression of the interleukin 8 (IL-8) production by epithelial cells. In fact, IL-8 is a neutrophil chemokine (namely a signaling protein) secreted by infected or damaged macrophages, after a pathogen recognition. Then, IL-8 acts as a chemoattractant that induces chemotaxis and guides the migration of other macrophages, in order to prevent the pathogen invasion. Moreover, this chemokine also expedites phagocytosis once neutrophils are on site. At the transcriptional level, the predominant control over IL-8 is exerted by the eukaryotic transcription factor NF-κB. Actually, PSP is

able to bind and dephosphorylate the p65 subunit of NF-κB and the p38 subunit of mitogen-activated protein kinase (MAPK, only described for *M.tb*). Hence, PSP prevents nuclear translocation of NF-κB p65 and subsequent transcription of the IL-8 gene: PSP inhibits an essential component of the innate immune system[86,91].

- **Remodeling of cytoskeletal architecture**: secondly, PSP facilitates invasion through remodeling of cytoskeletal architecture of the host cell. In fact, PSP dephosphorylates and activates cofilin (which causes host actin depolymerisation). The outcome of this interaction between PSP and cofilin is a remodeling of the dynamics of both the host microfilament and the microtubule cytoskeleton. Moreover, PSP is able to regulate the expression of genes that are involved in the actin dynamics[86,91]. This cytoskeletal modification has also been observed with the *M. avium* PSP (SerB)[90]. Modification of cytoskeletal architecture of the host cell for *P. gingivalis* PSP and *M.tb* PSP (SerB2) are also illustrated below.

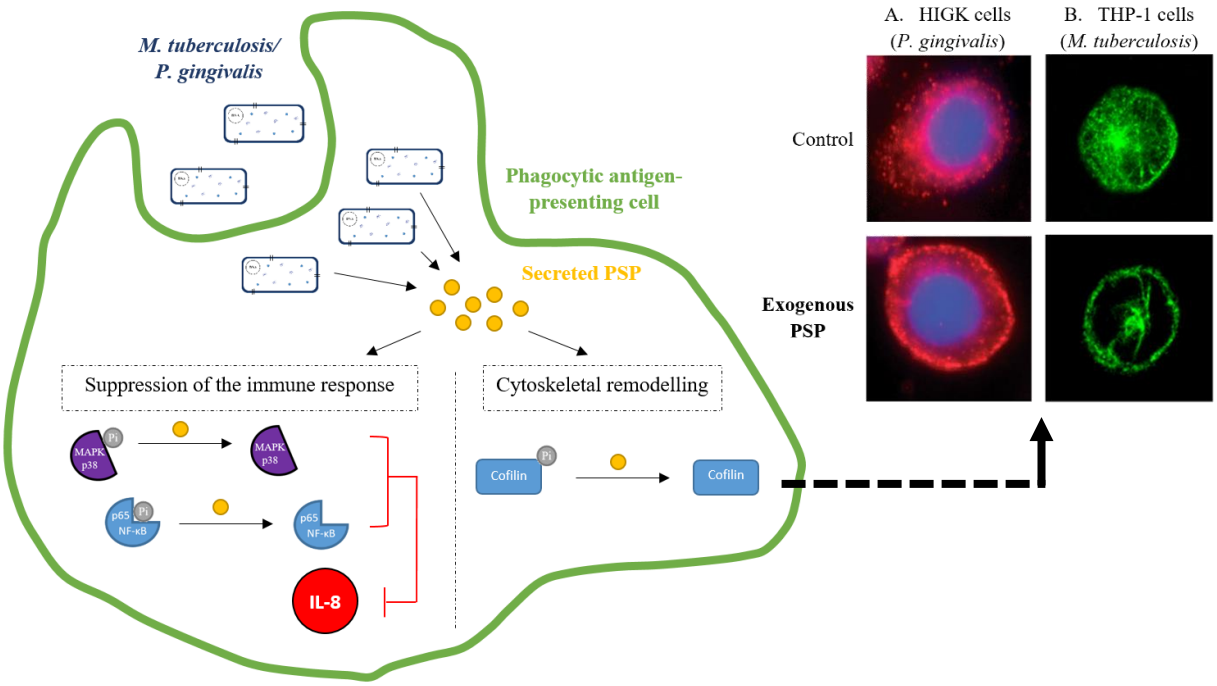

Figure 13 – Overview of PSP functions as virulence factor of *M.tb/P. gingivalis* (adapted from A.K. Sharma et al.[91]). Addition of exogenous *P. gingivalis* PSP on Human Immortalized Gingival Keratinocytes (HIGK) cells (A)[83] and exogenous *M.tb* PSP on THP-1 cells (B)[90] induces microtubule rearrangements (after 2 hours). Pictures are obtained with confocal microscopy.

2.2.3 Primary sequence of PSP is highly conserved

Among various pathogens, the primary sequence of PSP is highly conserved. As shown in the Figure 14, all of the aforementioned pathogenic mycobacteria possess a PSP with a very similar sequence of amino acids[89]. Hence, if a molecule used as curative agent leads to PSP inhibition for one pathogen, this inhibitor could be very effective on all of these mycobacteria because it is highly probable that amino acids implicated in the inhibition are identical and essential for the pathogen. This observation brings about the selectivity issue: a curative agent should not inhibit the human PSP (hPSP). However,

the pathogenic mycobacteria possess some additional domains that are not included in the human PSP sequence. The substrate specificity in PSP will be further discussed in the point 3.1.4.

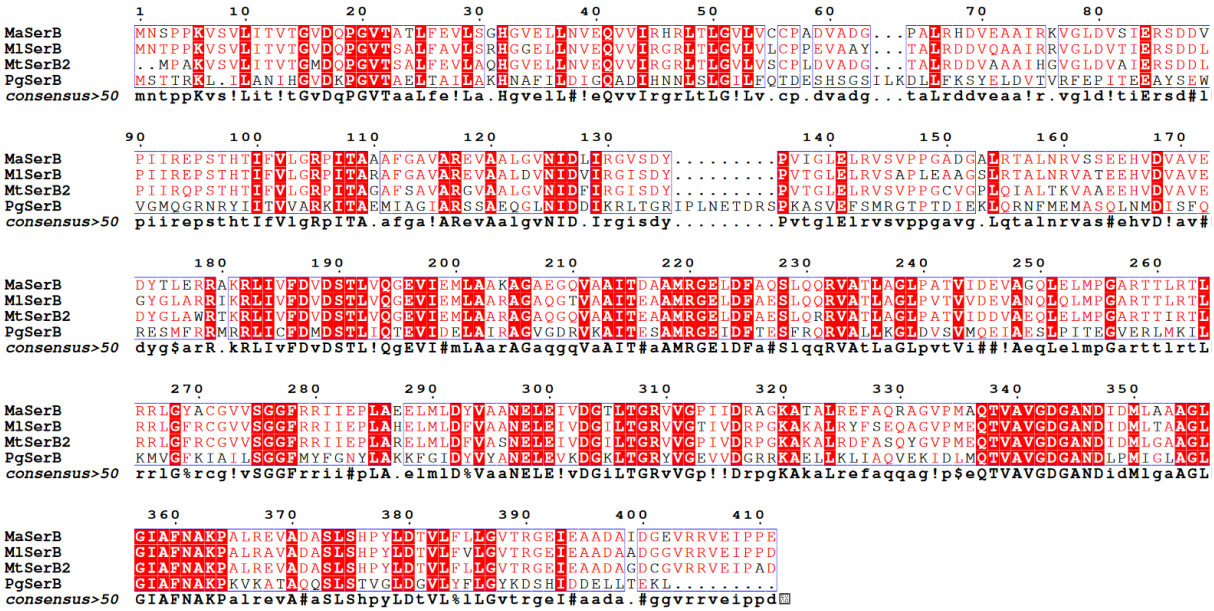

Figure 14 – Sequence alignment[3] for the PSP of *M. avium*, *M. leprae*, *M. tuberculosis* and *P. gingivalis*. The high level of homology is highlighted in red and can be quantified thanks to the following percentages of identity[4] with *M. avium* PSP: 84.7% with *M. leprae* PSP, 83.7% with SerB2 and 36.7% with *P. gingivalis* PSP.

[3] Sequence alignment is performed with MultAlin[139]: http://multalin.toulouse.inra.fr/multalin/
[4] The values are calculated with EMBOSS Needle (BLOSUM62): https://www.ebi.ac.uk/Tools/psa/emboss_needle/

3. PSP characterization

3.1 The HAD superfamily

In order to classify and avoid over-annotation problems, proteins are usefully assigned to a hierarchy of superfamilies and families. A superfamily is defined as a huge set of homologous proteins in which conserved sequence or structural characteristics can be associated with conserved functional characteristics. As a matter of fact, members of a protein superfamily are evolutionary linked together through a common ancestor and utilize a common mechanistic attribute (like a common intermediate or transition state)[92]. Hence, proteins are frequently annotated using computational sequence-alignment methods alone[93]. Actually, common biological traits like protein sequences and structures are an indication for divergence from a common ancestor and means of assigning phylogenetic relationships: divergent evolution leads to homologous proteins. However, because of shared chemical-physical constraints, proteins that evolved independently (without any close common ancestor) often converge on very similar molecular traits, including structure and sequence: convergent evolution leads to analogous proteins[94]. In order to avoid misannotation in enzyme superfamilies and improve prediction accuracy, A.M. Schnoes et al. have proposed a misannotation assessment protocol[93].

M. avium PSP (SerB) belongs to the Haloacid Dehalogenase (HAD) superfamily. The latter comprises numerous families (namely a set of proteins within a superfamily that perform an identical function by the same mechanism[93]), like P-type ATPases, phosphoserine phosphatase, phosphomannomutase, phosphoglycolate phosphatase, epoxide hydrolases and L-2-haloacid dehalogenases[95]. The HAD superfamily is a large, ancient, ubiquitous and diverse group of enzymes present in organisms from all three superkingdoms of life[96]. Although the overall sequence identity between HAD superfamily proteins with different catalytic activities is typically very low ($< 14\%$)[97], members of this superfamily show certain common features:

- **A highly conserved catalytic core**: HAD enzymes possess a catalytic core with a primary sequence (motif I, II and III) and a tertiary structure (Rossmann-like fold) highly conserved within the superfamily.
- **Mg^{2+}-dependent enzymes**: members of HAD superfamily use Mg^{2+} as an obligatory cofactor. This divalent metallic cation provides charge neutralization and helps to correctly orient and position the substrate through coordination.
- **A covalent acyl-phosphate intermediate**: the catalytic mechanism of HAD superfamily enzymes includes the formation of a covalent acyl-phosphate intermediate.
- **A wide substrate specificity**: HAD enzymes are hydrolases with a wide variability in substrate specificity.

3.1.1 A highly conserved catalytic core

The HAD superfamily enzymes contain three peptide motifs that are highly conserved[95,97-99]. In the particular case of HAD phosphatases family, four motifs have been identified[96,100]. Motifs are fold together and form a single binding cavity as enzymatic active site. The presence of these patterns provides a means of identifying superfamily and family members through amino acid sequence alignments. In fact, residues included in the conserved motifs are essential for activity: studies involving site-directing mutagenesis have shown that mutations within these motifs abolish enzymatic activity in solution[101]. The sequences of the aforementioned motifs are illustrated in Figure 15 and are detailed below according to the IUPAC one-letter code for amino acids: X indicates any amino acid and h represents a hydrophobic residue. Described sequences are observed for all HAD superfamily proteins and bold parts highlight residues especially found within the phosphatase family.

- Motif I has the consensus sequence $\mathbf{h_3}$DX(**D**/T/Y)X(T/V)(L/V)**h**. The first Asp residue is the functional nucleophile, essential for the catalytic mechanism. The second Asp participates in this phosphorylation through acid-base catalysis.
- Motif II is the consensus sequence $\mathbf{h_6}$(S/T). The conserved Ser/Thr allows to correctly orient the substrate for the nucleophilic attack through hydrogen bonds with the phosphoryl oxygen.
- Motif III is poorly conserved but can be described with the consensus sequence K(G/S)(D/S)X_3(D/N). The highly conserved Lys stabilizes the negative charge of the reaction intermediate whereas other less conserved residues interact with Mg^{2+}.
- Motif IV, found within phosphatases, is the sequence **(G/S)(D/S)$\mathbf{X_{3\text{-}4}}$(D/E).** Residues are also involved in the coordination of the divalent cation Mg^{2+}.

Moreover, all members of the HAD phosphatase superfamily share the same structural arrangement of the active core: the residues of the catalytic machinery are positioned in a Rossmannoid fold (aka. Rossman-like fold). It is composed of a series of alternating β-strand and α-helix segments wherein the β-strands are hydrogen bonded in order to form a central parallel β-sheet. As shown in Figure 16, this super-secondary structure includes five β-strands that are ordered 3-2-1-4-5, thereby orienting four loops including the four consensus motifs and α-helices which surround both faces of the sheet to produce a three stacked α/β sandwich[96,102].

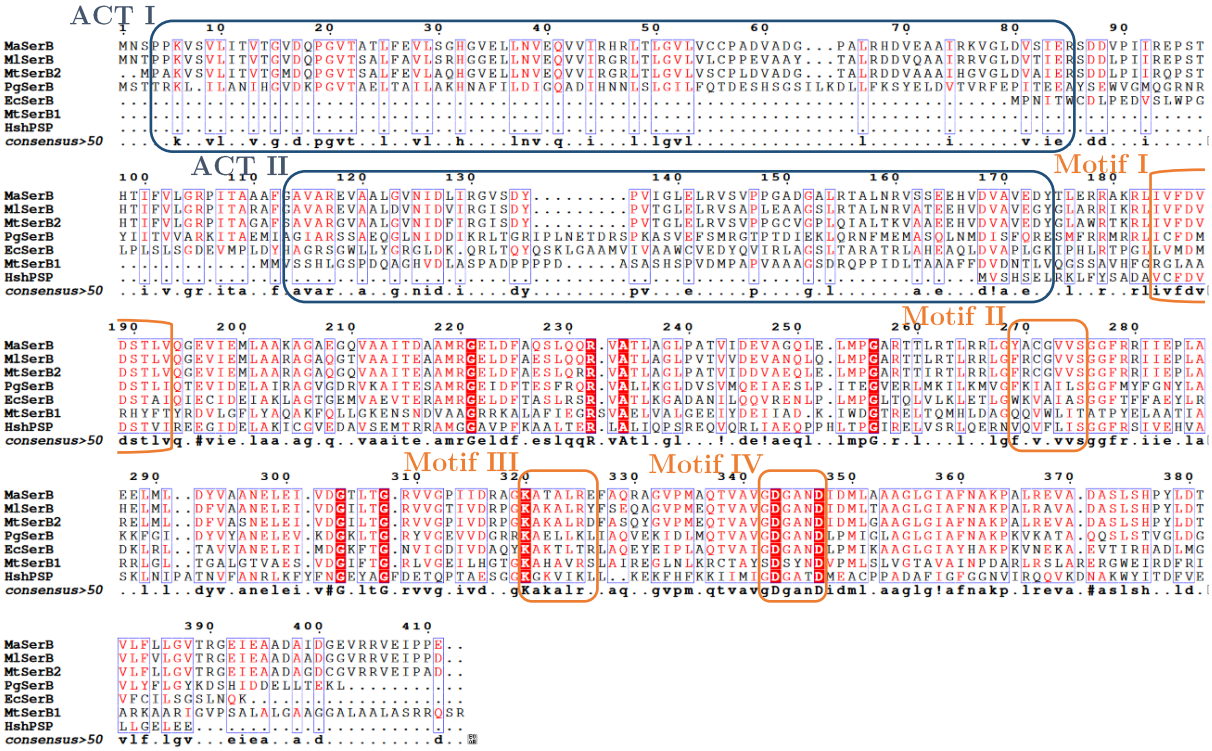

Figure 15 – Sequence alignment[5] for the PSP of *M. avium*, *M. leprae*, *M.tb* (SerB2), *P. gingivalis*, *E. coli*, *M.tb* (SerB1) and *H. sapiens* (human PSP). The high conserved domains I, II, III and IV are highlighted in orange frames whereas the additional ACT domains are highlighted in blue frames.

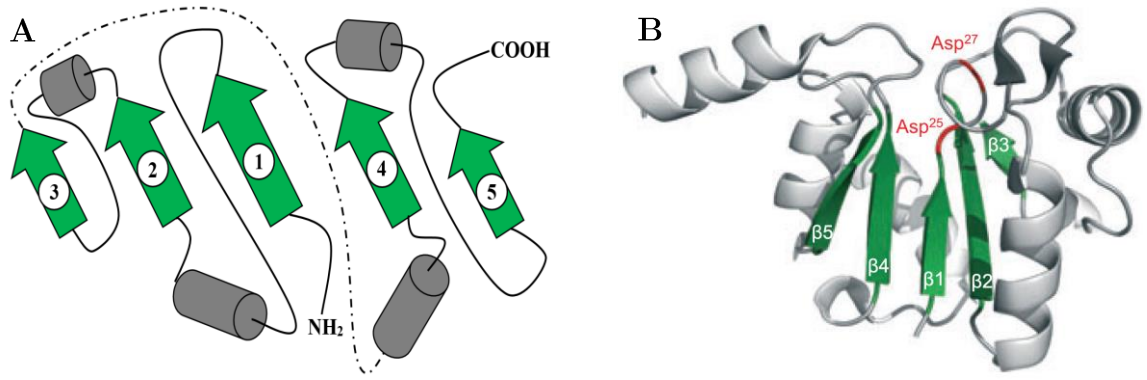

Figure 16 – Schematic representation of the Rossmann-like fold (A) and catalytic core of PDXP/Chronophin (adapted PDB: 2P69) (B)[96].

[5] Sequence alignment is performed with MultAlin[139]: http://multalin.toulouse.inra.fr/multalin/

3.1.2 Mg^{2+}-dependent enzymes

As mentioned before, numerous essential residues included in highly conserved motifs are involved in the coordination of Mg^{2+} as an obligatory cofactor. This metallic cation aids in the correct positioning of the substrate phosphoryl group, and electrostatically stabilizes the required close rapprochement between enzyme and substrate[96]. As shown in Figure 17-A/B, this Mg^{2+} is coordinated in an octahedral geometry *via* three Asp residues, the phosphate anion (from the substrate) and two water molecules[101]. In human PSP, other metal cations like Mn^{2+} and Co^{2+} also act as activators. However, in the case of *M.tb* PSP, all other tested divalent cations like Ca^{2+}, Ni^{2+}, Co^{2+}, Mn^{2+} and Zn^{2+} deactivate it, as shown in Figure 17-C[89].

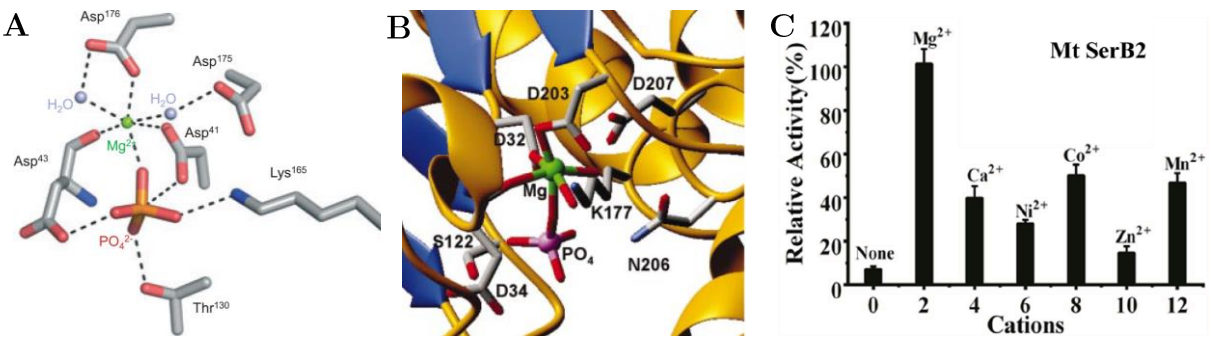

Figure 17 – Steric orientation of the catalytic core residues of the human mitochondrial deoxyribonucleotidase (adapted PDB: 1MH9) (A)[96] and of the human PHOSPHO1 (B)[101]. Relative activity of SerB2 depending on the divalent metallic cation in the catalytic site (C)[89].

3.1.3 A covalent acyl-phosphate intermediate

The characteristic feature of HAD enzymes is a phosphotransferase reaction including the formation of a covalent acyl-phosphate intermediate thanks to the highly conserved Asp residue (within the motif I). The susceptibility of the enzyme-substrate bond is increased by two interactions[97]:

- Interaction with Mg^{2+} helps to polarize the P-O bond thus increasing the electrophilicity of the P atom on the substrate.
- Interaction of the phosphate with conserved Ser/Thr (motif II) and Lys (motif III) could further increase the electrophilicity of the P atom for nucleophilic attack.

When the substrate is close enough to the enzyme, the phosphotransferase reaction occurs in a two-step mechanism within the catalytic site, described in Figure 18[96]:

- First, the Asp nucleophile (Asp^3) initiates a nucleophile attack on the phosphoryl group of the substrate, which results in the formation of a phosphoaspartyl enzyme intermediate and of the product, as substrate leaving group (R-OH). The second Asp of the motif I (Asp^7) assists this step through protonation of the leaving group.
- Secondly, a water molecule exerts a nucleophile attack on the covalent acyl-phosphate intermediate, thus releasing free phosphate and regenerating the catalytic Asp^3. The residue Asp^7 allows to deprotonate the water nucleophile during this second step.

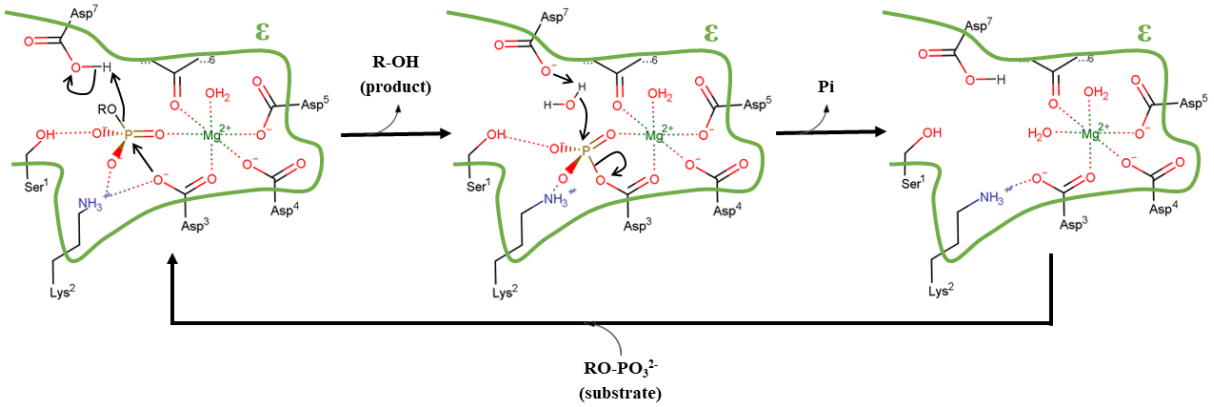

Figure 18 – General catalytic mechanism of HAD family enzymes (adapted from I.S. Ridder and B.W. Dijkstra[95] and from Seifried et al.[96]). Residues Asp^3 and Asp^7 belong to motif I, Ser^1 to the motif II, Lys^2 to the motif III and others are included in motif III or IV.

3.1.4 A wide substrate specificity among the superfamily

The HAD superfamily mainly catalyzes reactions resulting in cleavage of C-Cl, C-P, CO-P or PO-P bonds from a wide range of substrates and demonstrates remarkable functional diversity through a single protein fold[92,101]. Substrate recognition derives from structural accessorizing which for a majority of the HAD members involves additional smaller domains called cap modules. The latter can provide extensive shielding for the catalytic cavity and supply essential interactions for substrate selectivity. In addition, cap modules can be involved in variable oligomerization states. As illustrated in Figure 19, the HAD superfamily enzymes can be divided into three categories based on the organization of the cap domain[96,100]: subfamily I has a small α-helical bundle cap module (C1 cap) located between motifs I and II in the primary sequence, subfamily II has a mixed α/β domain (C2 cap) located between motifs II and III and subfamily III has the structural simplest modules which consist of loops or β-strands (C0 cap).

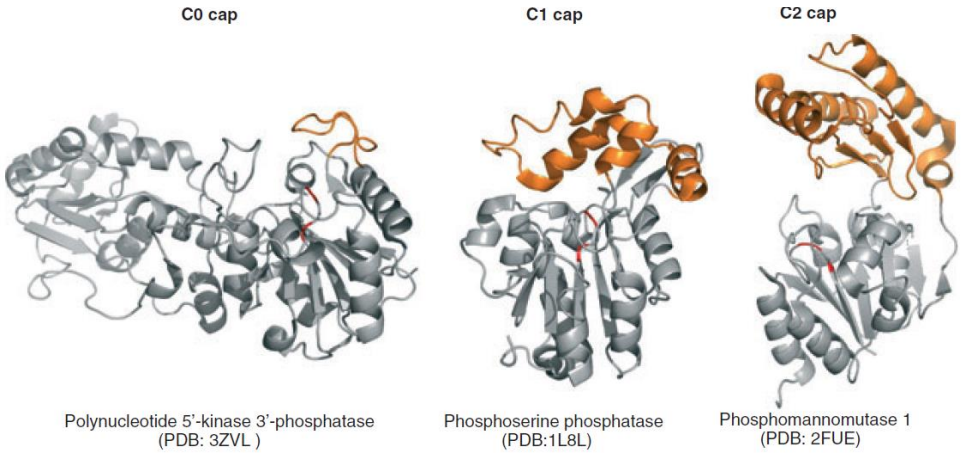

Figure 19 – Structural diversity of HAD phosphatase cap domains. The catalytic core is highlighted in grey, the cap domain in orange and the two catalytic Asp residues in red[96].

Substrate specificity in HAD enzymes can be explained by several phenomena[96]:

- Substrate selectivity is firstly provided by a number of invariant residues that restrict the entrance to the active site through unfavorable interactions.
- Enzymes belonging to subfamily III sterically restrict the entrance to the active site through "pseudocapping", namely by oligomerization via a "flap" segment.
- The presence of C1/C2 cap module (in subfamily I and II) also sterically restricts access to the catalytic cavity and allows enzymes to act on small molecules (which are sequestered within the active site in the "cap-closed" conformation).
- Cap modules include some substrate specificity domains which are sets of residues that interact with the substrate leaving group, define the electrostatic environment of the active site and activate the substrate for nucleophilic attack.

3.2 *M. avium* PSP and closest counterparts

The *M. avium* PSP (SerB) is poorly described in the literature. This enzyme was firstly described by SSGCID research group in 2011[103] and possess a C2 cap domain in addition to the Rossmannoid core, as shown in Figure 20. Moreover, SerB is naturally found in a homodimeric form and each monomer possesses a molecular weight of 44 kDa (415 residues).

As a matter of fact, SerB and its closest counterparts SerB2, *M. leprae* PSP and *P. gingivalis* PSP possess two characteristic ACT domains[6] as cap modules, which justify the hight level of homology, shown in Figure 15. These particular cap modules are widely common among proteins involved in amino acid and purine biosynthesis. The ACT domains have a regulatory role and are able to bind some small molecules like amino acids[104]. Indeed, crystallographic structures of SerB with L-serine near ACT domains have been recently proposed by S. Shree and R. Ramachandran (PDB: 5JLP and 5JLR, to be published). G.P. Yadav et al.[89] have studied the effect of different amino acids on the activity of SerB2. A few amino acids have no effect (Met, Ile, Leu, Asn and Cys) or activate the enzyme (Lys, Tyr and Phe) whereas all others present an inactivation effect. In addition, L-serine, which is the product of the catalyzed reaction and the best inhibitor among amino acids (IC_{50} = 0.78 µM), interacts with ACT domains of SerB2 and leads to the formation of an inactivated tetramer.

The most studied PSP is SerB2 because of the worldwide hazardous effect of *M.tb.* However, the crystallographic structure of this enzyme is still unknown. Hence, the known crystallographic structure of SerB is often used in order to generate a modeled structure of SerB2[89,105,106]. In fact, the closest counterpart of SerB2 is the *M. leprae* PSP

[6] The ACT domain is named after three enzymes that contain this domain: Aspartate kinase, Chorismate mutase and Tyr A (prephenate dehydrogenase).

(84.7%[7] of identity) but the latter has also an unknown crystallographic structure (as well as *P. gingivalis* PSP). Therefore, SerB is exploited as the closest SerB2 counterpart that can be crystallized (with 83.7%[7] of identity).

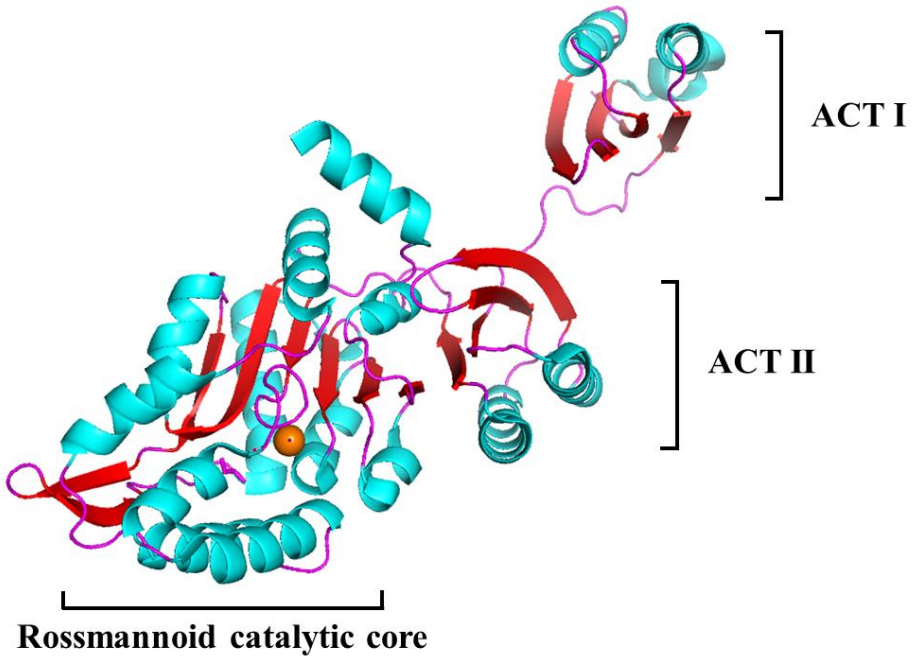

Figure 20 – Catalytic core and ACT domains in the structure of *M. avium* PSP (PDB: 3P96)[103].

[7] The values are calculated with EMBOSS Needle (BLOSUM62): https://www.ebi.ac.uk/Tools/psa/emboss_needle/

4. PSP inhibitors as therapeutic agents

After the identification of an interesting therapeutic target, associated therapeutic agents need to be found. A few PSP inhibitors have been highlighted in various organisms with different objectives. Until the year 1996, L-serine (shown in Figure 21) was the first and the only known micromolar human phosphoserine phosphatase inhibitor identified (IC_{50} = 456 µM)[107]. In 1997, the rat brain PSP was studied by J.E. Hawkinson et al.[108] in order to elucidate the mechanism regulating synaptic D-serine levels. Among other, *p*-chloromercuriphenylsulfonic acid (CMPSA, shown in Figure 21) was identified as potent, noncompetitive inhibitor (IC_{50} = 9 µM), L-α-glycerophosphorylcholine (also illustrated in Figure 21) was found to be an uncompetitive inhibitor (IC_{50} = 18 µM) and fluoride ion (IC_{50} = 770 µM) was also highlighted and may bind the active site like other Mg^{2+}-dependent enzymes. In addition, amino acids and numerous serine derivatives/analogs have been studied.

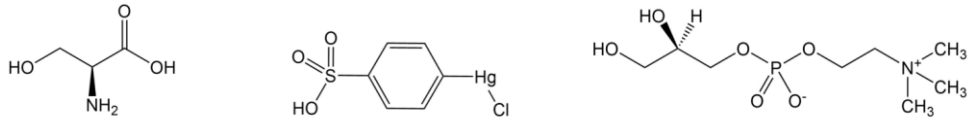

Figure 21 – Structure of the firstly discovered PSP inhibitors[107,108].

After the recognition of PSP as an interesting therapeutic target by Sassetti et al. in 2003[68], this enzyme has been further studied among pathogens. In 2012, the *P. gingivalis* PSP has been studied by Jung et al.[109]. A high-throughput screen of the Korea Chemical Bank has led to the discovery of three 3-acyl-2-phenylamino-1,4-dihydroquinolin-4-one derivatives with IC_{50} values under 10 µM, shown in Figure 22.

In 2014, G.P. Yadav et al.[89] have tested the inhibitors previously highlighted by J.E. Hawkinson et al.[108] on SerB2. Only the chlorpromazine (and the L-serine, cf. point 3.2) presented great inhibition effect with an IC_{50} value fixed at 0.92 µM, illustrated in Figure 23. During the same year, a high throughput screen of a library received from National Cancer Institute Developmental Therapeutic Program (NCIDTP) was performed by Arora et al.[105], in order to identify inhibitors specific for SerB2. Two most potent inhibitors are referred to NSC 76027 (IC_{50} = 3.8 µM) and NSC 693172 (IC_{50} = 4 µM), as shown in Figure 23. In addition, clorobiocin and rosaniline have been highlighted for their ability to kill and inhibit *M.tb* growth in liquid cultures and in infected macrophages: both compounds displayed the best MIC_{99}[8] values of 2 µM against *M.tb* and *M. bovis in vitro*.

[8] The minimum inhibitory concentration (MIC) value is the lowest inhibitor concentration which prevents more than 99% of the bacterial growth.

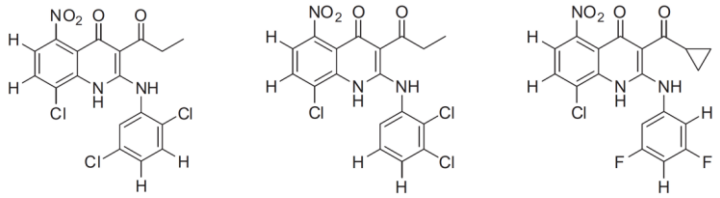

Figure 22 – The three best *P. gingivalis* PSP inhibitors among 3-acyl-2-phenylamino-1,4-dihydroquinolin-4-one derivatives[109].

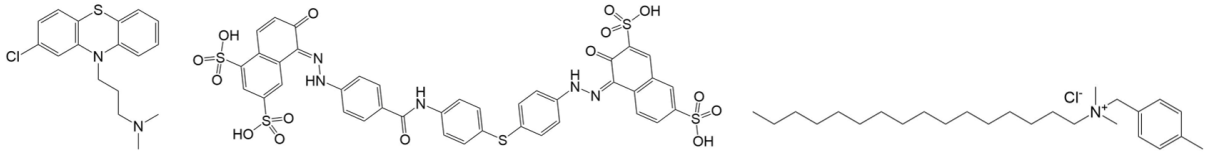

Figure 23 – Structure of potent SerB2 inhibitor discovered in 2014[89,105].

In 2016, Shree et al.[90] have identified clofazimine as an effective and competitive inhibitor (IC_{50} = 5 µM) of both SerB2 and SerB, with similar efficacy. Moreover, clofazimine seems to possess other inhibition effects like inhibition of K^+ transport, binding with DNA or formation of reactive oxygen species after reduction and oxidation within mycobacteria[110]. Although the mechanisms of action of clofazimine remains unclear, this curative agent has a MIC_{99} in a range of 0.3 to 10 µM against *M.tb*, which justify its presence among current therapy against tuberculosis and leprosy (cf. point 1.3.1/1.3.2).

Last year, our research group has performed a screening of NAMEDIC's chemo-library in order to find new SerB2 inhibitors[106]. Three harmine derivatives (with a common molecular structure shown in Figure 24) were discovered (referred to **88**, **91** and **95**) with IC_{50} values from 12.2 to 2.5 µM. In addition, a fourth harmine derivative (**124**) has been synthesized, based on the structure of the three previously discovered compounds. This synthesized compound seemed to present an IC_{50} value very similar to the best harmine derivative inhibitor. Our present research work is a further characterization of those potential therapeutic agents, through study of their efficiency on SerB.

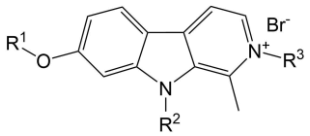

Figure 24 – General structure of discovered harmine derivatives[106].

Objectives and strategy

Objectives and strategy

Mycobacterium, and more specifically *M.tb*, is currently recognized as one of the biggest health issue. As a matter of fact, mycobacteria are frequently multidrug-resistant and numerous resistant *M.tb* strains are spreading worldwide. This situation highlights the obsolescence of the current treatment strategies: new relevant therapeutic targets and associated curative agents need to be found, in order to design new efficient drugs.

Several experiments in our research group focus on SerB2 as new therapeutic target, for the aforementioned reasons. As a result of our research, certain inhibitors have been discovered, thanks to the screening of NAMEDIC's chemo-library. The four most efficient of them have been selected and studied[106]. However, the study of the discovered inhibitors remains incomplete because the crystallographic structure of SerB2 has never been obtained to date.

The first aim of the present research project is the study of the closest counterpart of SerB2 (83.7% of identity[9]) that can be crystallized: the *Mycobacterium avium* phosphoserine phosphatase (SerB). Although researchers from the Seattle Structural Genomics Center for Infectious Diseases (SSGCID) have recently determined the three-dimensional protein structure of SerB[103], there is a significant lack of information in the literature about this enzyme. In this research work, three different ways are exploited in order to characterize SerB, as shown in Figure 25. Firstly, a kinetic study of the aforementioned SerB2 inhibitors on SerB is executed. Secondly, a study of several potential oligomerization states is performed in various conditions. Finally, as a final outcome of the first objective, a structural analysis of complexes with the inhibitors is conducted, after crystallization assays. An optimal purification procedure is required beforehand and is also set up in this research work.

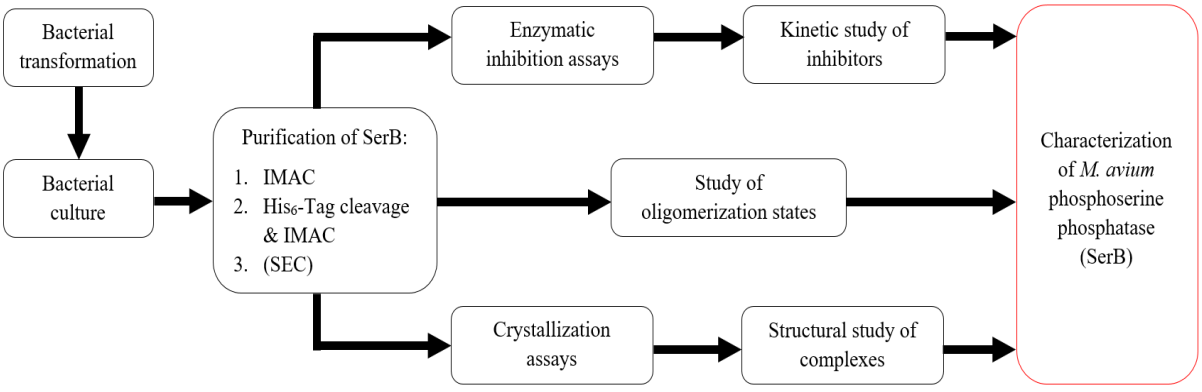

Figure 25 – Overview about the SerB characterization strategy.

[9] The value is calculated with EMBOSS Needle (BLOSUM62): https://www.ebi.ac.uk/Tools/psa/emboss_needle/

The second aim of this research work consists in a comparison between SerB and SerB2 characterization. As shown in Figure 26, studies of enzymatic kinetics and oligomerization states are compared respectively. Then, the high level of homology between both enzymes (initially observed through sequence alignment) is discussed and confirmed. That point allows to finally transpose the crystallographic study of SerB as a new source of information about SerB2 structure and inhibition in a relevant way.

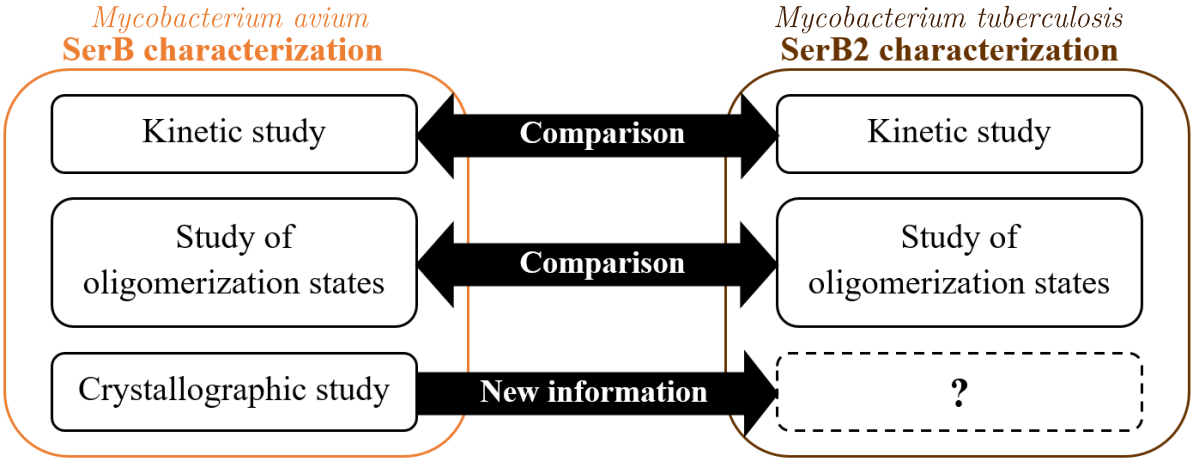

Figure 26 – Overview about the comparison between SerB (this research work) and SerB2[106].

Results

Results

The results of this research work are presented according to the subsequent steps summarized in Figure 27: bacterial transformation, SerB overexpression, SerB purification and finally SerB characterization.

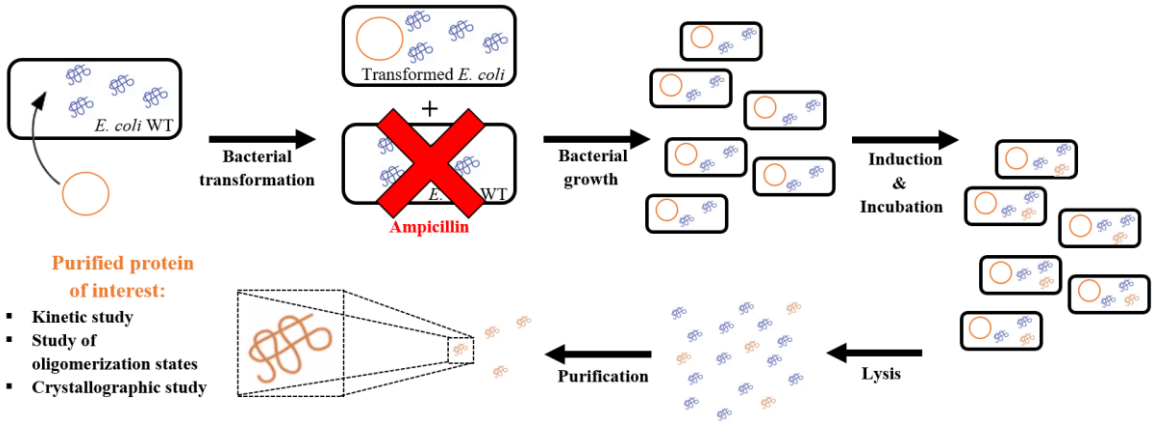

Figure 27 – Overview of the different required step leading to SerB characterization.

5. Bacterial transformation

The general procedure of this research work starts with the bacterial transformation. The plasmid that contains the coding gene for SerB, inserted near the LIC site[10] into a pAVA0421 vector (SSGCID standard bacterial expression vector[111,112]), was obtained from SSGCID. The plasmid includes a T7-promoter and terminator, a cleavable N-terminal hexahistidine tail (His_6-Tag) and a resistance gene against ampicillin, as shown in Figure 28. The pAVA vector is inserted in *E. coli* BL21 by thermoporation and numerous colonies of transformed bacteria are finally obtained.

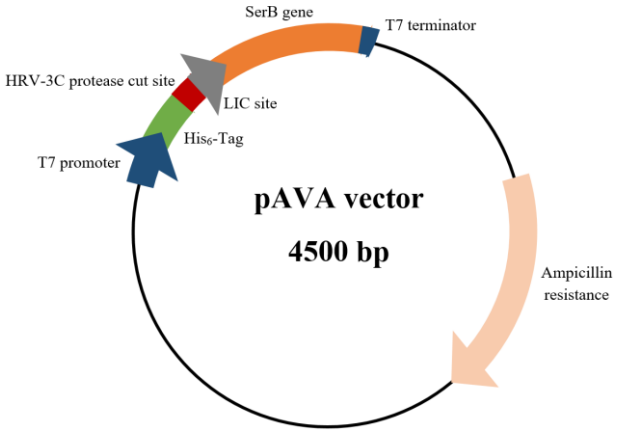

Figure 28 – Overview of the pAVA vector (adapted from S.N. Hewitt et al.[113]).

[10] Ligation Independent Cloning (LIC) is the methodology used in order to clone the purified PCR product (SerB gene) into expression vector (AVA0421), which does not require any restriction enzymes[140].

6. Optimal overexpression conditions

After bacterial transformation, optimal overexpression conditions need to be determined. Overexpression mainly depends on three parameters: the turbidity reached before induction, the amount of isopropyl β-D-1-thiogalactopyranoside (IPTG) added to perform the induction and incubation conditions (time and temperature) after induction.

- **Bacterial growth**: transformed *E. coli* BL21 grow in Lysogenic broth (LB) with ampicillin. This medium causes the apoptosis of wild type bacteria and select transformed bacteria. The growth of suspended *E. coli* is monitored thanks to turbidity measurements. As a matter of fact, increasing amount of bacteria makes the medium more turbid and this phenomenon can be quantified by light scattering with UV-VIS spectrophotometric measurements, generally at 600 nm (OD_{600nm})[114].
- **IPTG addition**: once the optimal medium turbidity is reached, induction must be induced. This phenomenon can be defined as an increased synthesis of enzymes in response to the presence of a particular substrate[115]. In this case, IPTG is used. This gratuitous inducer[11] is associated with the *lac* operon of *E. coli* and allows to start the transcription of the target gene. Actually, the classic mode of prokaryotic transcription is the negative transcription: most genes are "on" and are turned "off" when not needed, thanks to a repressor. Without IPTG, the *lac* repressor is naturally synthesized and transcription of the T7 gene 1 is then prevented, as shown in Figure 29. After IPTG addition, this substrate analogue inhibits the action of the lactose repressor *lac*I and therefore maintains transcription of the T7 RNA polymerase. The latter finally allows transcription of the target gene (SerB) within the inserted expression vector, as illustrated in Figure 30.

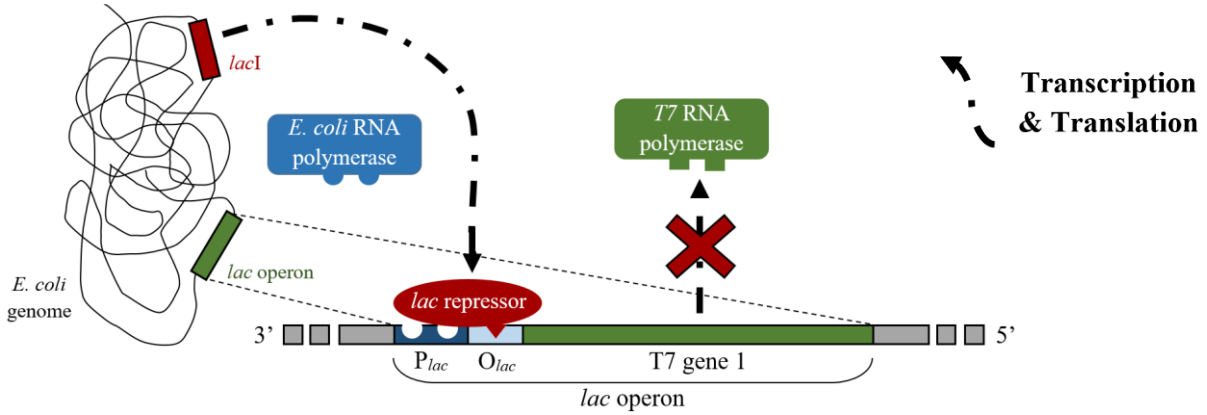

Figure 29 – Negative transcription in *E. coli*: without IPTG, transcription of T7 RNA polymerase is prohibited by the *lac* repressor.

[11] Gratuitous inducers are substrate analogues that can induce enzyme synthesis even if enzymes are incapable of metabolizing them[141].

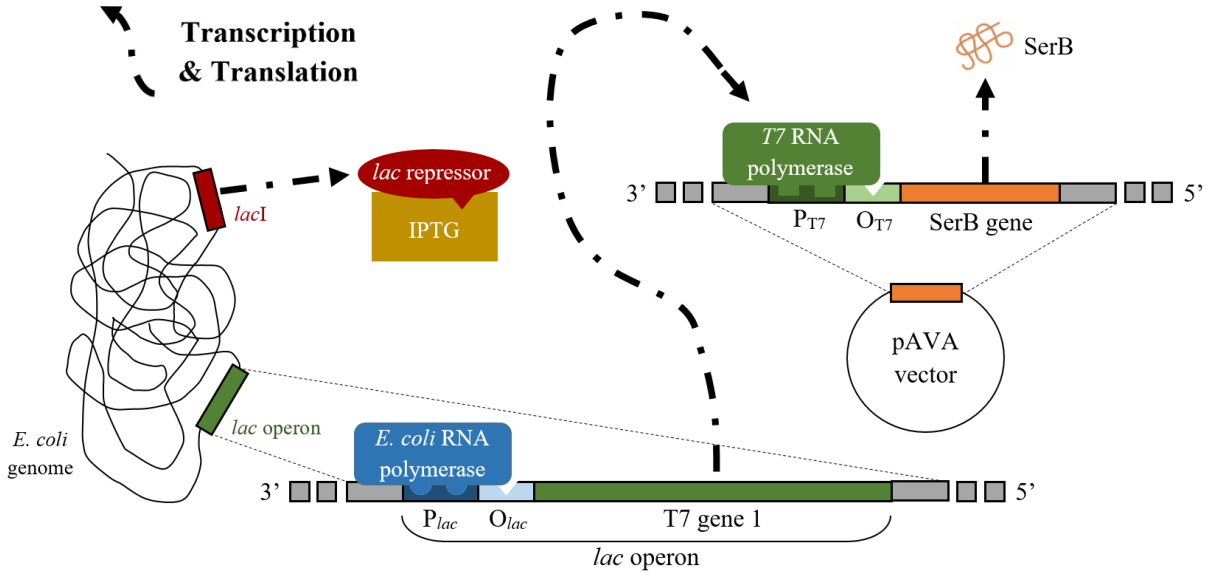

Figure 30 – Mechanism of action of IPTG induction: the presence of IPTG causes *lac* repressor inhibition. Therefore, T7 RNA polymerase is synthesised and is able to browse the expression vector in order to finally lead to SerB expression.

- **Incubation**: after IPTG addition, bacterial cultures are incubated in certain conditions (at a fixed temperature for a given time) in order to maximise SerB expression and lead to SerB overexpression within transformed bacteria.

The first step of this research work is the determination of optimal induction conditions. Twelve different induction conditions were tested and summarized in Table 1. After incubation, a fraction of each sample is collected in order to elaborate an SDS-PAGE (Sodium Dodecyl Sulfate-Polyacrylamide Gel Electrophoresis) analysis, shown in Figure 31. The analysis reveals that induction occurred in all tested conditions. At first glance, the IPTG concentration and the medium turbidity do not impact the induction. Therefore, IPTG concentration is fixed at 0.5 mM and OD_{600nm} is monitored to be located between 0.6 and 1.0, for next bacterial cultures. However, a slight difference in band intensity can be shown on the first gel: the band is scarcely more intense for incubation at 18°C overnight (1a-c) compared to incubation at 37°C during 3 hours (1d-f). In order to invalidate or confirm this observation, the protein concentration of subsequently grown bacterial cultures is measured thanks to Nanodrop Spectrophotometer measurements. After effective purification, the culture incubated at 18°C overnight shows a lower protein amount (~4.5 mg/400 mL of bacterial culture) than the one that has been incubated at 37°C during 3 hours (~5.3 mg/400 mL of bacterial culture). Hence, next cultures are managed thanks to the following optimal conditions:

- An optical density at 600 nm comprised between 0.6 and 1.0 before induction.
- IPTG concentration fixed at 0.5 mM.
- An incubation after induction during 3 hours at 37°C.

Table 1– Summary of different induction conditions which are tested.

	Induction conditions											
Culture turbidity	Culture 1 (OD_{600nm} = 0.6)						Culture 2 (OD_{600nm} = 1.0)					
Incubation conditions	18°C - overnight			37°C - 3h			18°C - overnight			37°C - 3h		
[IPTG] (mM)	0.1	0.5	1.0	0.1	0.5	1.0	0.1	0.5	1.0	0.1	0.5	1.0
Annotation	1a	1b	1c	1d	1e	1f	2a	2b	2c	2d	2e	2f

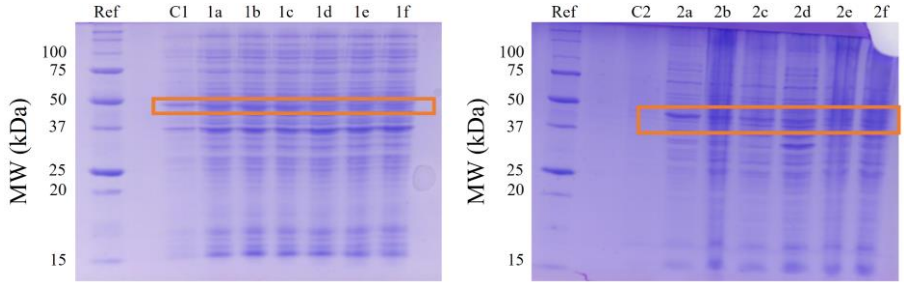

Figure 31 – SDS-PAGE analysis (12% SDS) of fractions in different conditions. On the left, the analysis for the culture 1 (OD_{600nm} = 0.6) and on the right, the analysis for the culture 2 (OD_{600nm} = 1.0). The band associated to SerB (44 kDa) is highlighted thanks to the orange frame. Samples C1 and C2 are fractions before induction. Ref is the molecular weight marker.

7. Set up of the optimal purification procedure

As shown in Figure 31, the bacterial culture after induction and lysis contains overexpressed SerB among numerous other proteins. In order to rigorously characterize SerB, an efficient purification procedure needs to be determined. Researchers from SSGCID have proposed a purification procedure which involves two subsequent Immobilized Metal Affinity Chromatography (IMAC) and one Size-Exclusion Chromatography (SEC). This purification pattern is discussed and detailed below.

7.1 IMAC as first purification step

An IMAC is a method of separating a protein mixture based on a specific affinity. As mentioned before, the expression vector inserted in transformed *E. coli* bacteria allows to express SerB with a cleavable N-terminal polyhistidine affinity tag (His_6-Tag). The latter is used in order to specifically interact with an immobilized metal matrix of a chromatography column, as shown in Figure 32. The latter is composed of nitriloacetic acid (NTA) covalently linked with an agarose matrix and complexed with the divalent cation Ni^{2+}. Actually, histidine residues act as electron donor groups and form coordination bonds with immobilized transition metal[116].

When the protein mixture (obtained after induction and lysis) is loaded on the column, His_6-Tagged SerB interacts with the immobilized cations Ni^{2+}. After washing of the matrix material with a first purification buffer A, proteins which strongly interact with the matrix stay on the column whereas other contaminants are eluted and collected as Flow Through (FT). In order to collect SerB bound on the column, a second purification buffer B_1 more concentrated in free imidazole is gradually added. The latter is a molecule that also strongly interacts with immobilized Ni^{2+} and causes elution of bound proteins by competitive interaction for the column. A purified protein mixture is finally obtained. This first IMAC is schematically represented in Figure 33. In order to optimize this first purification step, numerous purification buffers A/B_1 and elution programs have been tested. Optimal purification has been observed with these following parameters:

- Purification buffer A: 50 mM Tris-HCl, 300 mM NaCl, 20 mM imidazole, pH 7.4.
- Purification buffer B_1 : 50 mM Tris-HCl, 300 mM NaCl, 200 mM imidazole, pH 7.4.
- Elution program of the purification buffer B_1:
  - Flow fixed at 1 mL/min.
  - Buffer B_1 is progressively added from 0 to 100% during 50 minutes.
  - Buffer B_1 (100%) is further added during 10 minutes.

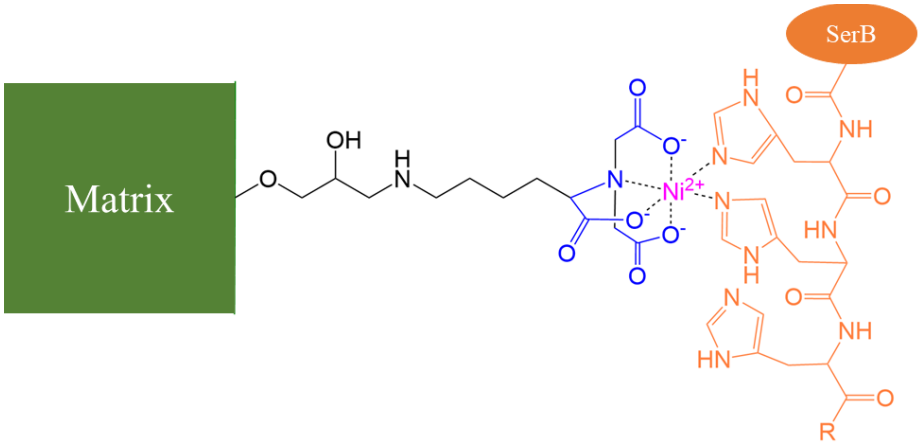

Figure 32 – Affinity between the polyhistidine affinity tag and the nickel-nitriloacetic acid (Ni^{2+}-NTA) matrix (adapted from J.A. Bornhorst and J.J. Falke[116]).

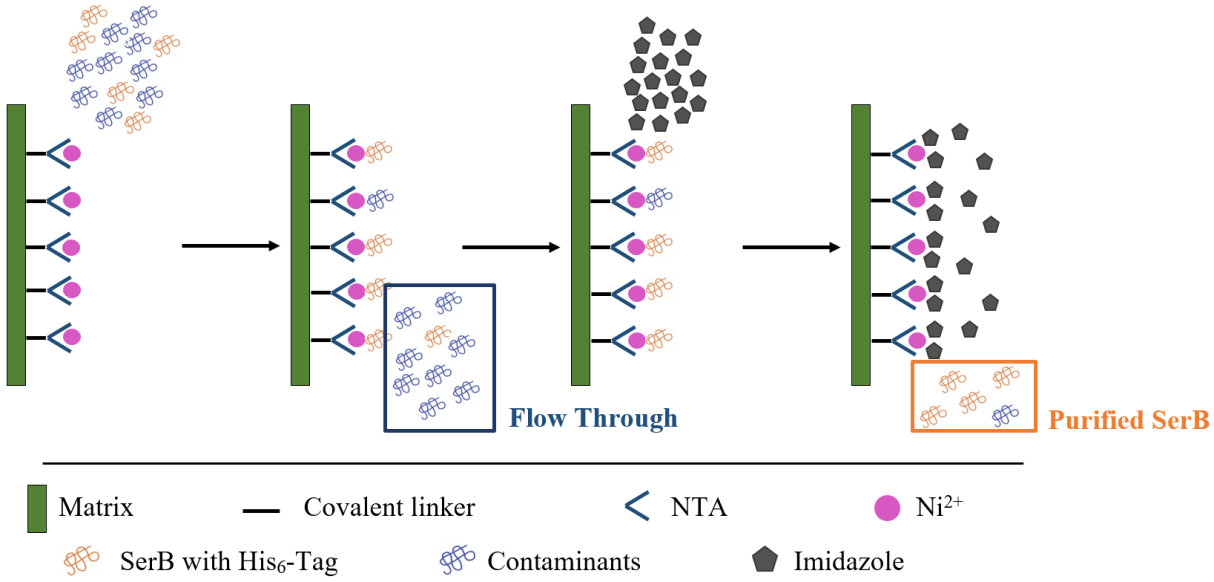

Figure 33 – Schematic representation of the first IMAC for SerB purification.

In order to assess the efficiency of this purification step and follow proteins elution during this process, the IMAC column is coupled with an UV-VIS spectrophotometer (absorbance measurements at 280 nm) and an electrical conductivity meter. A chromatogram is then obtained: the FT appears as a very large and intense absorbance peak and the purified SerB as a second smaller peak. In addition, SDS-PAGE analysis is performed on collected fractions. The chromatogram and associated SDS-PAGE analysis obtained with optimal purification parameters are presented in Figure 34. Despite optimization of this first purification step, SDS-PAGE analysis highlights the presence of numerous contaminants within the purified SerB fractions finally collected. At least one other purification step is required in order to obtain SerB with a high purity (especially for crystallographic assays). Hence, fractions 26 to 46 are pooled for the purpose of the second purification step.

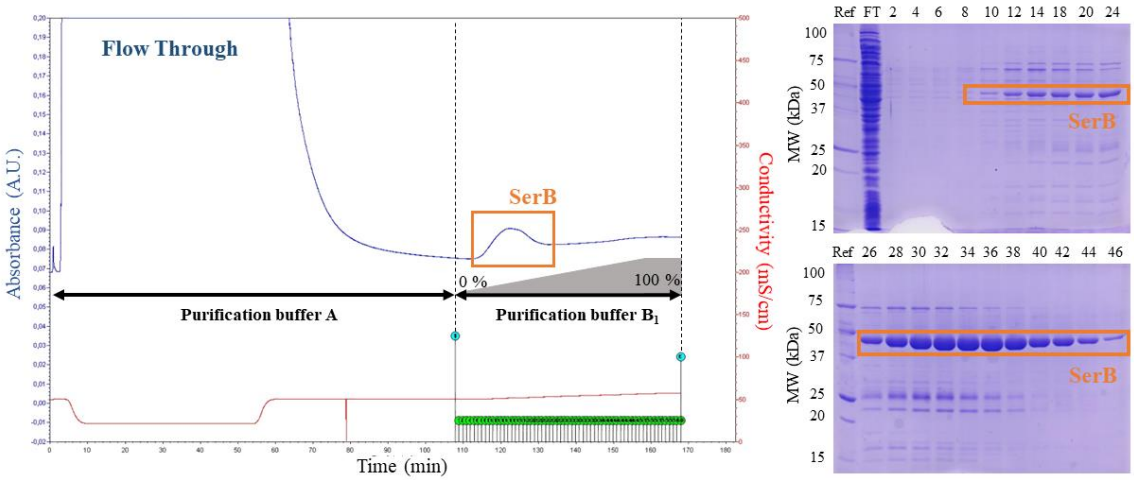

Figure 34 – Chromatogram obtained during the first step of the purification (IMAC) and SDS-PAGE analysis of the FT and collected fractions 2 to 46. Ref is the molecular weight marker.

7.2 Second purification step

7.2.1 His_6-Tag cleavage and dialysis

The second step of purification involves cleavage of the N-terminal His_6-Tag before the second IMAC. Actually, the presence of the His_6-Tag could significantly modify the spatial conformation of SerB and prevent its crystallization. Hence, His_6-Tag cleavage allows to perform an efficient second IMAC (cf. point 7.2.2) and to prevent future potential crystallization issues. As shown in Figure 28, the polyhistidine affinity tag is linked to the SerB gene through a "HRV-3C protease cut site". Hence, SerB is expressed with a set of residues between the enzyme and the His_6-Tag which are used as recognition site for the human rhinovirus 3C protease (HRV-3C protease). When this protease is added in the collected sample, the amino acid sequence LEVLFQGP is recognized and the proteolytic cleavage occurs between the Gln and Gly residues to leave a minimal four-amino-acid sequence at the N-terminus, as shown in Figure 35[113,117].

Figure 35 – SerB is expressed with a 3C protease cleavage site linked to the His_6-Tag.

In order to find optimal conditions for the purpose of His_6-Tag cleavage, four conditions are tested. After HRV-3C protease addition, the protein mixture is incubated during 12-24 hours at 4°C or during 8 hours at room temperature. In addition, a dialysis is performed (or not) simultaneously. In order to determine conditions under which cleavage is achieved, an SDS-PAGE analysis is executed. This analysis, illustrated in Figure 36, shows that cleavage occurs in all tested conditions. Hence, future cleavages will be performed simultaneously with a dialysis, within a reaction buffer which allows the peptide digestion and reduces concentration of free imidazole in the collected sample.

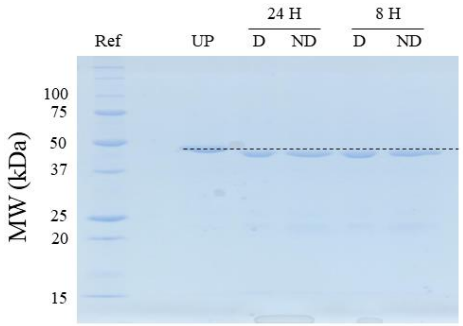

UP = Uncleaved Protein
D = Dialysis
ND = No dialysis

Ref = Molecular weight marker

Figure 36 – SDS-PAGE analysis of the sample after His_6-Tag cleavage in various conditions.

7.2.2 Second IMAC

After digestion, a second IMAC is performed in order to separate cleaved SerB from contaminants which strongly interact with immobilized Ni^{2+} (like the His_6-Tagged protease). As a matter of fact, the HRV-3C protease is initially His_6-Tagged and can be easily removed from the protein mixture by a second IMAC. The latter is very similar to the first IMAC, except that SerB no longer interacts with the column. When the protein mixture is loaded on the column and purification buffer A is added, cleaved SerB elutes as FT whereas other proteins (which strongly interact with immobilized cations) stay on the column. Finally, a purification buffer B_2 (more concentrated in free imidazole than the buffer B_1) is added in order to elute all contaminants. This second IMAC is schematically represented in Figure 37. The following purification buffers and elution program are used for this purification step:

- Purification buffer A: 50 mM Tris-HCl, 300 mM NaCl, 20 mM imidazole, pH 7.4.
- Purification buffer B_2: 50 mM Tris-HCl, 300 mM NaCl, 500 mM imidazole, pH 7.4.
- Elution program of the purification buffer B_2:
  - Flow fixed at 1 mL/min.
  - Buffer B_2 (100%) is added during 10 minutes after FT elution.

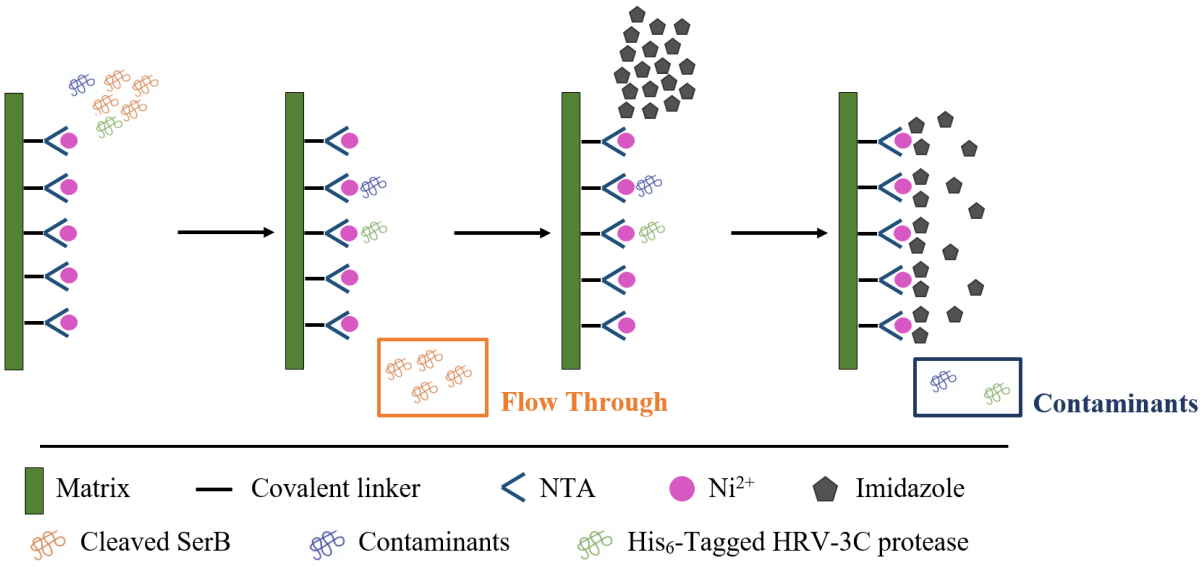

Figure 37 - Schematic representation of the second IMAC for SerB purification.

The chromatogram and associated SDS-PAGE analysis obtained after this second IMAC are presented in Figure 38. The FT (containing cleaved SerB) appears as a large absorbance peak whereas contaminants are detected as a second smaller peak. SDS-PAGE analysis shows that fractions collected as FT contain pure SerB (without any contaminants detected on the gel) except fractions 37 to 44. Fractions 56 to 58 correspond to the contaminants peak and present various proteins including small amount of uncleaved SerB. After second IMAC, fractions 7 to 35 are pooled and a batch of highly purified SerB is obtained. The presence of His_6-Tagged HRV-3C protease (27 kDa) cannot be clearly identified because its concentration is too low to be detected on the blue stained polyacrylamide gel.

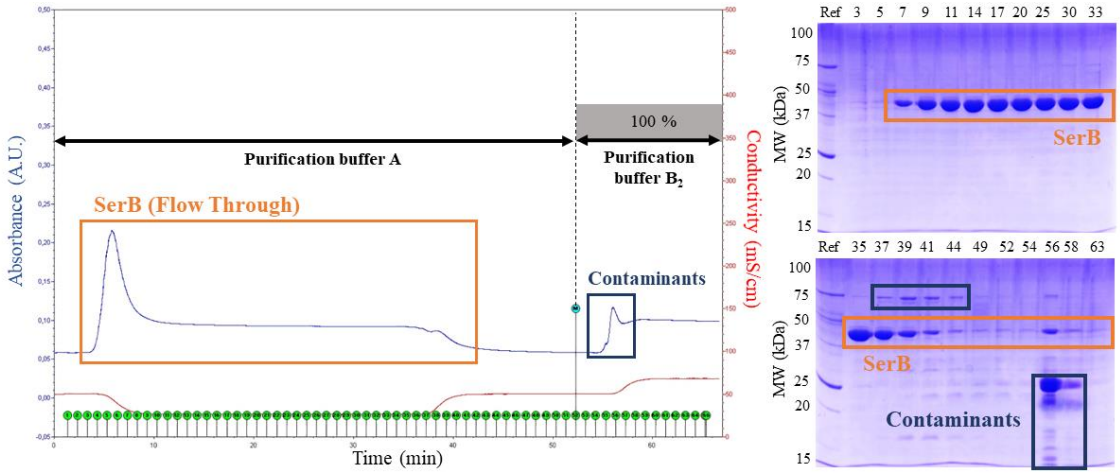

Figure 38 - Chromatogram obtained during the second step of the purification (IMAC) and SDS-PAGE analysis of the collected fractions 3 to 63. Ref is the molecular weight marker.

7.3 Optional SEC as last purification step

Size-Exclusion Chromatography (SEC) is a method in which components of a mixture are separated depending on their ability to enter the pores: molecules elute more or less quickly in function of their size[118]. The purified protein of interest can be then collected, without contaminants like enzymes or oligonucleotides. Before SEC, the sample with cleaved SerB is concentrated. After injection on the column, a purification buffer C containing DL-dithiothreitol (DTT) and glycerol is used in order to optimize the separation between compounds: DTT is a strong reducing agent and prevents bond formation between cysteine residues[119] whereas glycerol prevents protein aggregation[120]. The elution of compounds is monitored thanks to conductivity and absorbance (at 280 nm) measurements. Chromatogram obtained and SDS-PAGE analysis performed are shown in Figure 39. No contaminant is visible on the gels: fractions are pooled and this sample is completely purified. In order to evaluate the efficiency of this step, the absorbance ratio 260 nm/280 nm is measured before and after SEC: this average ratio decreases from 0.78 to 0.53 after purification. This diminution indicates that oligonucleotides are less present in the sample: SerB is obtained with a higher purity.

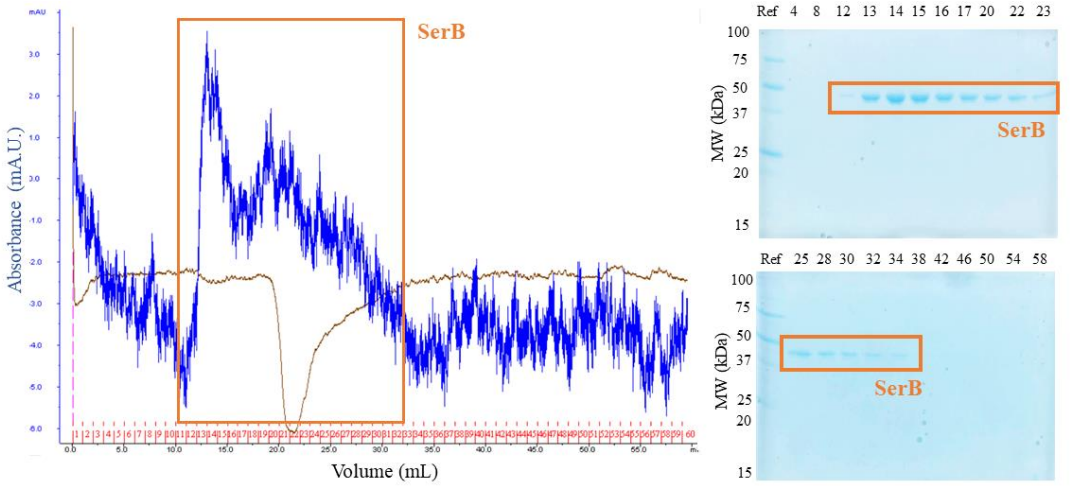

Figure 39 – Chromatogram obtained during the last step of the purification (SEC) and SDS-PAGE analysis of the collected fractions 4 to 58. Ref is the molecular weight marker.

Although the purity of the collected sample is increased, this last step drastically reduces the total amount of collected SerB, in our experiment. Moreover, it is superfluous for the purpose of crystallization and enzymatic assays. Indeed, fractions with cleaved SerB obtained after second purification step have been pooled and concentrated. Subsequently, a crystallization assay was performed by vapor diffusion sitting drop and SerB crystals appeared, under conditions described in SSGCID experiments. Therefore, SEC as last purification step will not be performed again for other bacterial cultures.

7.4 Review of the purification protocol

A review of the purification protocol can be performed by means of two analyses. Firstly, the average yield of each purification step can be evaluated and compared. For one liter of bacterial culture, ~20 mg of protein are obtained after the first purification step (IMAC), ~16 mg after the second step (second IMAC and dialysis) and only 9 mg after the last optional step (SEC). As previously mentioned, the last step dramatically reduces the amount of collected protein of interest and should be prevented.

Secondly, enzymatic assays are performed in order to assess if SerB has a preserved activity after each purification step. Enzymatic assays are performed through phosphate determination assays as detailed in the point 8.1. As shown in Figure 40, absorbance values increases proportionally with the SerB concentration, for the three purification steps. This increase indicates that SerB has a preserved activity: the general purification protocol established does not degrade the enzyme conformation.

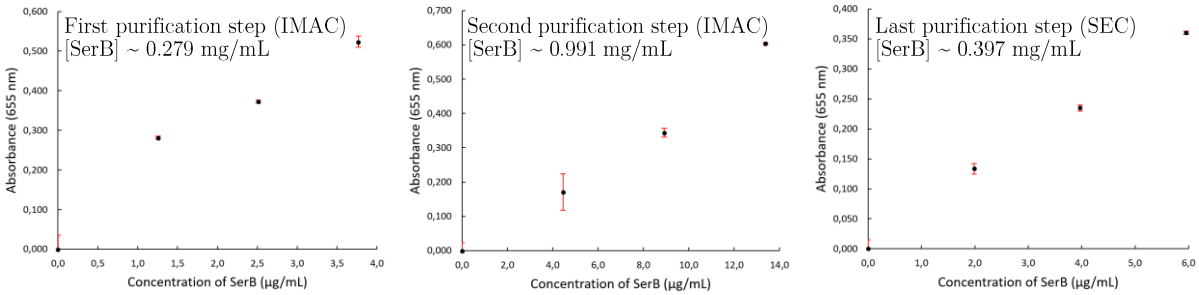

Figure 40 – Evolution of the absorbance at 655 nm depending on SerB concentration. Data cannot be quantitatively compared because enzymes come from various bacterial cultures

8. Kinetic study

The kinetic study of SerB includes study of the effect of harmine derivatives (as SerB2 inhibitors) and of some amino acids on the activity on SerB, through a phosphate determination assay. The kinetic behavior of SerB and SerB2 is thereafter compared (native conditions and with harmine derivatives or some amino acids).

8.1 Phosphate determination assay

In order to perform a kinetic study, the rate of the reaction catalyzed by SerB must be determined by measurements of either appearance of the products or disappearance of the reagents. In this case, SerB catalyzes a dephosphorylation (cf. Figure 11) and the rate can be usefully and easily determined by a phosphate determination assay. The latter is performed thanks to a colorimetric test, firstly proposed in 1966 by K. Itaya and M. Ui[121], on the basis of a green complex formed between phosphomolybdate and malachite green in acidic conditions. Then, the intensity, determined by spectrophotometric measurements, is proportional to the phosphate concentration according to Lambert-Beer's law[122]. As illustrated in Figure 41, the formation of the green complex occurs in three steps, when inorganic phosphate is added to an acidic solution composed of malachite green and ammonium orthomolybdate: formation of orthophosphoric acid (A), formation of phosphomolybdic acid (B) and finally, formation of the green complex (C). In this last step, the reactant is the protonated malachite green and it is only observed if the pH is lower than 2. Actually, malachite green has three acid-base forms (depending on the pH of the solution), as shown in Figure 42.

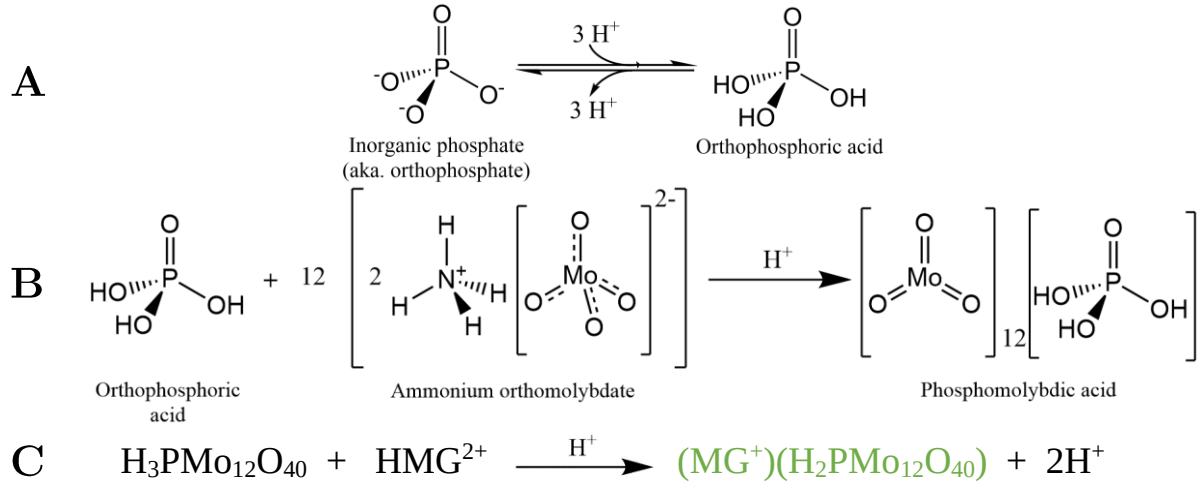

Figure 41 – Three steps for the formation of the green complex.

As detailed in the materiel and method chapter, assays are performed in triplicate, with two blanks (without substrate) for each triplicate. Solutions are incubated, dephosphorylation occurs and they are then added in a 96-multiwell plate containing malachite green and ammonium orthomolybdate in acidic medium. Released phosphate in each tested condition is then quantified by spectroscopic measurements at 655 nm.

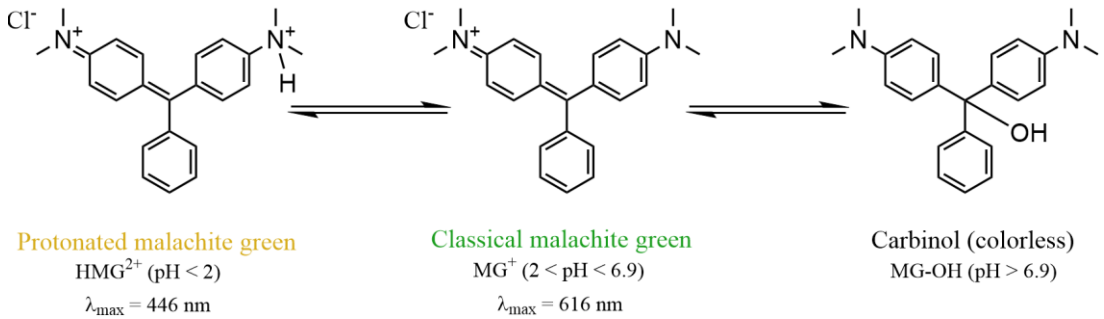

Figure 42 – Acid-base forms of malachite green (adapted from N.M. Cuong et al.[123]).

8.2 SerB batch for kinetic study

After effective purification procedure as previously described, a purified batch of SerB is selected and aliquots are stored at -80°C. All of the phosphate assays are executed thanks to this specific batch in order to perform comparative kinetic analysis. The SerB concentration of the batch is precisely evaluated thanks to the Pierce 660 nm protein assay. This dye-metal[12] complex-based total protein determination method, firstly described by B.S. Antharavally et al.[124] in 2009, is very reproducible and rapid compared to the Coomassie dye-based Bradford assay. Actually, this assay is based on a dye-metal complex binding to mainly basic amino acid residues in proteins. Thanks to spectroscopic measurements at 655 nm and a calibration curve based on bovine serum albumin (BSA), SerB concentration is evaluated at 0.18 mg/mL (±0.03 mg/mL) in the batch. Addition of a given volume of the batch in a tested condition can be easily converted to amount of SerB added in the solution.

8.3 Optimization of the phosphate determination assay

In order to perform kinetic study, conditions that maximize SerB activity must be determined. Arora et al.[105] have determined optimal SerB2 activity for a pH fixed at 7.4 and $MgCl_2$ concentration at 5 mM. Last year, E. Pierson[106] has performed a further characterization of SerB2 that highlights optimal activity with 1 mM DTT and when dephosphorylation occurs at 37°C during 10 minutes. In addition, experiments have shown that dimethyl sulfoxide (DMSO) does not significantly affect SerB2 activity (until 20%vol DMSO in the solution). These observations are used as initial postulate in our kinetic study of SerB. However, optimal amount of substrate and purified SerB need to be determined.

- In order to determine optimal SerB concentration, six concentrations are tested (from 0.23 µg/mL to 1.4 µg/mL) and the substrate concentration is temporarily fixed at 0.2 mM. The aim is to find a balance between high conversion rates and suitable absorbance values. This condition is observed for a SerB concentration of 0.452 µg/mL, with a yield of 4.5 % (after 10 minutes) and a range of absorbance value between 0.6 and 0.7.

[12] The dye-metal complex includes polyhydroxybenzenesulfonephtalein-type dye and transition metal.

- Subsequently, a wide range of substrate concentration is tested with this optimal SerB concentration. The curve obtained, illustrated in Figure 43, reveals that the evolution of the released orthophosphate in function of the substrate concentration follows the Michaelis-Menten kinetics. This curve, mathematically described by Equation 2, is a rectangular hyperbola, through the origin, defined by two asymptotes: [P-Ser] = -Km and v = Vmax[125]. These factors, called Michaelis-Menten parameters, are evaluated by nonlinear regression and characterize enzymatic kinetics: Vmax is the maximum rate achieved when the enzyme is oversaturated with substrate and Km is a quantitative indicator of the affinity between substrate and enzyme. The optimal substrate concentration is found in the linear part of the curve, near the Km value: 500 µM.

$$v = \frac{V_{max}[PSer]}{[PSer] + Km} \quad (2)$$

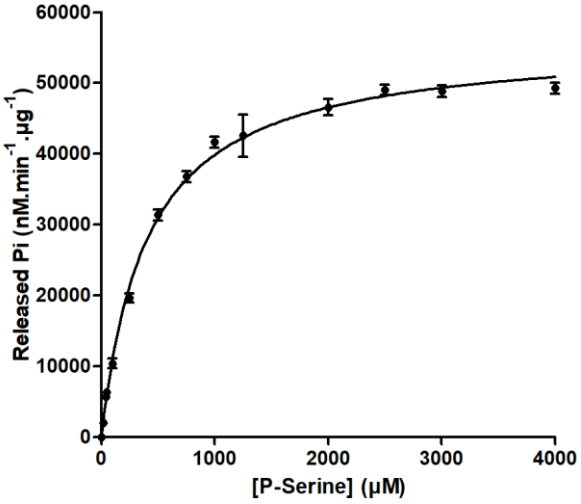

Km = 404.1 (± 16.6) µM
Vmax = 55 993 (± 596) nM.min^{-1}.µg^{-1}

R^2 = 0.9957

Figure 43 – Michaelis-Menten kinetics for SerB (*O*-phospho-L-serine (P-serine) as substrate).

8.4 Enzyme inhibition assay

8.4.1 Effect of harmine derivatives on SerB kinetics

As mentioned previously in this research work (cf. point 4), four efficient SerB2 inhibitors (**88**, **91**, **95** and **124**) are tested on SerB. In order to evaluate the inhibition effect of these inhibitors on SerB, enzyme inhibition assays are performed for the purpose of IC_{50} determination. As a matter of fact, IC_{50} value is the inhibitor concentration required in order to reach 50% of residual enzymatic activity (namely 50% of inhibition) and is useful to compare efficiency of various inhibitors, on a given enzyme. As shown in Figure 44, IC_{50} values are evaluated by following of the SerB activity with an increasing inhibitors concentration. Obtained IC_{50} values are included in the range of micromolar concentrations, which highlights the potential therapeutic aspect of these compounds against SerB. Inhibitors can be classified depending on their inhibition efficiency: **124** (best tested inhibitor with IC_{50} = 1.95 µM) > **91** (IC_{50} = 2.67 µM) > **95** (IC_{50} = 4.75 µM) >> **88** (worst tested inhibitor with IC_{50} = 61.81 µM).

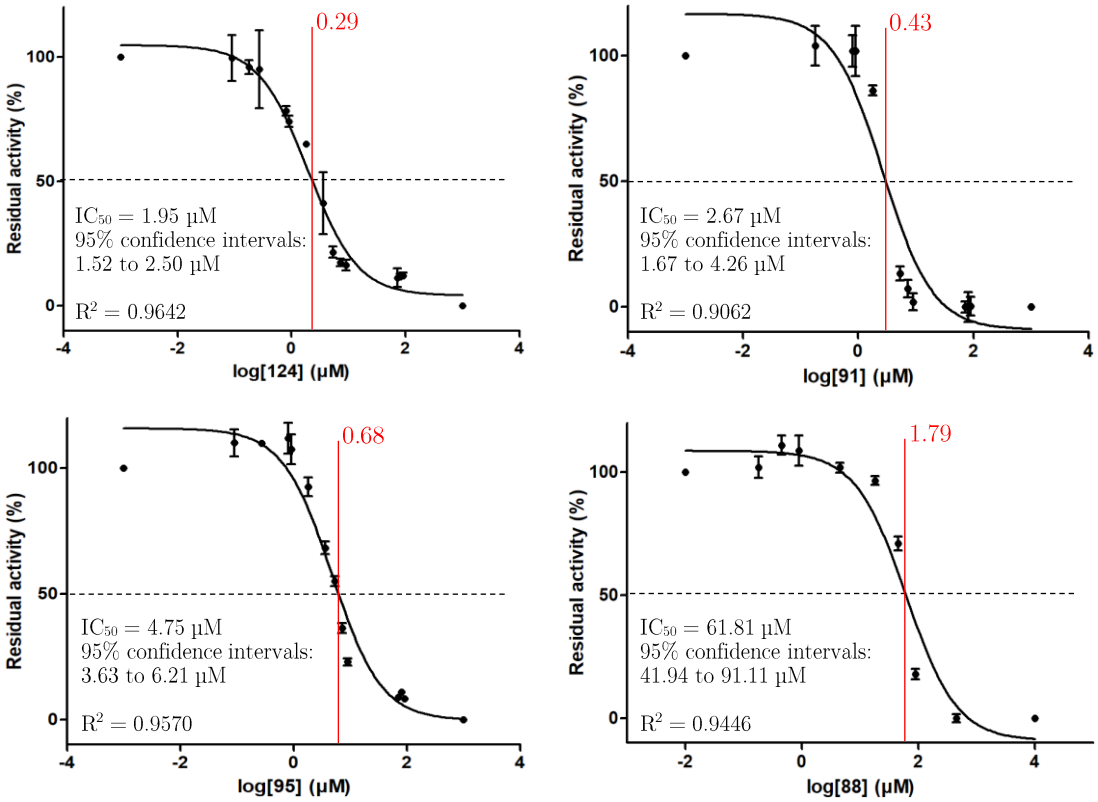

Figure 44 – Inhibition curves of SerB activity in presence of inhibitors **88**, **91**, **95** and **124**. Theoretical points are added for extreme values of log[inh.].

A similar range of inhibition efficiency is observed for both enzymes. However, IC_{50} values are enzyme-dependent and cannot allow rigorous comparison between SerB and SerB2 inhibition. For this comparison, Ki values need to be evaluated: inhibition constant value quantifies the inhibitor-enzyme affinity. To this end, a kinetic study of the inhibition mechanism of action must be performed beforehand. Indeed, inhibitor can be reversible or irreversible and there are three types of reversible inhibitors: competitive (interacts with the active site), uncompetitive (interacts with the enzyme-substrate complex) or mixed (both types of interactions). In order to characterize the mechanism of inhibition of harmine derivatives, the evolution of Michaelis-Menten parameters in function of the inhibitor concentration is analyzed. The parameters Km and Vmax are determined through nonlinear regression and Lineweaver-Burk plot (linear regression shown in Annex I). As shown in Figure 45, Km values increase with inhibitor concentration whereas Vmax remains in the same range of values. This phenomenon is typically observed for a competitive inhibitor. When the solution is saturated with substrate, inhibitor cannot easily encounter the enzyme even in high concentration. On the other hand, a competitive inhibitor causes loss of substrate affinity because it is in direct competition for the enzyme, as illustrated in Figure 46. Then, Ki values can be evaluated thanks to the linear relationship between apparent Km ($Km_{app.}$) and inhibitor concentration [I], based on the following Equation 3:

$$Km_{app.} = Km + \frac{Km}{Ki}[I] \quad (3)$$

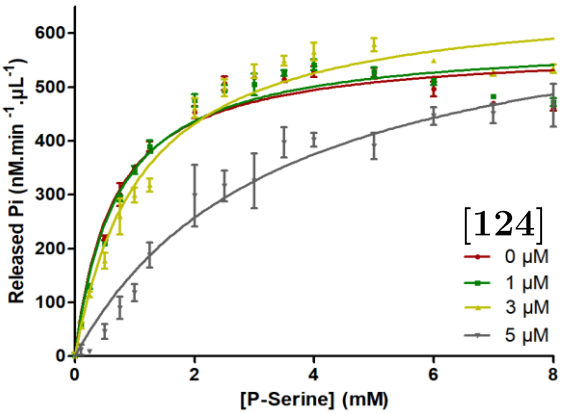

Table A (45) – Michaelis-Menten parameters depending on inhibitor **124** concentration.

[**124**] (µM)	Vmax (µM.min^{-1}.µL^{-1})	$Km_{app.}$ (mM)
0	605.4	0.80
1	667.3	1.06
3	747.7	1.57
5	577.7	1.96
Ki_{124} = 3.57 (± 0.07) (µM)		

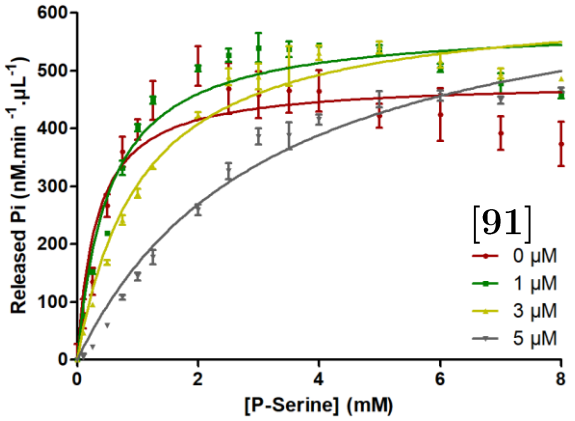

Table B (45) – Michaelis-Menten parameters depending on inhibitor **91** concentration.

[**91**] (µM)	Vmax (µM.min^{-1}.µL^{-1})	$Km_{app.}$ (mM)
0	541.5	0.57
1	634.5	0.79
3	721.2	1.61
5	989.3	5.90
Ki_{91} = 1.35 (± 0.16) (µM)		

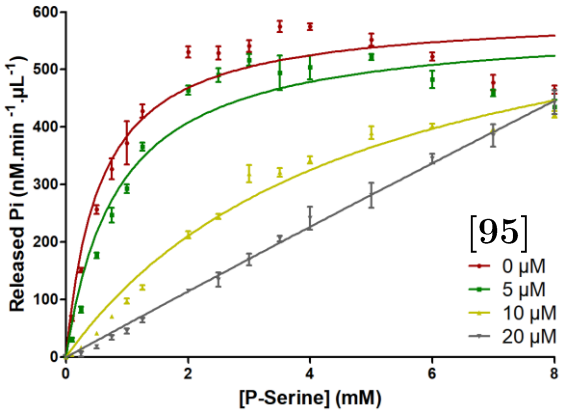

Table C (45) – Michaelis-Menten parameters depending on inhibitor **95** concentration.

[**95**] (µM)	Vmax (µM.min^{-1}.µL^{-1})	$Km_{app.}$ (mM)
0	678.4	0.89
5	646.9	1.23
10	690.0	4.26
20	-	-
Ki_{95} = 11.38* (± 2.50) (µM)		

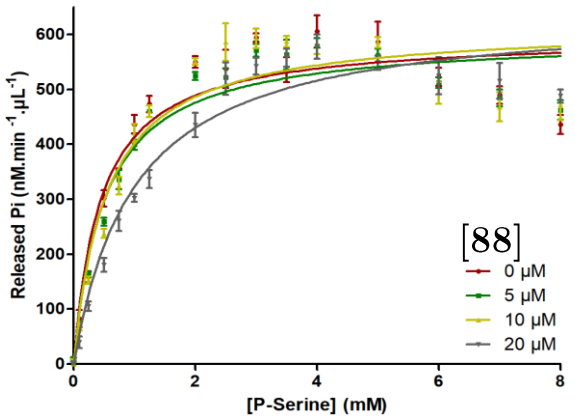

Table D (45) – Michaelis-Menten parameters depending on inhibitor **88** concentration.

[**88**] (µM)	Vmax (µM.min^{-1}.µL^{-1})	$Km_{app.}$ (mM)
0	650.4	0.69
5	661.3	0.78
10	710.0	0.94
20	729.6	1.47
Ki_{88} = 14.43 (± 1.33) (µM)		

Figure 45 – Kinetic curves of the inhibition of SerB activity by inhibitors **88**, **91**, **95** and **124**: evolution of the Michaelis-Menten kinetics depending on inhibitor concentration. (*O*-phospho-L-serine (P-serine) as substrate). *Ki_{95} value is not accurate enough because of rejected values.

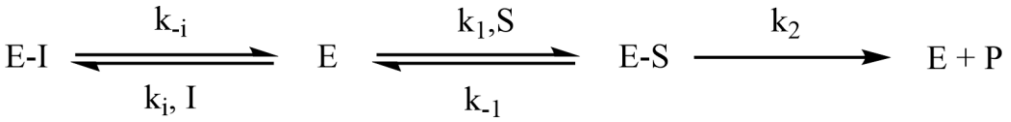

Figure 46 – Michaelis-Menten kinetics with competitive inhibitor I. Letters E, S and P are respectively the enzyme, the substrate and the product.

Inhibitors can be classified depending on their inhibition efficiency: **91** (best tested inhibitor with Ki = 1.35) > **124** (Ki = 3.57) > **95** (Ki = 11.38*) > **88** (worst tested inhibitor with Ki = 14.43). This classification is very similar to the previously established one, based on IC_{50} values. In this case, inhibitor **91** is the more efficient but IC_{50} and Ki values of **91** and **124** are very close and indicate that both inhibitors possess similar efficiency to inhibit SerB activity. In addition, in this classification, inhibitor **95** seems scarcely more efficient than **88**. However, Ki_{95} is less accurate because of rejected values. In fact, inhibitor **95** appears as barely less effective than **91** and **124** inhibitors (as highlighted in the IC_{50} classification) and Ki_{95} could be precisely determined with a range of inhibitor concentration between 1 and 5 µM (rather than 5 to 20 µM).

As shown in Figure 45, experimental points show a systematic decrease of released orthophosphate for high substrate concentration. This phenomenon is typically observed in the case of product inhibition: the product of the enzymatic reaction binds to the active site of the enzyme and inhibits its activity. In this case, kinetic curves highlight the fact that L-serine, as product of the reaction, could inhibit SerB. In order to assess this hypothesis, a study of the effect of certain amino acids on SerB kinetics is performed.

8.4.2 Effects of amino acids on SerB activity

G.P. Yadav et al.[89] have executed a study of effects of all amino acids on SerB2 (cf. point 3.2) and some of them have been selected. As a matter of fact, L-serine (IC_{50} = 0.78 µM), L-tryptophan (IC_{50} = 321.7 µM), L-glutamic acid (IC_{50} = 363 µM) and L-glycine (IC_{50} = 381.3 µM) have been identified as best SerB2 inhibitors whereas L-tyrosine (38% activation) seems to significantly activate SerB2. Hence, these amino acids are subsequently tested against SerB, with a concentration fixed at 10 and 100 µM, as shown in Figure 47. The residual activity is calculated through the Equation 4, where A, A_{blank} and $A_{100\%}$ are the absorbance respectively of the solution containing L-serine, of the blank and of the solution without L-serine. With a concentration fixed at 10 µM, amino acids generally do not impact SerB activity and the enzyme fully conserves its activity. At 100 µM, L-serine causes a dramatic drop of residual activity and the latter reaches 34%. This activity decrease is also observed, to a lesser extent, with L-tryptophan and residual activity reaches 66%. Other amino acids do not show significant activity variations between 10 and 100 µM. Therefore, L-glutamic acid, L-glycine and L-tyrosine do not seem to have an effect on SerB function (higher concentration should be tested). A slight activity increase is observed for L-glutamic acid and L-tyrosine but higher amino acids concentration should be tested in order to prescribe activation effect.

$$Residual\ activity\ (\%) = 100\left(\frac{A - A_{blank}}{A_{100\%} - A_{blank}}\right) \quad (4)$$

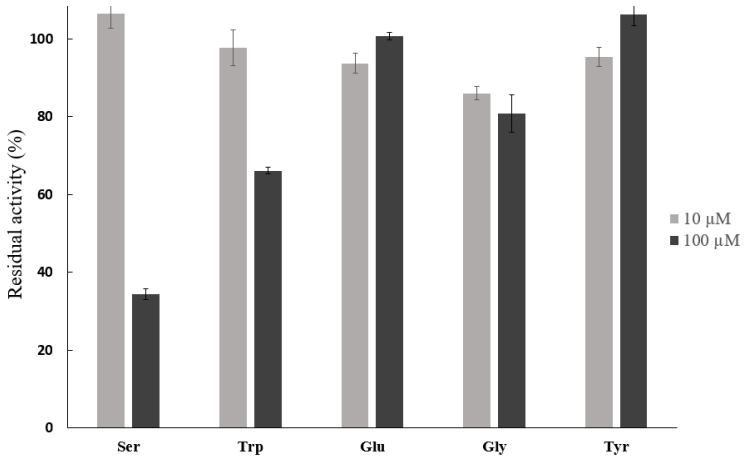

Figure 47 – Residual activity of SerB with 10 and 100 µM of selected amino acids.

Moreover, this experiment confirms that product inhibition occurs in the studied reaction. In order to quantify the SerB inhibition by L-serine, IC_{50} value is determined and the calculated value is 58.44 µM (Figure 48).

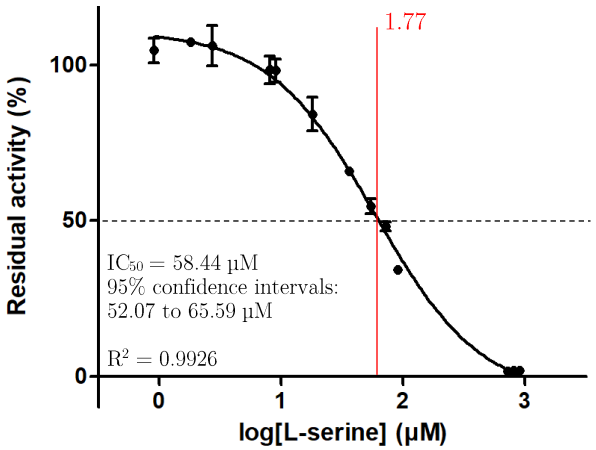

Figure 48 - Inhibition curves of SerB activity in presence of L-serine.

8.5 Comparison between SerB and SerB2

The kinetic study of SerB can be used to determine if SerB and SerB2 have a similar kinetic behavior. The Michaelis-Menten parameters of both enzymes are compared, without any inhibitors (values are determined by nonlinear regression). As shown in Figure 49, the enzymatic kinetics of SerB and SerB2 are very similar: Km and Vmax values are respectively close for both enzymes. It means that SerB and SerB2 have approximately the same affinity for the substrate and the same maximum rate when substrate is saturated in solution. Slight differences between the curves can be explained by imprecision on the enzyme concentration determination. Actually, an efficient purification procedure of SerB2 has not been determined yet. However, contaminant proteins do not possess phosphatase activity and enzymatic assays can be performed without significant effect of the contaminants.

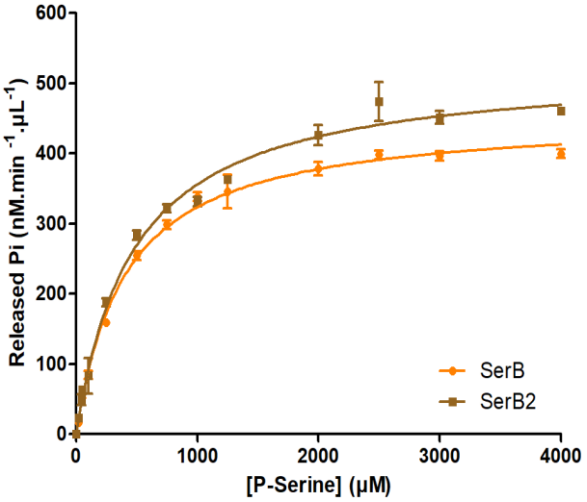

Table A (49) – Michaelis-Menten parameters of SerB and SerB2 in native conditions.

ε	Vmax ($nM.min^{-1}.\mu L^{-1}$)	Km (µM)	R^2
SerB	454.2±4.8	404±16	0.996
SerB2	524.5±8.8	473±29	0.991

Figure 49 – Michaelis-Menten kinetics for SerB (this research work) and SerB2[106].

The efficiency of harmine derivative inhibitors on both enzymes can be quickly evaluated through evaluation of inhibition percentage with inhibitor concentration at 10 and 100 µM, as shown in Figure 50. The inhibition percentage can be determined based on Equation 5, where A, A_{blank} and $A_{100\%}$ are respectively the absorbance of the solution containing inhibitor, of the blank and of the solution without any inhibitor. Generally, inhibitors possess similar inhibition potential on both enzymes. Percentage differences between SerB and SerB2 do not exceed 5%. In addition, these small variations of the inhibition percentages between the two experiments can be explained by imprecise measurements of the enzyme concentration. An exception is the inhibitor **88**. The latter seems good inhibitor against SerB2 but it is not very effective on SerB: at 10 µM, SerB activity remains almost totally conserved. This graph highlights the fact that SerB2 inhibitors also have a considerable effect against SerB, which illustrates the high level of homology between the enzymes.

$$Inhibition\ (\%) = 100 - Residual\ activity\ (\%) = 100 - 100\left(\frac{A - A_{blank}}{A_{100\%} - A_{blank}}\right) \quad (5)$$

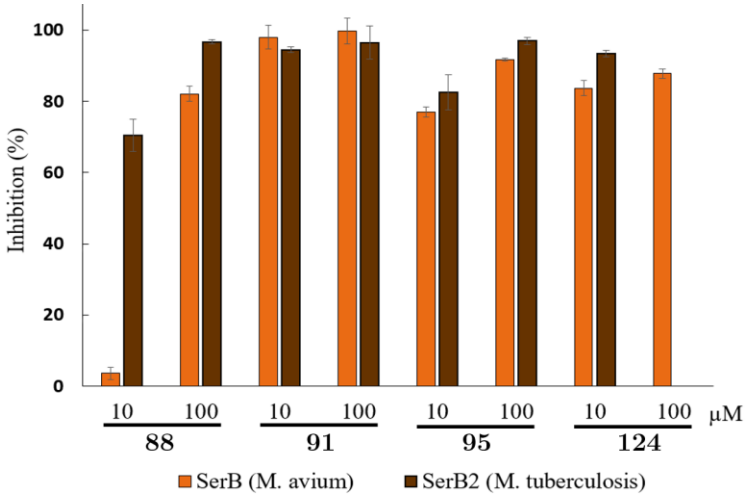

Figure 50 – Inhibition percentages of compounds **88**, **91**, **95** and **124** on SerB (this research work) and SerB2 activity[106], at 10 and 100 µM (100 µM of **124** on SerB2 not available).

Moreover, inhibition constant values can be used in order to compare inhibition on SerB and SerB2. The Table 2 includes $Ki_{\mathbf{88}}$ and $Ki_{\mathbf{91}}$ on both enzymes. Inhibitors seem more effective on SerB2, especially for inhibitor **88** which is the weaker inhibitor on SerB. In order to determine if this difference between both enzyme is really significant, Ki_{95} and Ki_{124} must be evaluated against SerB2.

As previously detailed, L-serine is the best inhibitor on both SerB and SerB2, among amino acids. The associated IC_{50} values are also listed in the Table 2. Values show that L-serine inhibits much more SerB2 than SerB. Among tested amino acids, L-tryptophan is the second best inhibitor on both enzymes. However, SerB inhibition is globally less effective than SerB2 inhibition by amino acids. Once again, further experiments need to be performed in order to confirm if the inhibition by amino acids is generally less effective on SerB compared to SerB2 inhibition.

Table 2 - Ki values of inhibitors **88** and **91** on SerB (this research work) and SerB2[106] and IC_{50} values of L-serine on SerB (this research work) and SerB2[89].

ε	$Ki_{\mathbf{88}}$	$Ki_{\mathbf{91}}$	L-serine IC_{50} (µM)
SerB	14.43	1.35	58.44
SerB2	1.75	0.18	0.78

8.6 Summary of the kinetic study

After determination of Michaelis-Menten parameters, kinetic study of SerB highlights the fact that harmine derivatives found as SerB2 inhibitors are also efficient on SerB with the following classification: **124** $\cong$ **91** > **95** >> **88**. This relative efficiency is not observed on SerB2 because on this enzyme, inhibitor **88** is more effective than **95**. Moreover, inhibitors seem scarcely more efficient on SerB2 but this observation needs to be confirmed by further experiments. In the same way, amino acids inhibit generally more SerB2 than SerB. However, the relative efficiency of amino acids seems respected: L-serine as best inhibitor and L-tryptophan as second best inhibitor, for both enzymes. Generally, inhibition mechanisms of harmine derivatives (reversible and competitive inhibitors) and of amino acids are very similar. Nevertheless, inhibition of SerB seems generally less effective than SerB2 inhibition.

9. Study of oligomerization states

G.P. Yadav et al.[89] performed further studies about the effect of L-serine on SerB2. Thanks to SEC and native poylyacrylamide gel (PAGE), they have shown that the dimeric population of SerB2 is shifted to a tetramer in the presence of ~0.8 molar ratio of L-serine (shown in Figure 51-A). Comparison between native enzyme and mutants (catalytic core without ACT domains) shows that L-serine interacts with ACT domains and leads to the formation of an higher order oligomeric form. This tetrameric form of SerB2 is totally inactive and mainly justify the inhibition effect of L-serine on SerB2.

As previously described (cf. point 7.3), SEC is not a relevant method in order to analyze SerB. The native PAGE is therefore used in order to compare oligomerization states of SerB and SerB2. This method is very similar to SDS-PAGE anaysis, except the fact that SDS is prevented and the protein conformation is therefore conserved. As shown in Figure 51-B, SerB is added on the gel after 10 minutes of incubation in solutions with various L-serine concentrations. When SerB is heated at 100°C in presence of SDS, only the monomeric form is observed. On the other hand, when the protein conformation is conserved, only the dimeric form is detected. Furthermore, the same analysis is performed after 1 hour and 2 days of incubation and an identical band pattern is observed in both cases (shown in Annexe II).

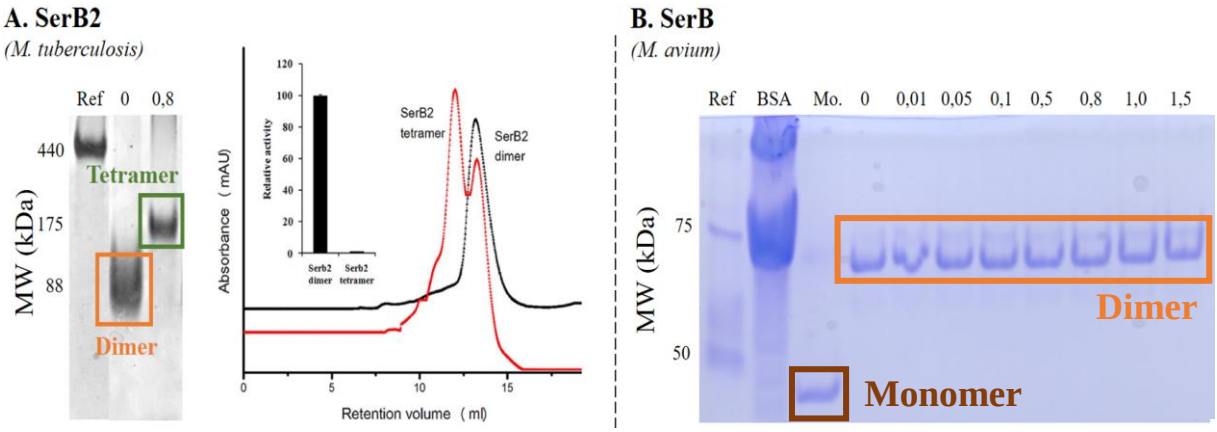

Figure 51 – Oligomerization states of SerB2[89] (A) and SerB (B). For SerB2 (A), Ref is Ferritin (MW = 440 kDa) and 0.8 indicates a molar ratio of L-serine. For SerB (B), native PAGE is obtained after 10 minutes of incubation, within solution of various L-serine concentrations (0 to 1.5 M). Ref is the molecular weight marker, BSA is used as second reference (MW = 66.5 kDa) and Mo. is the monomeric form of SerB (completely denatured: heated at 100°C and SDS added).

This experiment suggests that L-serine does not induce a modification of the SerB oligomerization states (with a molar ratio of L-serine >> 0.8) whereas the native dimeric form of SerB2 is completely modified into tetramer, in similar conditions. This observation can be justified by the fact that residues Gly^{20} and Gly^{110} in SerB2[13] (recognized as essential for amino acids-ACT domains binding) are not conserved in the

[13] Residues Gly^{20} and Gly^{110} are referred to Gly^{18} and Gly^{108} according to G.P. Yadav et al.[89].

primary sequence of SerB (Gly^{20} and Ala^{110} respectively). Hence, the side chain of the residue Gly^{110} included in the primary sequence of SerB2 could be essential in order to ensure interactions which induce a tetrameric form.

Because this tetramer is an inactive form of SerB2, this result should explain the dramatic difference of L-serine inhibition on SerB and SerB2. Indeed, SerB, which does not possess tetrameric form, is less inhibited by L-serine because all of the native dimeric form potentially has an enzymatic activity whereas all of the tetrameric form of SerB2 is completely inactivated.

10. Crystallographic study

A crystallographic study of SerB requires a concentrated, homogeneous and active sample, free of contaminants (protein that is at least 95% pure). To fulfill these conditions, a relevant protein purification procedure must be established beforehand. Then, SerB is crystallized by vapor diffusion sitting drop in optimized conditions. SerB crystals are harvested and stored in liquid nitrogen until X-ray crystallography analysis. A diffraction pattern is converted into electron density map. The latter is finally interpreted to get an atomic model of SerB with a good resolution.

10.1 Optimization of crystal growing experiments

In this research work, the crystallization of SerB is performed by sitting drop vapor diffusion crystallization. This method is based on a drop of concentrated protein in vapor equilibration with a liquid reservoir of reagents. The nature and the concentration of these reagents define a tested condition. Typically, the drop contains a lower (half) reagent concentration than the reservoir. To reach an equilibrium, water vapor leaves the drop. The protein is concentrated until precipitation and/or crystals formation.

The crystal growing experiments are firstly based on the condition established by SSGCID researchers[103]. This condition includes a polymer used as precipitant (20% polyethylene glycol (PEG 6000), a buffer that fixes a given pH (0.1 M 2-(N-morpholino)ethanesulfonic acid (MES) with a pH fixed at 6.0) and some additives which ensure protein conformation (0.2 M $MgCl_2$). Moreover, SSGCID researchers recommend a SerB concentration of 27.45 mg/mL. Crystal growth is performed in a 24-multiwell sitting drop crystallization plate and previously described condition is exploited ($MgCl_2$ is modified from 0.1 to 0.4 M and pH is varied from 6.0 to 6.5). Purified SerB sample is concentrated to reach ~25 mg/mL. As shown in Figure 52, SerB crystals are obtained after one night at room temperature, in the given condition. Moreover, in the range comprised between 6.0 and 6.5, pH does not influence the crystallization. On the other hand, optimal $MgCl_2$ concentration is observed for 0.3-0.4 M. Few SerB crystals appear in lower concentration but their size was significantly smaller, as shown in Figure 52-A.

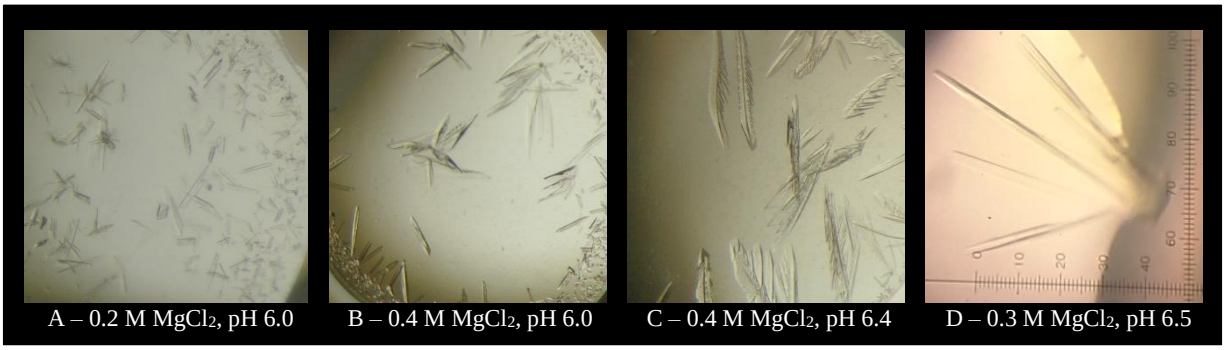

Figure 52 – Picture of SerB crystals obtained in various conditions (PEG 6000 and MES fixed at respectively 20% and 0.1 M), after one night at room temperature. Scale unit, visible on picture D, is in micrometer: obtained crystals have a size comprised between 50 and 100 µm.

Although SerB crystals are obtained, crystallization conditions are not optimal because of the twinning on the crystal growth mechanism. As a matter of fact, twinned crystals are not relevant for the purpose of X-ray crystallography: additional diffraction pattern(s) can be observed and the computational analysis becomes more difficult. In order to prevent crystals twinning, the growing rate need to be decreased. Two solutions are proposed in this research work: decrease the temperature or decrease the PEG 6000 concentration. Firstly, a crystal growing experiment is executed at 4°C. As shown in Figure 53, the general amount of crystals in each well is decreased but their size is globally bigger. The growing rate of crystal is dramatically decelerated: most SerB crystals appear after 48 hours at 4°C (cf. Figure 53-C/D). In addition, twinning of crystals is decreased but not totally avoided. Hence, temperature decreasing in order to prevent twinned crystals is not recommended.

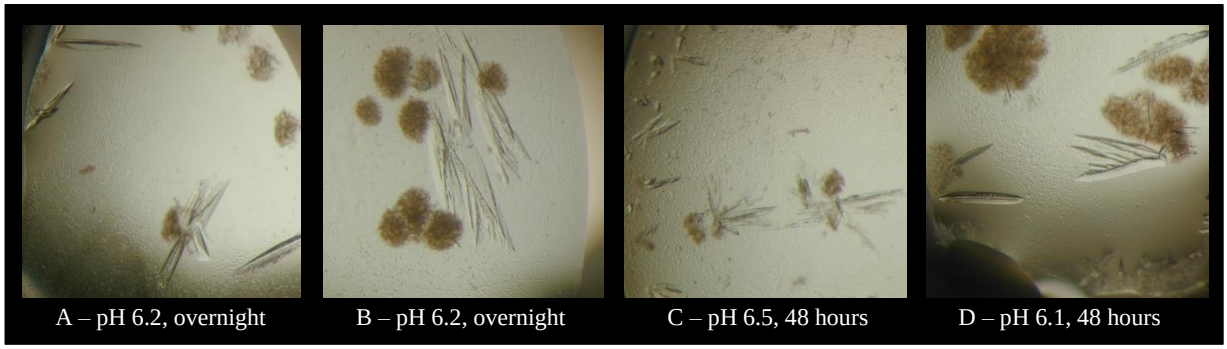

Figure 53 – Picture of SerB crystals obtained in fixed condition (20% PEG 6000, 0.1 M MES, 0.3 M $MgCl_2$), after one night or 48 hours at 4°C.

The second adopted way in order to decelerate crystal growing is to decrease PEG 6000 concentration in tested conditions. First test is performed with PEG concentration comprised between 14 and 20%. High PEG concentration (18-20%) leads to formation of numerous twinned crystals as shown in Figure 54-C/D. Although some wells with 16% PEG 6000 have shown big single crystals (cf. Figure 54-B), twinned crystals remain observed in lower PEG concentration, as illustrated in Figure 54-A.

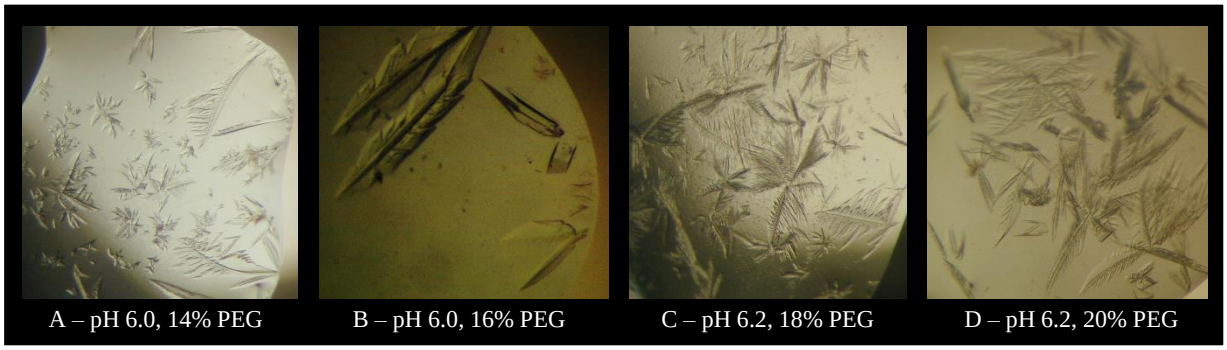

Figure 54 – Picture of SerB crystals obtained in various conditions (0.1 M MES, 0.3 M $MgCl_2$), after one night at room temperature.

A second test is executed with lower PEG 6000 concentration, ranging from 8 to 14%. At very low concentration (8-10%), only few conditions have led to crystals formation. However, the latter possess a massive structure, as shown in Figure 55-A. This second test has confirmed the fact that 14% PEG concentration does not prevent twinned crystals, as illustrated in Figure 55-D. The optimal concentration which allows single crystal growth with high reproducibility is 12% PEG 6000. This polymer concentration is therefore recommended in order to rationally reduce SerB crystals growth and obtain single crystals, relevant for harvesting and X-ray crystallography.

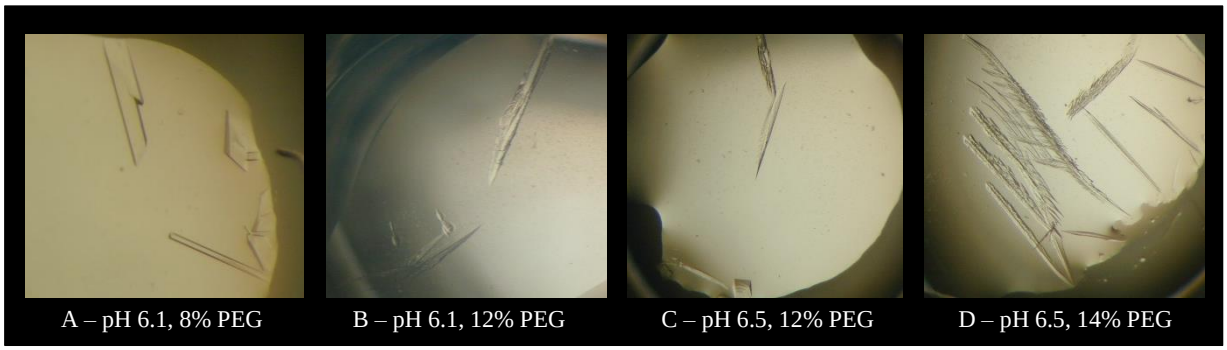

Figure 55 – Picture of SerB crystals obtained in various conditions (0.1 M MES, 0.3 M $MgCl_2$), after one night at room temperature.

10.2 Co-crystallization with amino acids

After determination of optimal SerB crystallization, co-crystallization assays are performed with the set of amino acids previously analyzed in the kinetic study: L-glycine, L-glutamic acid, L-tyrosine and L-tryptophan. For co-crystallization, the ligand (tested amino acids) is added to the protein directly during crystallization setup[126]. Hence, the amino acid concentration is fixed at 0.2 M in each condition and crystals are observed in the same way as native SerB crystallization. For each tested amino acid, one crystal is harvested for the purpose of X-ray crystallography.

10.3 Soaking with harmine derivatives

Ligand co-crystallization typically requires more resources compared to soaking[127]. Because harmine derivatives **88**, **91**, **95** and **124** are a limited resource (compared to commercially available amino acids), this last method is employed in order to get crystals of SerB complexed with inhibitor. However, soaking requires some conditions:

- The first need is a soakable crystal form, namely a crystal form with an accessible ligand-binding site. In fact, the SSGCID has successfully performed an iodide ion soaking on SerB crystals[103], which highlights the fact that this first requirement is satisfied: soaking (with small ligands) can be therefore executed on SerB crystals.
- A second requirement is a reasonable ligand (inhibitors **88**, **91**, **95** or **124**) solubility in order to maximize the probability of encounter between ligand and enzyme. Because studied inhibitors are solubilized in DMSO, the effect of this solvent on SerB crystals needs to be studied. Crystallization assays in optimized conditions is

performed, with an increasing DMSO concentration (from 5 to 20%). As shown in Figure 56-A, SerB crystals appears until 15% DMSO concentration. Hence, SerB crystals are not too sensitive to the presence of this solvent.

After formation of SerB crystals in certain conditions, some of them are selected and 0.100 µL of harmine derivatives 100 mM solvated in DMSO are added in the crystallization drop, as shown in Figure 56-B. The cover slide is repositioned after this addition. The high DMSO concentration does not immediately dissolve SerB crystals, as illustrated in Figure 56-C. However, the soaking was performed one week before X-ray analysis and many soaked crystals disappeared during this period. Hence, proposed soaking conditions are not effective. Two protocols should resolve this issue: either directly add solid powder of inhibitor in the crystallization drop (DMSO is avoided but low solubility limits inhibitor diffusion) or perform soaking few hours before X-ray analysis (DMSO used but short incubation time limits inhibitor diffusion).

Figure 56 – Picture of SerB crystals obtained in optimized condition (12% PEG 6000, 0.1 M MES, 0.3 $MgCl_2$), after one night at room temperature (A). Picture of the soaking procedure, before and after injection of inhibitor (**88**, **91**, **95** or **124**) solubilized in DMSO, within the crystallization drop (B-C).

10.4 Structural analysis

After crystal growing and equilibrium of vapor pressures between the crystallization drop and the reserve, SerB crystals are obtained. The latter is a solid material defined by a periodic and infinite repetition of a crystal lattice in all directions. When an energetic X-ray beam is projected on the crystal, incident beam is scattered according to some preferential directions: a diffraction pattern is observed. This phenomenon, schematized in Figure 57, is called X-ray diffraction. The diffraction pattern is arranged as highly ordered spots. This is governed by the geometry (size and shape) of the crystal unit cell and the X-ray wavelength (synchrotron beam has been fixed at a wavelength of 0.97857 Å). Each spot is defined by a position and an intensity[127]:

- The positions of the spots are directly defined by the reciprocal lattice, based on the locations of all atoms in the cell (namely the crystal lattice). Macromolecules like proteins have a very large unit cell with sparse atoms. The reciprocal lattice is very dense and numerous spots, which are close from each other, are observed as diffraction pattern. Hence, the latter allows to determine the primitive cell of the crystal.

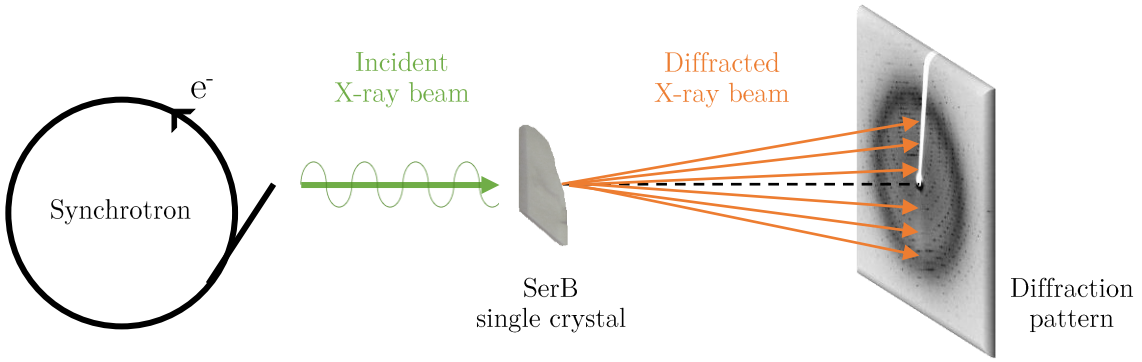

Figure 57 – X-ray diffraction of a single crystal of SerB (Sc-XRD).

- The observed intensity of the spots is influenced by the position and the nature of each atom within the unit cell. Rigorously, the experimental intensity is mathematically linked with the structure factor (aka. $\overrightarrow{F_{hkl}}$ value), which represents the reflection amplitudes and phases. Although the phases cannot be experimentally determined, several methods are used in protein crystallography in order to determine the phases and solve this issue.

Finally, the diffraction pattern can be computationally interpreted. Typically, the Fourier transform of the structure factor leads to an initial approximate electronic density distribution in the crystal. This electron density map is then chemically interpreted in terms of atoms and molecules. Finally, the atomic model is refined: cartesian coordinates and *B*-factor of each atom are optimized in order to achieve the best agreement between the observed reflection amplitude (F_{obs}) and those calculated from the model (F_{calc}). The crystallographic *R*-factor allows to quantify and evaluate this refinement process. All information about experimental crystallographic structures are detailed in Annexe III.

In practice, some SerB crystals are harvested and stored in liquid nitrogen for the purpose of X-ray diffraction. Thanks to this analysis, native structure of SerB was obtained with a good resolution (2.07 Å). Unfortunately, none of the analyzed crystals possess an harmine derivative within the active site. The soaking method needs to be improved as previously described (cf. point 10.3). Nevertheless, a co-crystal of SerB with L-tyrosine was obtained with a relatively good resolution (2.50 Å). Indeed, additional electron densities are shown near the ACT1 domain and within the active site. After refinement process, it appears that L-tyrosine interacts with the ACT domain, known to bind amino acids. Within the active site, electron density seems to be associated with two conformations of MES (with a fitting ratio of 50/50). The experimental structure of SerB complexed with L-tyrosine and MES is illustrated in Figure 58.

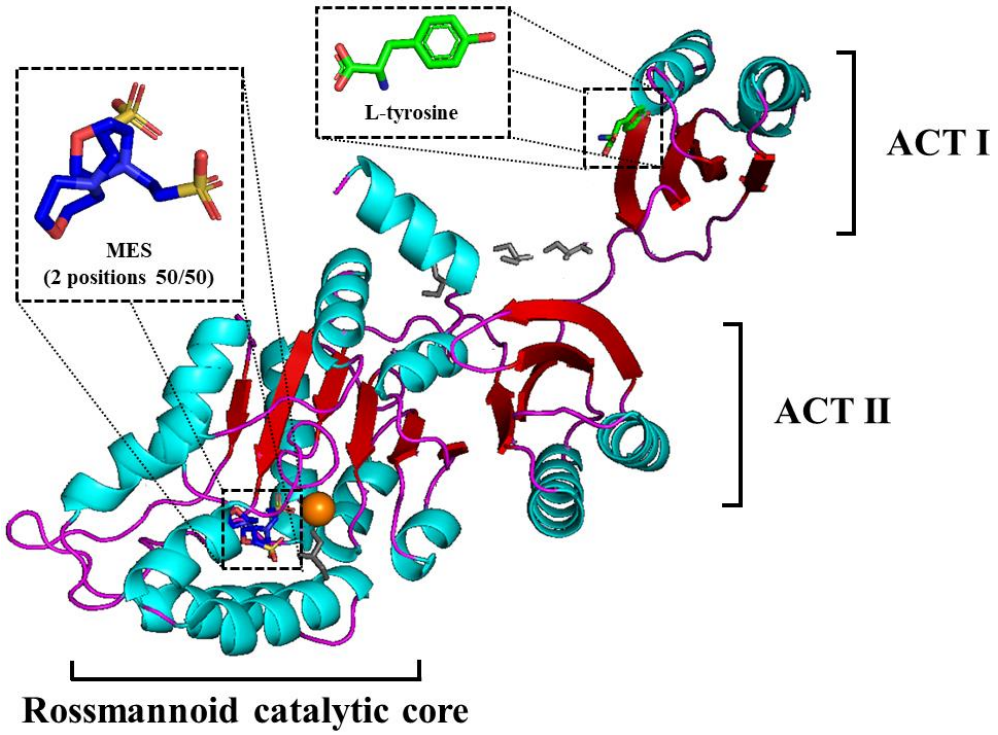

Figure 58 – Structure of SerB co-crystallized with L-tyrosine within the ACT I domain and MES (with two visible positions) within the active site. L-tyrosine is colored in green, MES in dark blue, glycerol in grey and the cation Mg^{2+} in orange.

10.4.1 MES within the active site

After interpretation of the experimental electronic density, it appears that MES, which is the buffer used in crystallographic study, is able to interact favorably within the active site of SerB. In order to optimally fit the observed electron density, two positions are proposed. These conformations are mainly differentiated by the localization of the sulfate group. The first observed position A consist of MES oriented like the substrate (*O*-phospho-L-serine) within the active site: as shown in Figure 59, the sulfate group of MES interacts like the phosphate group of the substrate (cf. Figure 18):

- The oxygen O1(A) forms charge assisted H bonds with the residues Lys^{320} (3.2 Å), which belongs to the motif III, and Asn^{346} which belongs to the motif IV (2.1 Å).
- The second oxygen O2(A) interacts (H-bonds) with three water molecules (2.5, 2.6 and 3.7 Å). This oxygen is located near the cation Mg^{2+} (~3.9 Å) but does not directly interact with the latter. On the other hand, phosphate group directly interacts with the divalent cation in order to achieve the formation of the covalent acyl-phosphate intermediate, with the nucleophile Asp^{187} residue (motif I).
- The last oxygen O3(A) forms H bonds with the residues Lys^{320} (2.4 Å), one water molecule (2.4 Å) and the protonated Ser^{275} (3.5 Å), which belongs to the motif II.

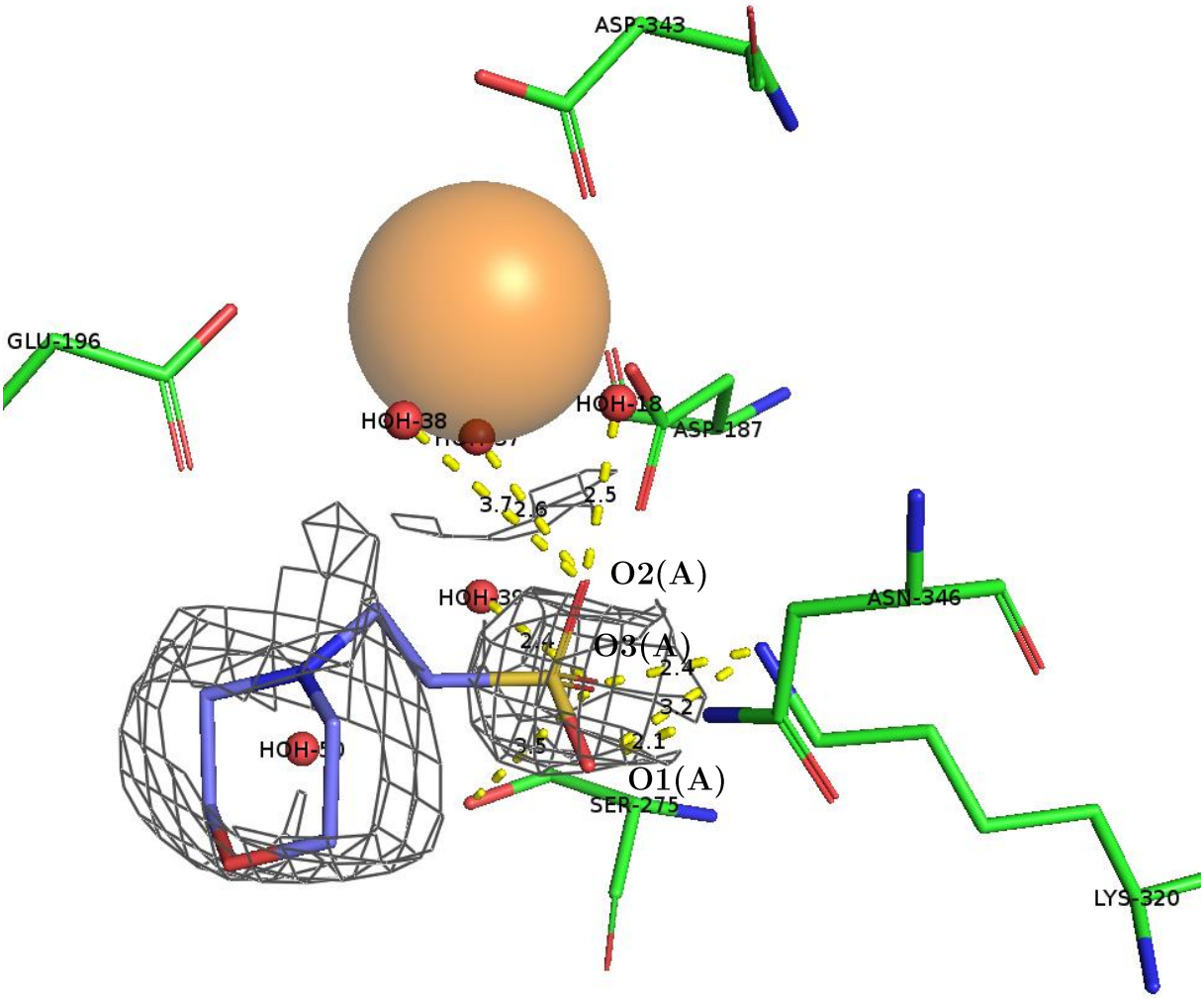

Figure 59 – Position A of the MES within the active site of SerB. Molecular structure (C in green, N in blue, O in red and S in yellow) and experimental electronic densities around ligand (at 0.5 σ in grey) are illustrated. The MES molecule is shown in blue. The sulfate group interacts with some residues through H bonds and/or ionic interactions, highlighted by dashed yellow lines and indicated distances are measured in Angström (Å). Water molecules are schematized by little pink spheres and the divalent cation Mg^{2+} by an orange sphere. The nucleophilic residue Asp^{187} belongs to the motif I, Ser^{275} to the motif II, Lys^{320} to the motif III and the residue Asn^{346} to the motif IV.

With the second position B shown in Figure 60, the MES sulfate group interacts with the residue Arg^{232} (2.0 Å and 2.4 Å) through two oxygen atoms (O1(B) and O2(B) respectively) and one water molecule (2.9 Å) with the last oxygen O3(B). In addition, the oxygen within the MES heterocycle is able to form H bonds with one water molecule (2.7 Å) and the peptide amine group of the residues Val^{197} and Ile^{198} (3.3 and 3.2 Å).

Positions A and B of MES are observed in a 50/50 ratio: one position is not especially favored compared with the other. Indeed, the position A allows several interactions only with the sulfate group whereas the position B allows few interactions with the sulfate group but also few interactions with the MES heterocycle. Globally, the MES molecule is stabilized as well with the position A as the position B.

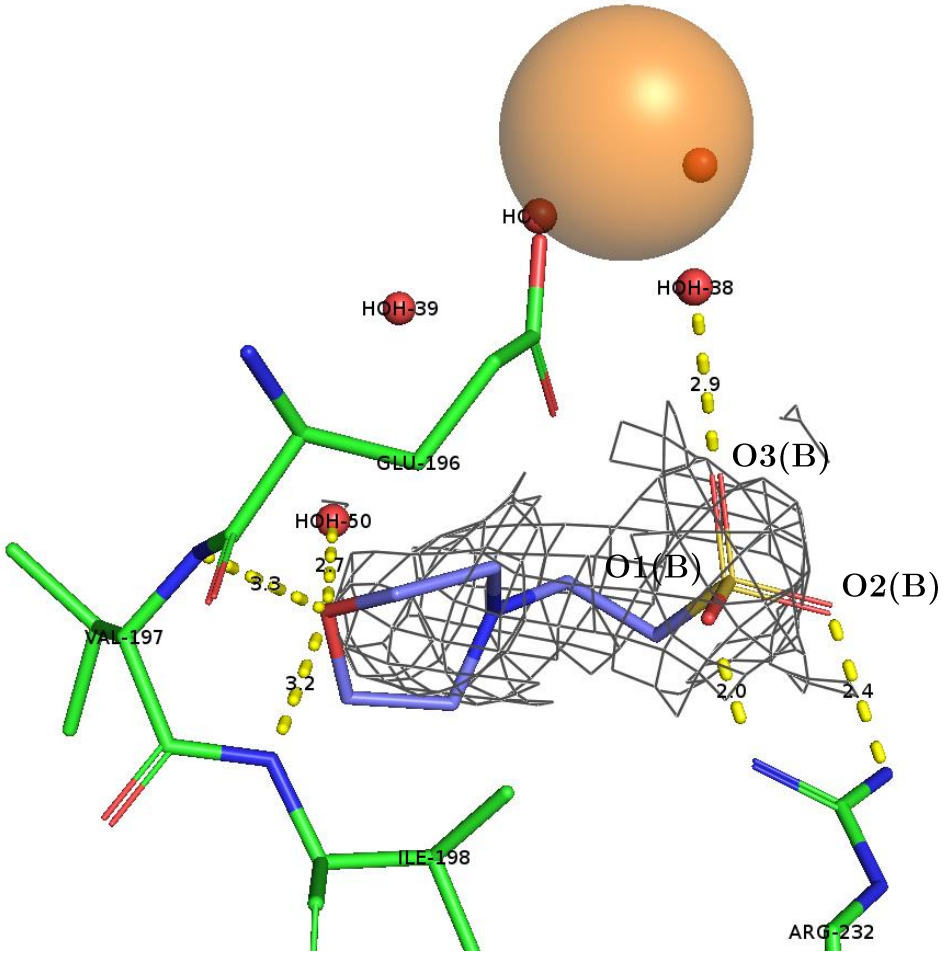

Figure 60 – Position B of the MES within the active site of SerB. Molecular structure (C in green, N in blue, O in red and S in yellow) and experimental electronic densities around ligand (at 0.5 σ in grey) are illustrated. The MES molecule is shown in blue. The sulfate group interacts with some residues through H bonds and/or ionic interactions, highlighted by dashed yellow lines and indicated distances are measured in Angström (Å). Water molecules are schematized by little pink spheres and the divalent cation Mg^{2+} by an orange sphere.

10.4.2 L-tyrosine interacts with ACT I domain

As a matter of fact, the ACT domain is commonly involved in the binding of small regulatory molecules, like amino acids. In this case, experimental electronic density shows that L-tyrosine interacts with the ACT I domain of SerB. As shown in Figure 61-A, the phenol group of the amino acid forms H bonds with peptide nitrogen of residues Gly^{20} (3.5 Å), Val^{21} (3.4 Å), Thr^{22} (3.1 Å) and Ala^{23} (3.6 Å). Only the last residue is not conserved in SerB2 (Ser^{23}). The ammonium group of the amino acid interacts with the residue Asp^{17} (2.3 and 3.7 Å). Moreover, some water molecules allow to further stabilize L-tyrosine through additional H-bonds.

In order to assess this interpretation, the experimental structure of SerB complexed with L-tyrosine can be compared with the structure of SerB in complex with L-serine at ACT domain, obtained by S. Shree and R. Ramachandran (PDB: 5JLP, to be published). The Figure 61 highlights the fact that the two amino acids interact within the same regulatory site of SerB (residues comprised between Asp^{17} and Ala^{23}), thanks to similar

interactions with identical residues. Hence, the latter could be essential in order to design new inhibitors based on the impediment to ACT domains regulatory effects. However, L-serine and L-tyrosine present opposite effect on enzymatic kinetics: L-tyrosine activates whereas L-serine is the best inhibitor (cf. point 8.4.2). A hypothesis to justify their opposite effect could be based on the fact that interactions with L-tyrosine are generally stronger (namely smaller intermolecular distances) than interactions with L-serine because of variation of their side chain lengths. Therefore, these two amino acids could impact differently the regulatory domain of SerB.

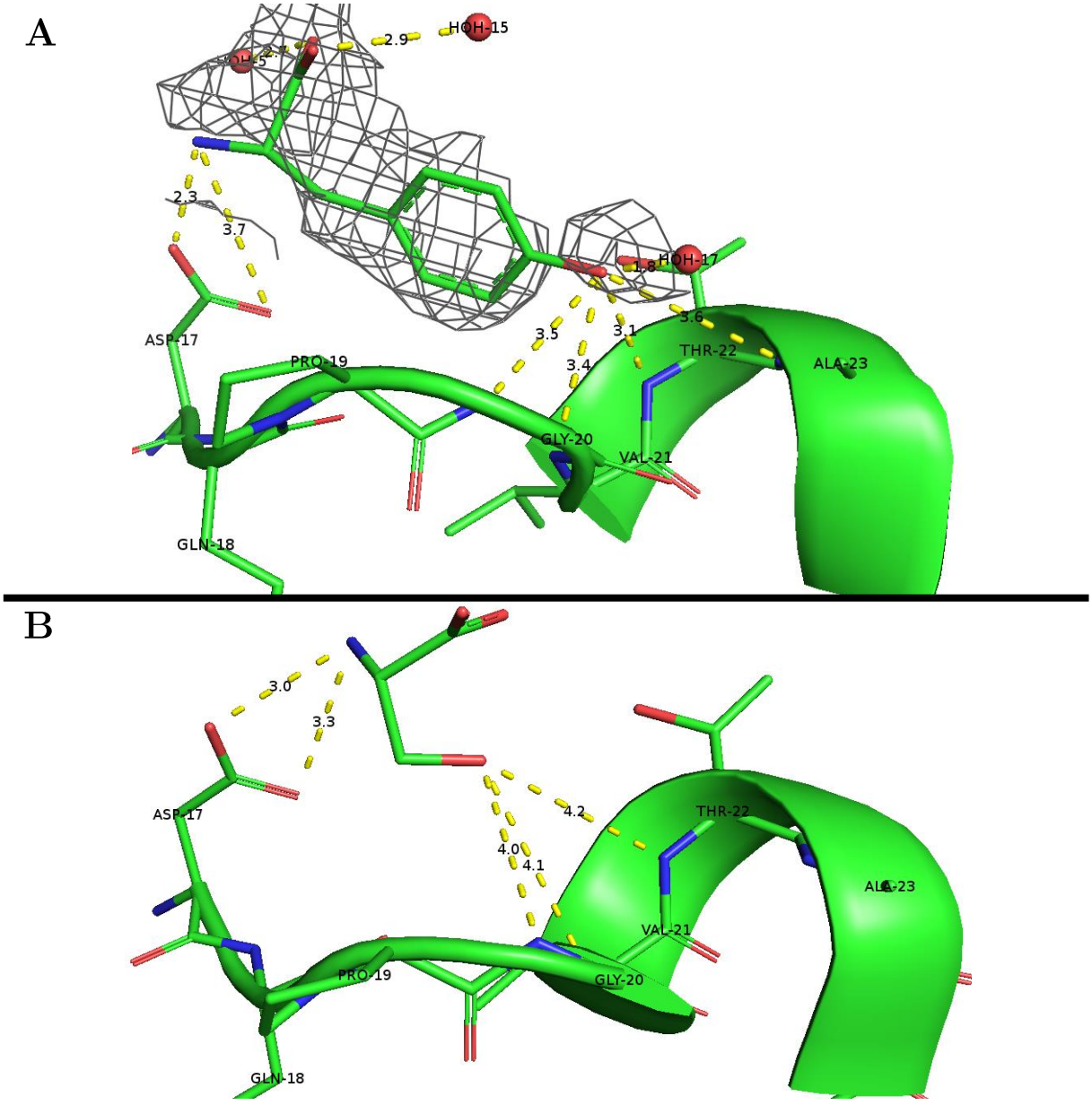

Figure 61 – Interaction between L-tyrosine (A, this research work) or L-serine (B, PDB: 5JLP not published) and the ACT I domain of SerB. Molecular structure (C in green, N in blue and O in red) and experimental electronic densities around ligand (at 1.0 σ in grey) are illustrated. The L-tyrosine and L-serine molecules are shown with the same orientation within the ACT I domain. Amino acids interact with some residues through H bonds, highlighted by dashed yellow lines and indicated distances are measured in Angström (Å).

10.5 Phosphate assay: MES as new inhibitor against SerB?

The presence of MES within the active site is associated with some favorable interactions, as previously detailed. Hence, MES should be a potential good competitive inhibitor on SerB. In order to assess this hypothesis, an additional phosphate assay is performed in order to analyze the evolution of the residual activity depending on the MES concentration. As shown in Figure 62, MES leads to SerB inhibition at high concentration (with an estimated $IC_{50} > 10$ mM). It indicates that SerB interacts much more specifically with its substrate than with MES: at low concentration (10-100 µM), MES impacts scarcely the SerB activity. Nevertheless, with a high MES concentration (10 mM), inhibition becomes significant and residual activity decreases.

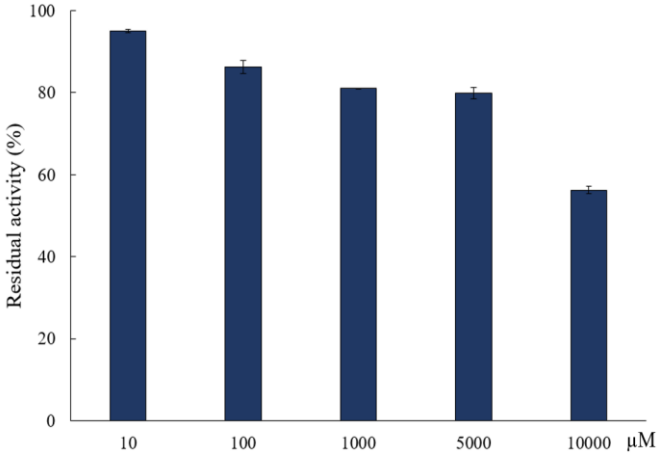

Figure 62 – Residual activity of SerB with an increasing MES concentration.

10.6 Summary of the structural study

Optimal crystallization condition of SSGCID researchers is tested and SerB crystals are obtained. However, this research work shows that SerB crystal morphology can be improved (namely, avoid twinned crystals) with the following condition: 12% PEG 6000, 0.1 MES, 0.3 $MgCl_2$ and a pH included in a range between 6.0 and 6.5. Thanks to this optimal condition, co-crystallization with some amino-acids is successfully performed and crystallographic structures of SerB are obtained. No crystallographic structure of SerB complexed with harmine derivatives (compounds **88**, **91**, **95** or **124**) was obtained because an effective soaking procedure needs to be found (some relevant protocols have been proposed but they are not executed in this research work).

The crystallographic structure of a co-crystal shows that L-tyrosine interacts with ACT I domain of SerB. The L-tyrosine interacts with SerB exactly at the same site than L-serine, with a residue Asp especially important for optimal interactions. This site can be recognized as regulatory site of SerB, with a high affinity for amino acids. In the catalytic site, MES molecule is observed, with two distinct conformations (observed with a 50/50 ratio). The first position maximizes interactions of the sulfate group and is mainly similar to the position of the substrate within the enzyme: sulfate group of the

MES interacts with numerous highly conserved amino acids among HAD superfamily enzymes. The second position of MES is based on few interactions that implicate the sulfate group and also the MES heterocycle. This result indicates that MES should be a potential competitive inhibitor of SerB. However, additional phosphate assay has shown that MES only inhibits SerB at very high concentration (> 10 mM).

Conclusion and outlooks

Conclusion and outlooks

The two main goals of this research work were to improve the general scientific knowledge about the *M. avium* phosphoserine phosphatase (SerB) and to compare this enzyme with one of its closest counterpart: *M. tuberculosis* phosphoserine phosphatase (SerB2). As matter of fact, the latter is essential for the survival of *M. tuberculosis*, the pathogen responsible for tuberculosis, which is a global health issue. This comparison between SerB and SerB2 is performed through studies of enzymatic kinetics and oligomerization states. Finally, the result of this comparison allows to determine if the crystallographic study of SerB can be transposed as structural information about SerB2, in a relevant way. Indeed, the crystallographic structure of SerB2 remains unknown because this enzyme has never been crystallized to date.

11. New information about SerB

This research work started with the plasmid coding for SerB, obtained from SSGCID. After bacterial transformation, optimal overexpression and induction conditions have been determined. Best conditions have been found for an optical density at 600 nm comprised between 0.6 and 1.0 before induction, an IPTG concentration fixed at 0.5 mM and an incubation after induction during 3 hours at 37°C.

The second step before SerB study was the establishment of an effective purification protocol. Two steps have been recommended for the purpose of an effective purification. A first IMAC was performed with a purification buffer A (50 mM Tris-HCl, 300 mM NaCl, 20 mM imidazole, pH 7.4), a purification buffer B_1 (50 mM Tris-HCl, 300 mM NaCl, 200 mM imidazole, pH 7.4) and an elution program for which buffer B_1 is progressively added from 0 to 100% during 50 minutes and kept constant at 100% during 10 minutes. Fractions have been selected and pooled. The cleavage of the His_6-Tag was executed simultaneously with a dialysis in a reaction buffer. The sample was then collected for the purpose of a second IMAC with the same purification buffer A and a purification buffer B_2 (50 mM Tris-HCl, 300 mM NaCl, 500 mM imidazole, pH 7.4), directly added (100%) during 10 minutes. After this step, purified SerB was collected. A SEC as last purification step could be performed but this last step dramatically reduced the total amount of SerB. For one liter of bacterial culture, ~20 mg of protein were collected after the first purification step (IMAC), ~16 mg after the second step (second IMAC and dialysis) and only 9 mg after the last optional step (SEC).

After effective purification protocol, SerB was collected as a pure protein solution which could be used for the purpose of further characterizations. In this research work, the study of SerB was based on three distinct ways:

- The kinetic study firstly allowed to determine the Michaelis-Menten parameters of SerB in native conditions: Km was evaluated as 404.1 (± 16.6) µM and Vmax was determined as 55 993 (± 596) $nM.min^{-1}.\mu g^{-1}$. Then, four harmine derivatives, which had been identified as good SerB2 inhibitors, were tested on SerB. They also possess an inhibition effect. The IC_{50} values were determined and harmine derivatives were classified: **124** (best tested inhibitor with IC_{50} = 1.95 µM) > **91** (IC_{50} = 2.67 µM) > **95** (IC_{50} = 4.75 µM) >> **88** (less active tested inhibitor with IC_{50} = 61.81 µM). Moreover, evolution of the Michaelis-Menten kinetics depending on the inhibitor concentration showed that harmine derivatives act as reversible and competitive inhibitors. Finally, the effect of selected amino acids on SerB kinetics was studied. L-serine and L-tryptophan appeared to be respectively the best (IC_{50} = 58.44 µM) and the second best inhibitor. Other tested amino acids (L-glycine, L-glutamic acid and L-tyrosine) did not impact significantly the SerB activity.
- The study of oligomerization states was executed through native polyacrylamide gel. The results have shown that SerB possesses a native dimeric form, and the latter was conserved even in presence of L-serine in high concentration (until 1.5 M). At first glance, SerB did not possess an inactive tetrameric form with L-serine.
- The crystallographic study started with an optimization of the crystal growing conditions. Optimal conditions were found in order to quickly obtain single crystals (twinned crystals are prevented). These conditions were defined as 12% PEG 6000, 0.1 MES, 0.3 $MgCl_2$, a pH included in a range between 6.0 and 6.5 and a protein concentration fixed at ~25 mg/mL. Thanks to these conditions, SerB was co-crystallized with some amino acids and soaking assays with harmine derivatives were performed. The soaking protocol used in this research work needs to be improved because an exceedingly high concentration of DMSO led to SerB crystals dissolution. Moreover, none of harvested crystals possessed one of the harmine derivatives within the active site. Nevertheless, an experimental crystallographic structure was obtained and SerB was co-crystallized with two compounds: MES within the active site (in two distinct positions) and L-tyrosine near the ACT I domain. In addition, MES appears to mainly interact with the active site like the substrate (*O*-phospho-L-serine), through H bonds with highly conserved residues among HAD superfamily enzymes. The L-tyrosine molecule interacts in the periphery of the ACT I domain, with the same (even more) residues than L-serine, as observed in the crystallographic structure of SerB, proposed by S. Shree and R. Ramachandran (PDB: 5JLP, to be published). This result has shown that this spot in the ACT I domain could be the regulatory site of SerB, which possesses a high affinity for amino acids. An additional kinetic study was performed in order to evaluate the inhibition effect of MES on SerB but the activity was decreased only for high MES concentration (> 10 mM).

12. Comparison between SerB and SerB2

A rigorous comparison between SerB and SerB2 can be executed based on the first two ways of SerB study, as previously detailed. Both enzymes are analyzed depending on the effect of harmine derivatives and amino acids on their activity and depending on their oligomerization states. Results obtained for SerB in this research work are used and compared to SerB2 characterization (E. Pierson[106] and G.P. Yadav[89]).

At first glance, both enzymes have a similar enzymatic kinetics with close Michaelis-Menten parameters: Km_{SerB} = 404±16 µM, Km_{SerB2} = 473±29 µM, $Vmax_{SerB}$ = 454.2±4.8 $nM.min^{-1}.\mu L^{-1}$ and $Vmax_{SerB2}$ = 524.5±8.8 $nM.min^{-1}.\mu L^{-1}$. Nevertheless, inhibition effect of harmine derivatives or amino acids seems generally more efficient on SerB2. This hypothesis can be confirmed through comparison of inhibition constants for some harmine derivatives: $Ki_{\mathbf{88}/SerB}$ = 14.43 > $Ki_{\mathbf{88}/SerB2}$ = 1.75 and $Ki_{\mathbf{91}/SerB}$ = 1.35 > $Ki_{\mathbf{91}/SerB2}$ = 0.78. The IC_{50} values of L-serine on both enzymes can also be used: $IC_{50/SerB}$ = 58.44 µM > $IC_{50/SerB2}$ = 0.78 µM. Despite this difference of inhibitors' efficiency, the relative classification of inhibitors is very similar for both enzymes: L-serine and L-tryptophan are the best inhibitors among amino acids, and harmine derivatives are classified as **124** ≅ **91** > **95**. Nevertheless, compound **88** inhibits very differently both enzymes: it is the worst tested inhibitor on SerB but it is more efficient than **95** on SerB2. All kinetic parameters are summarized in the Table 3. Concerning oligomerization states, both enzymes act very differently. The active and native form of SerB and SerB2 is a homodimer. However, SerB2 is able to adopt an inactive tetrameric form in presence of L-serine. This tetramer is not observed for SerB in our experiments.

Table 3– Summary of Ki and IC_{50} values for SerB (this research work) and SerB2[89,106]. The symbol * indicates that the value is not accurate.

ε	Param. (µM)	88	91	95	124	L-serine
SerB	Ki	14.43	1.35	11.38*	3.57	-
	IC_{50}	61.81	2.67	4.75	1.95	58.44
SerB2	Ki	1.75	0.78	-	-	-
	IC_{50}	6.0	2.5	12.2	-	0.78

Although SerB and SerB2 are very close counterparts (83.7% of identity[14]) and seem identical concerning enzymatic kinetics (without any inhibitor) and oligomerization states (native dimeric form), both enzymes seem barely different. As a matter of fact, slight variations in the nature of some residues near the active site could explain difference of affinity and therefore difference of inhibition percentages. However, further crystallographic study of SerB could be precious information about SerB2 inhibition for

[14] The value is calculated with EMBOSS Needle (BLOSUM62): https://www.ebi.ac.uk/Tools/psa/emboss_needle/

most inhibitors. Some exceptions, like the compound **88**, need to be carefully interpreted because of big significant differences of affinity between both enzymes. In fact, the good inhibition effect of **88** on SerB2 could be based on a specific residue that is not included in the primary sequence of SerB. Hence, a rigorous comparison of the effect of a given inhibitor on the enzymatic kinetics of SerB and SerB2 should be executed before exploitation of a crystallographic study of complexed SerB as new information about SerB2 inhibition. Nevertheless, this research work has highlighted the potential regulatory domain of SerB and SerB2 which includes conserved residues (Asp[17] until Ala[23]), as shown in Figure 63.

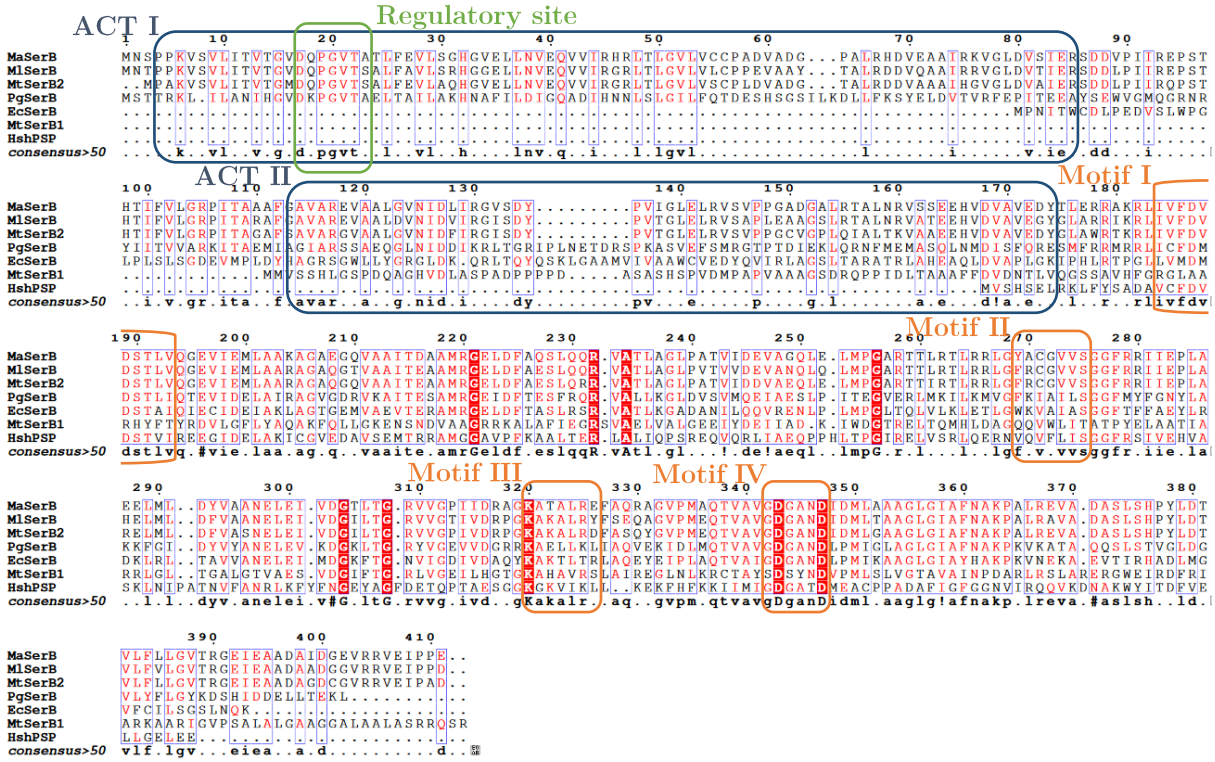

Figure 63 – Sequence alignment[15] for the PSP of *M. avium*, *M. leprae*, *M.tb* (SerB2), *P. gingivalis*, *E. coli*, *M.tb* (SerB1) and *H. sapiens* (human PSP). The high conserved domains I, II, III and IV are highlighted in orange frames whereas the additional ACT domains are highlighted in blue frames. The regulatory site described in this research work is shown in green frame.

[15] Sequence alignment is performed with MultAlin[139]: http://multalin.toulouse.inra.fr/multalin/

13. Outlooks

SerB is poorly described in the scientific literature and numerous further characterization experiments should be executed, especially kinetic analysis with other kinds of inhibitor and other amino acids (with a larger range of tested concentrations for each amino acid). In addition to native polyacrylamide gel analysis, the nonexistence of the tetrameric form of SerB should be confirmed by small-angle X-ray scattering (SAXS) or dynamic light scattering (DLS) analysis. In order to assess if the side chain of Gly^{110} (found in the SerB2 sequence) is essential for the formation of a tetrameric form, native PAGE analysis could be performed on a mutant of SerB that includes Gly^{110} instead of Ala^{110}. In addition, the soaking protocol needs to be improved in order to obtain crystallographic structure of SerB co-crystallized with a harmine derivative or other kinds of inhibitors.

In order to rigorously compare SerB and SerB2 for a given inhibitor, the affinity between enzyme and inhibitor could be studied by isothermal titration calorimetry (ITC). Furthermore, comparison of the results should be additional information to confirm analysis only based on the comparison of Ki or IC_{50} values.

After identification of an efficient inhibitor on SerB2 and the study of its interactions within the active site through crystallographic analysis of SerB, numerous experiments need to be performed for the purpose of the elaboration of a new efficient drug against *M. tuberculosis*. As a matter of fact, finding a new therapeutic target and associated curative agent is the beginning of the wide challenge of drug design: therapeutic agent should be able to cross the highly impermeable cell wall of *M.tb*, should not lose its effect in the metabolism and should not be easily ejected out of mycobacteria. Thereafter, various pre-clinical and clinical experiments should be performed, before potential marketing authorization. Actually, a further description of interactions between harmine derivatives and SerB could be important for a better understanding of SerB2 inhibition, which is an essential threshold in the wide process of new drug design.

Materials and methods

Materials and methods

14. SerB overexpression

A precise protocol of SerB overexpression has never been detailed in the literature. Hence, the following manipulations are initially based on a standard protein overexpression protocol that is subsequently improved and adapted for SerB.

14.1 Bacterial transformation

In order to execute the bacterial transformation, thermoporation is employed. All of following manipulations are executed under a Bunsen burner, in sterile conditions. Firstly, plasmids and thermocompetent *E. coli* BL21 bacteria are incubated together on ice during 30 minutes. The mixture is then placed in a thermostatic bath at 42°C during 2 minutes. Meanwhile, Lysogenic broth (LB) is prepared with LB agar and ampicillin (1 mM). Subsequently, 1 mL of LB is added in the sample and the latter is incubated at 37°C during 40 minutes. Thereafter, 100 µL of the sample is scattered thanks to a few glass beads on the first Petri dish, which contain LB. The rest of the sample is concentrated through centrifugation (4000 rpm for 5 minutes) and also scattered on a second Petri dish with LB. Petri dishes are finally closed and incubated overnight at 37°C. As shown in Figure 64, several colonies of transformed *E. coli* BL21 appeared. The latter can be conserved at 4°C a few days, for the purpose of the elaboration of an aliquots reserve of transformed bacteria.

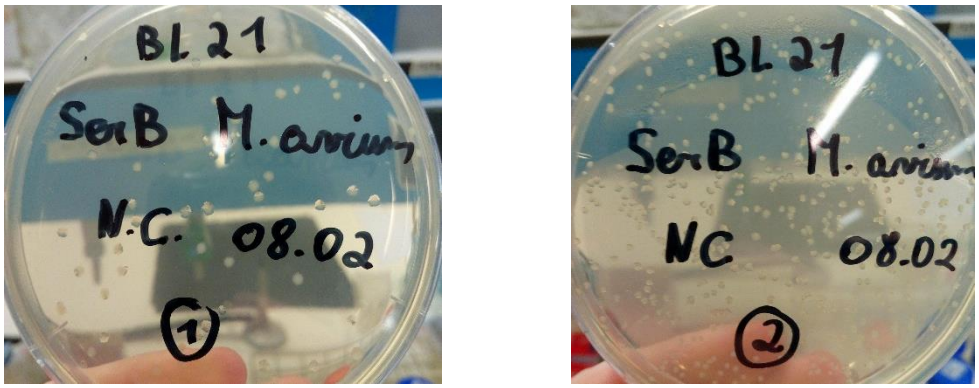

Figure 64 – Colonies of transformed *E. coli* BL21 (incubation overnight at 37°C).

14.2 Aliquots reserve of transformed bacteria

Colonies of transformed *E. coli* BL21 are exploited in order to elaborate an aliquots reserve easily storable at -80°C. As previously, the following manipulations are executed in sterile conditions. Firstly, 3 or 4 colonies of the first Petri dish are scraped and suspended in 10 mL of liquid LB with ampicillin (1 mM). The sample is then stirred overnight at 37°C. The manipulation is reiterated for the second Petri dish. Finally, several fractions are stored at -80°C, in glycerol 20%.

14.3 Bacterial growth

After the elaboration of an aliquots reserve, numerous bacterial cultures can be matured. The first step is the preparation of a primary culture under sterile conditions. A fraction of transformed bacteria is added with a volume ratio of 1/50 in liquid LB with ampicillin (final concentration of 1 mM). The sample is stirred overnight at 37°C, in a suitable container at least three times larger than the sample volume (a third of sample for two-thirds of air). The second step is the preparation of a bacterial culture from the primary culture. Under sterile conditions, the latter is added with a volume ratio of 1/20 in liquid LB with ampicillin (final concentration of 1 mM). The sample is then stirred at 37°C in a suitable striped container (see above), until the optical density at 600 nm (OD_{600nm}) is comprised between 6.0 and 1.0.

14.4 Induction

When the OD_{600nm} of the medium reaches a suitable value, the expression of SerB is induced through the addition of a given volume of isopropyl β-D-1-thiogalactopyranoside (IPTG). Thereafter, samples are stirred under certain conditions. Various incubation conditions and IPTG concentrations are discussed in the results. Conditions are finally optimized with a IPTG concentration of 0.5 mM and incubation during 3 hours at 37°C.

14.5 Bacterial lysis

After incubation, the sample is centrifuged at 4 000 rpm for 30 minutes at 4°C. Supernatant is eliminated and the bacterial pellet is suspended in a lysis buffer (50 mM Tris-HCl, 100 mM NaCl, pH 7.4) supplemented by EDTA-free Complete protease inhibitor ($Roche^{TM}$). The cell lysis is induced by several successive sonication cycles (10 watts of output power during 10 cycles of 30 seconds). The lysate is centrifuged at 12 500 rpm ($Beckman^{TM}$ coulter Avanti J-E High-Speed Centrifuge) for 1 hour at 4°C in order to separate heavy organelles from soluble compounds (like SerB with His_6-tag). Finally, the supernatant is filtered (0.45 µm and 0.20 µm) and conserved for the purpose of purification

15. SerB purification

In this research work, the purification of SerB is based on the protocol established by researchers from SSGCID[103]. Several purification buffers and elution programs were tested. After optimization, the following protocol is currently the best established one.

15.1 First IMAC

The first step of the SerB purification is an Immobilized Metal Affinity Chromatography (IMAC) using a *HiTrap*^{TM} IMAC FF 1 mL column loaded with $NiSO_4$ (0.1 M) beforehand. The column is pre-equilibrated with a first purification buffer A (50 mM Tris-HCl, 300 mM NaCl, 20 mM imidazole, pH 7.4) and the protein sample is thereafter loaded on the column. After the Flow Through (FT) elution, proteins which are bond on the column are progressively eluted thanks to a gradual addition of a second purification buffer B (50 mM Tris-HCl, 300 mM NaCl, 200 mM imidazole, pH 7.4). The gradual addition is monitored thanks to the following elution program: with a flow fixed at 1 mL/min, the buffer B is progressively added from 0 to 100 % during 50 minutes and 100 % in buffer B is applied during 10 minutes. After SDS-PAGE analysis, collected fractions are polled and activity test is performed. In addition, the protein concentration is evaluated by measurement at 280 nm with a Nanodrop 2000 Microvolume Spectrophotometer (cf. point 16.2.1).

15.2 His_6-Tag cleavage and dialysis

The second step of the SerB purification involves simultaneously a dialysis and the cleavage of the N-terminal His_6-Tag, by addition of commercial HRV-3C protease (*Sigma Aldrich*). Thanks to the protein concentration measurement, the total amount of collected SerB can be evaluated. The HRV-3C protease is then added to the sample for a mass ratio of 1/500. The latter is finally placed in a tubular semipermeable membrane (6-8 kDa as cut-off) immersed within a reaction buffer (25 mM Tris-HCl, 150 mM NaCl, 1 mM DTT, 1 mM ethylenediaminetetraacetic acid (EDTA) and pH 7.5). Dialysis is executed during 12-24 hours at 4°C or during 8 hours at room temperature.

15.3 Second IMAC

The next step of the SerB purification is a second IMAC with the same column (loaded with $NiSO_4$ and pre-equilibrated with the same purification buffer A). The dialyzed sample is then loaded and the FT corresponds to cleaved SerB. After its elution, a purification buffer B more concentrated in imidazole (500 mM instead of 200 mM) is added during 10 minutes: contaminants are eluted from the column. After SDS-PAGE analysis, fractions of pure SerB are pooled and activity test and concentration measurements are performed in the same way as mentioned earlier.

15.4 Optional SEC

The last facultative step of the SerB purification is a Size-Exclusion Chromatography (SEC). The purified sample is concentrated by centrifugation cycles (7 000 rmp during 5 minutes at 4°C) in order to reach a volume comprised between 50 and 150 µL, thanks to *Vivaspin*^{TM} ultrafiltration spin column (*Sartorius*) with a cut-off of 15 kDa. The protein concentration and the ratio 260 nm/280 nm are thereafter measured by Nanodrop. Then, the concentrated sample is loaded on the S200-10-30 column pre-equilibrated with a third purification buffer C (25 mM Tris-HCl, 500 mM NaCl, 2 mM DTT, 5% glycerol, pH 7.0). After SDS-PAGE analysis, pure fractions are pooled. Activity test, concentration measurements and ratio 260 nm/280 nm determination are performed as before.

15.5 SerB batch storage

After the last step of the purification, the purified batch of SerB is stored at -80°C, as several 1 mL aliquots with 10% glycerol.

16. Purification assessment

16.6 SDS-PAGE analysis

The Sodium Dodecyl Sulfate–Polyacrylamide Gel Electrophoresis (SDS-PAGE) is the most common analysis in order to check the successful performance of a purification step. The associated protocol is widely described in the literature[128-130].

16.1.1 SDS gel preparation

A SDS-PAGE gel is divided into two parts: the separating gel (fractions migration) and the stacking gel (fractions loading). The SDS percentage of the separating gel must be adapted to the protein size in order to provide effective separation during the migration: a 12% SDS gel is prepared for SerB (~46 kDa). The precise gel composition is detailed in the Table 4.

Firstly, the separating gel is prepared and immediately poured in an empty mini gel cassette (*Novex*^{TM}). About 1-1.5 cm above the top level of the gel are allowed for the addition of the stacking gel. The freshly poured gel is thereafter covered by a thick layer of an ethanoic solution. Polymerization occurs during approximately 40 minutes. Then, the ethanoic solution is removed and replaced by the stacking gel freshly prepared. The comb (well template with different numbers of pockets) is immediately placed on the top of the stacking gel. The SDS-PAGE gel finally formed can be easily stored few days in an electrode running buffer (25 mM Tris, 200 mM glycine and 0.1% SDS).

Table 4 – Composition of the running (10 mL) and the stacking (5 mL) gels for one SDS-PAGE gel. The compounds addition is performed depending on the order indicated in the table: ammonium persulfate (APS) and tetramethylethylenediamine (TEMED) catalyze the polymerization and are lastly added in the solution.

Running gel (12% SDS)		Stacking gel	
Compound	Volume (mL)	Compound	Volume (mL)
Distilled water	3.390	Distilled water	3.000
Buffer 1.5 M Tris-HCl, pH 8.8	2.500	Buffer 0.5 M Tris-HCl, pH 6.8	1.260
SDS	0.100	SDS	0.050
Acrylamide Mix (30%)	3.960	Acrylamide Mix (30%)	0.660
APS (10%)	0.050	APS (10%)	0.025
TEMED	0.005	TEMED	0.005

16.1.2 Sample preparation

For each analysed fractions, 15 µL are introduced in 5 µL of sample buffer (66 mM Tris-HCl pH 6.8, 20% glycerol, 2% SDS and 10.5 µg/mL bromophenol blue). Samples are firstly incubated in a water bath at 100°C during approximately 5 minutes, and are secondly centrifuged at 6 000 rpm during 10 seconds (*Mini centrifuge*).

16.1.3 Electrophoresis

The cassette with polymerized SDS-PAGE gel is firstly placed in the electrophoresis tank and the central reservoir is filled with the electrode running buffer (described in point 16.1.1). The well template is removed from the stacking gel: each prong leaves a pocket in the stacking gel. Then, 8 µL of the molecular weight marker (*Precision Plus Protein™ All Blue Standards*) is loaded on the first pocket and 15 µL of each prepared sample is also disposed in the following pockets. One third of the electrophoresis tank is filled with the electrode running buffer and the electrophoresis apparatus is connected to the power pack. The migration occurs at 200 V until the tracking dye reaches the base of the gel (approximately 40 minutes).

16.1.4 Gel staining

Upon completion of the electrophoresis, gels are removed from between glass plates and immerged respectively in a Coomassie Brilliant Blue solution (3 mM Coomassie Brilliant Blue, 45% methanol and 10% acetic acid) during 1 hour, in a discoloration solution (30% methanol and 10% acetic acid) during approximately 30 minutes and in distillated water overnight, under slight stirring.

16.2 Determination of the SerB concentration

16.2.1 Nanodrop Spectrophotometer measurements

The most usual and fast way to determine protein concentration is measurements with a Nanodrop 2000 Microvolume Spectrophotometer: absorbance of a 2 µL sample is easily determined and SerB concentration is calculated using the molar attenuation coefficient (7 575 M^{-1}) and the molecular weight (45 949.72 Da) both calculated from the known primary sequence of SerB[16]. After each purification step, SerB concentration is evaluated thanks to spectrophotometer measurements at 280 nm.

16.2.2 Pierce protein assay

A more precise way to determine protein concentration is the Pierce protein assay. The procedure is detailed by the supplier of the *Pierce™* reagent (*Thermo Fisher Scientific*)[131]. Firstly, the protein sample is diluted depending on various dilution factors (1x, 1.25x, 2x, 2,5x, 4x, 8x). Then, solutions summarized in the Figure 65 are prepared in a 96-multiwell plate. After 5 minutes, the reaction is quenched and colorization remains stable for spectrophotometric measurements at 660 nm with a 96-multiwell plate reader (*Bio-Rad™* model 680). The Pierce protein assay is performed only for the batch used for the purpose of the kinetic study of SerB.

[16] The values are calculated with Protparam: https://web.expasy.org/protparam/

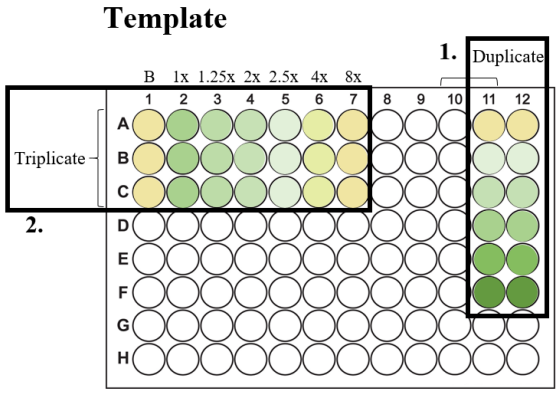

Wells composition

1. Calibration curve

Table A (65) – Solutions required for the calibration curve establishment.

1 µg/µL BSA (µL)	0	1	2.5	5	7.5	10
Distillated water (µL)	10	9	7.5	5	2.5	0
Pierce reagent (µL)	150	150	150	150	150	150
Final BSA concentration (µg/mL)	**0**	**6.25**	**15.62**	**31.25**	**46.88**	**62.50**

2. Pierce protein assay

For each diluted sample, 10 µL are added in 150 µL of Pierce reagent (dilution factors of samples are summarized on the top of the template). The blank (B) is prepared by addition of 150 µL of Pierce reagent in 10 µL of distillated water.

Figure 65 – Overview of the Pierce protein assay. Spectrophotometric measurements are calibrated thanks to a commercial bovine serum albumin (BSA) standard (*Sigma Aldrich*).

17. SerB characterization

17.1 Study of the oligomerization states: native PAGE

In this project, SEC is not a reliable method in order to study oligomerization states. The alternative method proposed in this research work is the native polyacrylamide gel electrophoresis (native PAGE). The protocol is adapted from Arndt et al.[132].

17.1.1 Gel preparation

The employed gel possesses a unique and uniform composition, summarized in the Table 5. The gel is prepared and immediately poured in an empty mini gel cassette (*Novex*^{TM}). A well template is thereafter added on the top of the gel. Polymerization occurs during approximately 1 hour. The gel is then ready to use.

Table 5 - Composition of the gel for the purpose of native PAGE. The compounds addition is performed depending on the order indicated in the table: APS and TEMED catalyze the polymerization and are lastly added in the solution.

Compound	Volume (mL)
Distilled water	4.170
Buffer 1.5 M Tris-HCl, pH 8.8	2.500
Acrylamide Mix (30%)	3.330
APS (10%)	0.050
TEMED	0.010

17.1.2 Sample preparation

Solutions (with various tested conditions) are prepared for a SerB concentration of ~0.2 mg/mL and a final volume of 100 µL. Then, 10 µL of each protein solution is added in 10 µL of sample solution (0.2 M Tris-HCl, 30% glycerol, 80 µg/mL bromophenol blue and pH 6.8). A "monomeric sample" and BSA (1 mg/mL) are used as reference and are prepared with addition in a classical sample solution (cf. point 16.1.2) before incubation in a water bath at 100°C during approximately 5 minutes. All samples are finally centrifuged at 6 000 rpm during 10 seconds (*Mini centrifuge*).

17.1.3 Electrophoresis

The protocol for this part is basically identical for both native PAGE and SDS-PAGE. (cf. point 16.1.3). Electrophoresis occurs at 150 V until the tracking dye reaches the base of the gel (approximately 1 hour).

17.1.4 Gel staining

See the SDS-PAGE protocol (cf. point 16.1.4).

17.2 Kinetic study: malachite green phosphate assay

Activity of SerB can be measured by following the release of inorganic phosphate (Pi) during the catalyzed reaction (cf. Figure 11), thanks to spectroscopic detection of the complexe of phosphomolybdate and malachite green in acidic conditions. The protocol is adapted from M. O'Toole[133] and from E. D'Angelo[134].

17.2.1 General procedure

The malachite green phosphate assay requires two initial solutions:

- The phosphate reagent is prepared by mixing 1 volume of 6.3% ammonium heptamolybdate in 7.5 M HCl with 3 volumes of 0.3% malachite green. The phosphate reagent is freshly prepared, stirred 15 minutes and filtered (0.20 µm) before using.
- The test buffer is composed of 100 mM Tris-HCl, 5 mM $MgCl_2$, 1 mM DTT (freshly added before use) with a pH fixed at 7.4.

Assays imply mixing enzyme (SerB) and substrate (*O*-phospho-L-serine) in various conditions which can affect the enzyme activity. Firstly, enzyme solutions are prepared (batch of 5 solutions for each tested condition) by dilution of enzyme sample in the test buffer (with possibly other compounds) and 180 µL of each enzyme solution are incubated during ~5 minutes in a thermostatic bath at 37°C. Then, substrate solutions are prepared by dilution of phosphoserine in the test buffer. One tested condition requires 3 substrate solutions because assays are always performed in triplicate (with substrate), with two blanks (without substrate) for each triplicate. Thereafter, 20 µL of substrate solutions are added in enzyme solutions and samples still incubated 10 minutes in the same bath. Meanwhile, 50 µL of phosphate reagent is added in each used well of a 96-multiwell plate. Eventually, 150 µL of each incubated sample are introduced in the used wells: the 200 µL final mixture becomes green which quantifies the formation of the green complex. After ~30 minutes in the dark at room temperature, colorization remains stable and the absorbance at 655 nm is measured with a 96-multiwell plate reader. Released Pi is quantified with a calibration curve and the associated solutions are incubated in the same thermostatic bath and simultaneously as aforementioned samples. All of the general procedure is summarized in the Figure 66. Michaelis-Menten parameters (Km and Vmax) are determined through linear (Lineweaver–Burk plot) and nonlinear (Michaelis-Menten kinetics) regressions with *GraphPad Prism* 5.04[135].

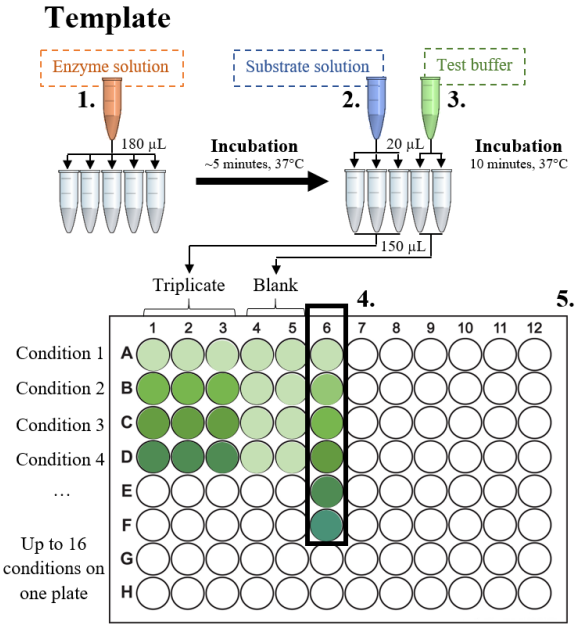

Sample composition

2. Enzyme solution

The enzyme solution is composed of SerB in the test buffer with possibly others compounds (inhibitors, solvent, etc.): tested conditions.

1. Substrate solution

The substrate solution is composed of phosphoserine in the test buffer.

3. Test buffer

5. Calibration curve

Table A (66) – Solutions required for the calibration curve establishment.

0.1 M Pi (µL)	0	10	20	30	40	50
TB (µL)	200	190	180	170	160	150
Final Pi concentration (µM)	**0.0**	**5.0**	**10.0**	**15.0**	**20.0**	**25.0**

4. Malachite green phosphate assay

Each well of the 96-multiwell plate is composed of 50 µL of phosphate reagent with 150 µL of the sample after incubation.

Figure 66 – Overview of the Malachite green phosphate assay. Spectrophotometric measurements are calibrated thanks to a commercial phosphate (Pi) standard (*Sigma Aldrich*).

17.2.2 Enzyme activity after purification steps

After each purification step, a malachite green phosphate assay is performed in order to assess if SerB has a preserved activity. This assay requires:

- Substrate solution: 2 mM phosphoserine in the test buffer.
- Enzyme solutions (4 conditions): 0, 5, 10 and 15 µL of a SerB sample (variable concentrations) in the test buffer, for a final volume of 1 mL.

17.2.3 Native enzymatic assay

The first step of the kinetic study is the determination of conditions that maximize SerB activity. Firstly, optimal enzyme concentration determination requires:

- Substrate solution: phosphoserine concentration is fixed at 2 mM.
- Enzyme solutions (7 conditions): the SerB concentrations are tested from 0.000 to 1.353 µg/mL by step of 0.226 µg/mL.

Subsequently, optimal substrate concentration determination is executed and requires:

- Substrate solutions (16 conditions): 0.00, 0.10, 0.25, 0.50, 0.75, 1.00, 1.25, 2.00, 2.50, 3.00, 3.50, 4.00, 5.00, 6.00, 7.00, 8.00 mM phosphoserine are tested.
- Enzyme solution: optimal SerB concentration previously determined (0.451 µg/mL).

17.2.4 Enzymatic inhibition assay

In this research work, selected inhibitors are characterized through IC_{50} and Ki determination. In addition, an initial assay is performed beforehand in order to quickly assess the efficiency of SerB2 inhibitors on SerB. The latter requires:

- Substrate solution: optimal substrate concentration previously determined (0.5 mM).
- Enzyme solutions (1 condition for the blank without inhibitor and 2 conditions for each inhibitor): optimal SerB concentration previously determined (0.451 µg/mL) with 10.0 and 100.0 µM of inhibitor and a DMSO concentration fixed at 5%.

The IC_{50} determination requires:

- Substrate solution: optimal substrate concentration previously determined (0.5 mM).
- Enzyme solutions (1 condition for the blank without inhibitor and 11 conditions for one inhibitor): optimal SerB concentration previously determined (0.451 µg/mL) with 0.1, 0.2, 0.3, 0.9, 1.0, 2.0, 4.0, 6.0, 8.0, 10.0, 80.0, 90.0 and 100.0 µM of inhibitor and a DMSO concentration fixed at 5%.

The Ki determination requires:

- Substrate solutions (16 conditions): 0.00, 0.10, 0.25, 0.50, 0.75, 1.00, 1.25, 2.00, 2.50, 3.00, 3.50, 4.00, 5.00, 6.00, 7.00, 8.00 mM phosphoserine are tested.
- Enzyme solutions (1 condition for the blank without inhibitor and 3 conditions for one inhibitor): optimal SerB concentration previously determined (0.451 µg/mL) with 0.00, 5.00, 10.00 and 20.00 µM of inhibitor and a DMSO concentration fixed at 5%. If the inhibitor is very efficient, the inhibitor concentrations are slightly decreased (0.00, 1.00, 3.00 and 5.00 µM).

17.3 Structural study: crystallization assay

SerB crystals have been obtained thanks to crystallization conditions described by SSGCID researchers[103]. In this project, the conditions are exploited and improved in order to optimize the crystal growth.

17.3.1 Vapor diffusion sitting drop

As shown in Figure 67, vapor diffusion sitting drop is performed in a 24-multiwell sitting drop crystallization plate. Each well test one condition defined by the composition of the reservoir solution. The crystallization drop is formed by addition of 1 µL of the reservoir solution in 1 µL of concentrated pure SerB sample (min. 25 mg/mL). The latter is obtained by several centrifugation cycles (7 000 rpm during 5 minutes at 4°C) after efficient purification procedure. The sample is concentrated thanks to *Vivaspin*^{TM} ultrafiltration spin column (*Sartorius*) with a cut-off of 15 kDa. Thereafter, each well is sealed thanks to siliconized glass circle cover slide (22 mm) and high vacuum grease. After one night at room temperature, SerB crystals appear in favorable conditions.

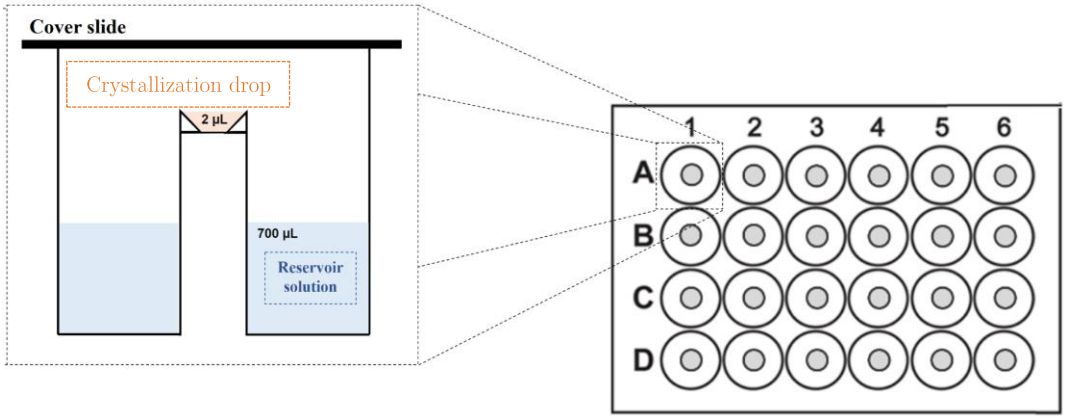

Figure 67 – Schematic representation of the vapor diffusion sitting drop.

17.3.2 Harvesting and cryo-cooling SerB crystals

SerB crystals are harvested with a tiny nylon loop. The crystal is then immerged few minutes in a drop composed of the reservoir solution, with 25% glycerol (cryoprotecting conditions). The SerB crystal is subsequently harvested and immediately cryo-cooled within liquid nitrogen. Loops and crystals can be stored until crystallographic analyses.

17.3.3 Structural determination and refinement

Cryo-cooled crystals are analyzed in the synchrotron facility SOLEIL (Gif-sur-Yvette, France) on beamline PROXIMA 2 (PX2) using PILATUS 6M (*Dectris Ltd.*) detector at a wavelength of 0.9801 Å. Incident X-Ray on crystals lead to X-Ray diffraction and a diffraction pattern is observed with a given resolution. The pattern is computationally processed using XDS/XSCALE[136]. Initial phases are calculated by molecular replacement using the program Phaser in PHENIX[137] and a starting model based on the known crystallographic structure of SerB (PDB: 3P96)[103]. The new SerB structure is finally built thanks to Coot program[138] and refined with PHENIX.

Bibliography

Bibliography

[1] T. Rogall et al., Towards a Phylogeny and Definition of Species at the Molecular Level within the Genus *Mycobacterium*, *International Journal of Systematic Bacteriology*, 40, 1990, 323-330.

[2] T. Rogall et al., Differentiation of *Mycobacterium* species by direct sequencing of amplified DNA, *Journal of General Microbiology*, 136, 1990, 1915-1920.

[3] J.M. Grange, Infection and disease due to the environmental mycobacteria, *Transactions of the Royal Society of Tropical Medecine and Hygiene*, 81, 1987, 179-182.

[4] J.L. Dahl, Electron microscopy analysis of *Mycobacterium tuberculosis* cell division, *FEMS Microbiology Letters*, 240, 2004, 15-20.

[5] C.T. Dow and L.A. Sechi, Environmental Triggers of Type 1 Diabetes Mellitus – *Mycobacterium avium* subspecies *paratuberculosis*, D. Wagner (ed.), Type 1 Diabetes – Pathogenesis, Genetics and Immunotherapy, London: *IntechOpen*, 2011.

[6] T.M. Shinnick and R.C. Good, Mycobacterial Taxonomy, *European Journal of Clinical Microbiology & Infectious Diseases*, 13, 1994, 884-901.

[7] E.H. Runyon, Anonymous Mycobacteria in Pulmonary Disease, *Medical Clinics of North America*, 43, 1959, 273-290.

[8] E.H. Runyon, International Working Group for Mycobacterial Taxonomy, *International Journal of Systematic Bacteriology*, 22, 1972, 124.

[9] L.G. Wayne et al., A Co-operative Numerical Analysis of Scotochromogenic Slowly Growing Mycobacteria, *Journal of General Microbiology*, 66, 1971, 255-271.

[10] G.P. Kubica et al., A Co-operative Numerical Analysis of Rapidly Growing Mycobacteria, *Journal of General Microbiology*, 73, 1972, 55-70.

[11] G. Meissner et al., A Co-operative Numerical Analysis of Nonscoto- and Nonphotochromogenic Slowly Growing Mycobacteria, *Journal of General Microbiology*, 83, 1974, 207-235.

[12] H. Saito et al., Cooperative Numerical Analysis of Rapidly Growing Mycobacteria, *International Journal of Systematic Bacteriology*, 27, 1977, 75-85.

[13] L.G. Wayne et al., A Co-operative Numerical Analysis of *Mycobacterium gastri*, *Mycobacterium kansasii* and *Mycobacterium marinum*, *Journal of General Microbiology*, 109, 1978, 319-327.

[14] L.G. Wayne et al., Serovar Determination and Molecular Taxonomic Correlation in *Mycobacterium avium*, *Mycobacterium intracellulare*, and *Mycobacterium scrofulaceum*: a Cooperative Study of the International Working Group on Mycobacterial Taxonomy, *International Journal of Systematic Bacteriology,* 43, 1993, 482-489.

[15] L.G. Wayne et al., Semantide- and Chemotaxonomy-Based Analyses of Some Problematic Phenotypic Clusters of Slowly Growing Mycobacteria, a Cooperative Study of the International Working Group on Mycobacterial Taxonomy, *International Journal of Systematic Bacteriology*, 46, 1996, 280-297.

[16] B.A. Brown et al., *Mycobacterium wolinskyi* sp. nov. and *Mycobacterium goodii* sp. nov., two new rapidly growing species related to *Mycobacterium smegmatis* and associated with human wound infections: a cooperative study from the International Working Group on Mycobacterial Taxonomy, *International Journal of Systematic* Bacteriology, 49, 1999, 1493-1511.

[17] L.G. Wayne et al., First Report of the Cooperative, Open-Ended Study of Slowly Growing Mycobacteria by the International Working Group on Mycobacterial Taxonomy, *International Journal of Systematic Bacteriology,* 31, 1981, 1-20.

[18] L.G. Wayne et al., Second Report of the Cooperative, Open-Ended Study of Slowly Growing Mycobacteria by the International Working Group on Mycobacterial Taxonomy, *International Journal of Systematic Bacteriology*, 33, 1983, 265-274.

[19] L.G. Wayne et al., Third Report of the Cooperative, Open-Ended Study of Slowly Growing Mycobacteria by the International Working Group on Mycobacterial Taxonomy, *International Journal of Systematic Bacteriology*, 39, 1989, 267-278.

[20] L.G. Wayne et al., Fourth Report of the Cooperative, Open-Ended Study of Slowly Growing Mycobacteria by the International Working Group on Mycobacterial Taxonomy, *International Journal of Systematic Bacteriology,* 41, 1991, 463-472.

[21] P.J. Freidlin, A New Paradigm for Genus *Mycobacterium* Population Structure, *Journal of Bacteriology and Parasitology*, 4, 2013, 1-11.

[22] R.S. Gupta et al., Phylogenomics and Comparative Genomic Studies Robustly Support Division of the Genus *Mycobacterium* into an Emended Genus *Mycobacterium* and Four Novel Genera, *Frontiers in Microbiology*, 9, 2018, 1-41.

[23] L.J. Alderwick et al., The *Mycobacterium* Cell Wall - Peptidoglycan and Arabinogalactan, *Cold Spring Harbor Perspectives in Medicine*, 5, 2015, 1-15.

[24] V.V. Lévy-Frébault and F. Portaels, Proposed Minimal Standards for the Genus *Mycobacterium* and for Description of New Slowly Growing *Mycobacterium* Species, *International Journal of Systematic Bacteriology,* 42, 1992, 315-323.

[25] R.C. Ellis and L.A. Zabrowarny, Safer Staining method for acid fast bacilli, *Journal of Clinical Pathology*, 46, 1993, 559-560.

[26] R. Bansal-Mutalik and H. Nikaido, Mycobacterial outer membrane is a lipid bilayer and the inner membrane is unusually rich in diacyl phosphatidylinositol dimannosides, *Proceedings of the National Academy of Sciences,* 111, 2014, 4958-4963.

[27] C.E. Barry et al., Mycolic Acids: Structure, Biosynthesis and Physiological Functions, *Progress in Lipid Research*, 37, 1998, 143-179.

[28] J. Asselineau and E. Lederer, Structure of the Mycolic Acids of Mycobacteria, *Nature,* 166, 1950, 782-783.

[29] S. Akira et al., Pathogen Recognition and Innate Immunity, *Cell,* 124, 2006, 783-801.

[30] B.S. Dyer et al., Synthesis and Structure of Phosphatidylinositol Dimannoside, *The Journal of Organic Chemistry,* 72, 2006, 3282-3288.

[31] G.E. Louw et al., A Balancing Act: Efflux/Influx in Mycobacterial Drug Resistance, *Antimicrobial Agents and Chemotherapy,* 53, 2009, 3181-3189.

[32] P.A. Lambert, Cellular impermeability and uptake of biocides and antibiotics in Gram-positive bacteria and mycobacteria, *Journal of Applied Microbiology Symposium Supplement,* 92, 2002, 46S-54S.

[33] H.H. Kwon et al., Distribution and characterization of βlactamases of mycobacteria and related organisms, *Tubercle and Lung Disease,* 76, 1995, 141-148.

[34] A.R. Flores et al., Genetic analysis of the βlactamases of *Mycobacterium tuberculosis* and *Mycobacterium smegmatis* and susceptibility to β-lactam antibiotics, *Microbiology,* 151, 2005, 521-532.

[35] H.W. van Veen et al., Basic Mechanisms of Antibiotic Resistance: Molecular Properties of Multidrug Transporters, *Malaysian Journal of Microbiology,* 4, 1998, 56-66.

[36] F. Wang et al., Crystal Structure and Activity Studies of the *Mycobacterium tuberculosis* {beta}-Lactamase Reveal Its Critical Role in Resistance to {beta}-Lactam Antibiotics, *Antimicrobial Agents and Chemotherapy,* 50, 2006, 2762-2771.

[37] P.J. Brennan, The Envelope of Mycobacteria, *Annual Review of Biochemistry,* 64, 1995, 29-63.

[38] S.E.G. Vasconcellos et al., Distinct genotypic profiles of the two major clades of *Mycobacterium africanum*, *BMC Infectious Diseases,* 10, 2010, 1-16.

[39] J. van Ingen et al., Characterization of *Mycobacterium orygis* as *M. tuberculosis* Complex Subspecies, *Emerging Infectious Diseases,* 18, 2012, 653-655.

[40] World Health Organization, Global tuberculosis report 2018. Geneva: *World Health Organization*, 2018.

[41] S. Ahmad, Pathogenesis, Immunology, and Diagnosis of Latent *Mycobacterium tuberculosis* Infection, *Clinical and Developmental Immunology,* 2011, 2011, 1-17.

[42] S. Sarkar and M.R. Suresh, An Overview of Tuberculosis Chemotherapy - A Literature Review, *Journal of Pharmaceutical Sciences,* 14, 2011, 148-161.

[43] M.P. Golden and H.R. Vikram, Extrapulmonary Tuberculosis: An Overview, *American Family Physician,* 72, 2005, 1761-1768.

[44] J.F. Murray et al., Treatment of Tuberculosis - A Historical Perspective, *Annals of the American Thoracic Society,* 12, 2015, 1749-1759.

[45] World Health Organization, Rapid Communication: Key changes to treatment of multidrug- and rifampicin-resistant tuberculosis (MDR/RR-TB), Geneva: *World Health Organization*, 2018.

[46] M.S. Hughes et al., PCR studies of feline leprosy cases, *Journal of Feline Medicine and Surgery,* 6, 2004, 235-243.

[47] X.Y. Han et al., Comparative Sequence Analysis of *Mycobacterium leprae* and the New Leprosy-Causing *Mycobacterium lepromatosis*, *Journal of Bacteriology,* 191, 2009, 6067-6074.

[48] K. Prabhakaran, Biochemical studies on *Mycobacterium leprae*, *Journal of Basic Microbiology,* 26, 1986, 117-126.

[49] R.O. Akinola et al., A Systems Level Comparison of *Mycobacterium tuberculosis*, *Mycobacterium leprae* and *Mycobacterium smegmatis* Based on Functional Interaction Network Analysis, *Journal of Bacteriology and Parasitology,* 4, 2013, 1-11.

[50] J.R. de Sousa et al., Leprosy As a Complex Infection: Breakdown of the Th1 and Th2 Immune Paradigm in the Immunopathogenesis of the Disease, *Frontiers in Immunology,* 8, 2017, 1-8.

[51] M. Romero-Montoya et al., Evaluation and Monitoring of *Mycobacterium leprae* Transmission in Household Contacts of Patients with Hansen's Disease in Colombia, *PLoS Neglected Tropical Disease,* 11, 2017, 1-11.

[52] World Health Organization, Weekly epidemiological record - Global leprosy update, 2015: time for action, accountability and inclusion, Geneva: *World Health Organization*, 2016.

[53] F.E.F. Pardillo et al., Methods for the Classification of Leprosy for Treatment Purposes, *Clinical Infectious Diseases,* 44, 2007, 1096-1099.

[54] World Health Organization, Guidelines for the diagnosis, treatment and prevention of leprosy - Executive summary, Geneva: World Health Organization, 2018.

[55] N. Radomski et al., Determination of Genotypic Diversity of *Mycobacterium avium* Subspecies from Human and Animal Origins by Mycobacterial Interspersed Repetitive-Unit-Variable-Number Tandem-Repeat and IS1311 Restriction Fragment Length Polymorphism Typing Methods, *Journal of Clinical Microbiology,* 48, 2010, 1026-1034.

[56] M.S. Philips and C.F. von Reyn, Nosocomial Infections Due to Nontuberculous Mycobacteria, *Clinical Infectious Diseases,* 2001, Vol. 33, 1363-1374.

[57] M-F. Thorel et al., Numerical Taxonomy of Mycobactin-Dependent Mycobacteria, Emended Description of *Mycobacterium avium*, and Description of *Mycobacterium avium* subsp. *avium* subsp. nov., *Mycobacterium avium* subsp. *paratuberculosis* subsp. nov., and *Mycobacterium avium* subsp. *silvaticum* subsp. nov., *International Journal of Systematic Bacteriology,* 40, 1990, 254-260.

[58] W. Mijs et al., Molecular evidence to support a proposal to reserve the designation *Mycobacterium avium* subsp. *avium* for bird-type isolates and "*M. avium* subsp. *hominissuis*" for the human/porcine type of *M. avium*, *International Journal of Systematic and Evolutionary Microbiology,* 52, 2002, 1505-1518.

[59] D.E. Griffith et al., An Official ATS/IDSA Statement: Diagnosis, Treatment, and Prevention of Nontuberculous Mycobacterial Diseases, *Amercian Journal of Respiratory and Critical Care Medicine,* 175, 2007, 367-416.

[60] P.M. Cassidy et al., Nontuberculous Mycobacterial Disease Prevalence and Risk Factors: A Changing Epidemiology, *Clinical Infectious Diseases,* 49, 2009, 124-129.

[61] M.M. Jones et al., Epidemiology of nontuberculous mycobacterial infections in the U.S. Veterans Health Administration, *PLoS ONE,* 13, 2018, 1-13.

[62] A. Renvoisé and C. Bernard, Traitement des infections à *Mycobacterium avium* complex, *Journal des Anti-infectieux,* 16, 2014, 199-206.

[63] L. Heifets et al., *Mycobacterium avium* Strains Resistant to Clarithromycin and Azithromycin, *Antimicrobial Agents and Chemotherapy,* 37, 1993, 2364-2370.

[64] L. Danalishvili et al., Genomic Approach to Identifying the Putative Target of and Mechanisms of Resistance to Mefloquine in Mycobacteria, *Antimicrobial Agents and Chemotherapy,* 49, 2005, 3707-3714.

[65] D.E. Griffith et al., Clinical and Molecular Analysis of Macrolide Resistance in *Mycobacterium avium* Complex Lung Disease, *American Journal of Respiratory and Critical Care Medicine,* 174, 2006, 928-934.

[66] G.A. Pankey and L.D. Sabath, Clinical Relevance of Bacteriostatic versus Bactericidal Mechanisms of Action in the Treatment of Gram-Positive Bacterial Infections, *Clinical Infectious Diseases,* 38, 2004, 864-870.

[67] K. Raman et al., targetTB: A target identification pipeline for *Mycobacterium tuberculosis* through an interactome, reactome and genome-scale structural analysis, *BMC Systems Biology,* 2, 2008, 1-21.

[68] C.M. Sassetti et al., Genes required for mycobacterial growth defined by high density mutagenesis, *Molecular Microbiology,* 48, 2003, 77-84.

[69] S. Anishetty et al., Potential drug targets in *Mycobacterium tuberculosis* through metabolic pathway analysis, *Computational Biology and Chemistry,* 29, 2005, 368-378.

[70] D.F. Warner et al., A derivative of *Mycobacterium smegmatis* mc2155 that lacks the duplicated chromosomal region, *Tuberculosis,* 86, 2006, 438-444.

[71] N. Jamshidi and B.O. Palsson, Investigating the metabolic capabilities of *Mycobacterium tuberculosis* H37Rv using the in silico strain iNJ661 and proposing alternative drug targets, *BMC Systems Biology,* 1, 2007, 1-20.

[72] X. Fang et al., Development and analysis of an in vivo-compatible metabolic network of *Mycobacterium tuberculosis*, *BMC Systems Biology,* 4, 2010, 160-184.

[73] G. Bai et al., Dysregulation of serine biosynthesis contributes to the growth defect of a *Mycobacterium tuberculosis* crp mutant, *Molecular Microbiology,* 82, 2011, 180-198.

[74] S. Dey, Structural Insights Into the Enzymes of the Serine and Biontin Biosynthetic Pathways in *Mycobacterium tuberculosis,* College Station (Texas) : *Texas A&M University*, 2008.

[75] A. Ichihara and D.M. Greenberg, Further Studies on the Pathway of Serine Formation from Carbohydrate, *Journal of Biological Chemistry,* 224, 1957, 331-340.

[76] G.A. Grant, Regulatory Mechanism of *Mycobacterium tuberculosis* Phosphoserine Phosphatase SerB2, *Biochemistry,* 56, 2017, 6481-6490.

[77] J. Jaeken et al., Phosphoserine phosphatase deficiency in a patient with Williams syndrome, *Journal of Medical Genetics,* 34, 1997, 594-596.

[78] F. Coulibaly et al., Structure of phosphoserine aminotransferase from *Mycobacterium tuberculosis*, *Acta Crystallographica Section D Biological Crystallography,* D68, 2012, 553-563.

[79] A.W. El-Hattab, Serine biosynthesis and transport defects, *Molecular Genetics and Metabolism,* 118, 2016, 153-159.

[80] Y. Izumi et al., L-serine production by a methylotroph and its related enzymes, *Applied Microbiology and Biotechnology,* 39, 1993, 427-432.

[81] T-Y. Jung et al., Identification of a novel ligand binding site in phosphoserine phosphatase from the hyperthermophilic archaenon *Thermococcus onnurineus*, *Proteins,* 81, 2013, 819-829.

[82] A. Koul et al., Interplay between Mycobacteria and Host Signalling Pathways, *Nature Reviews Microbiology*, 2, 2004, 189-202.

[83] G.D. Tribble et al., A *Porphyromonas gingivalis* haloacid dehalogenase family phosphatase interacts with human phosphoproteins and is important for invasion, *Proceedings of the National Academy of Sciences,* 103, 2006, 11027-11032.

[84] B. Bainbridge et al., Role of *Porphyromonas gingivalis* Phosphoserine Phosphatase Enzyme SerB in Inflammation, Immune Response, and Induction of Alveolar Bone Resorption in Rats, *Infection and Immunity,* 78, 2010, 4560-4569.

[85] C.E. Moffatt et al., *Porphyromonas gingivalis* SerB-mediated dephosphorylation of host cell cofilin modulates invasion efficiency, *Cellular Microbiology,* 14, 2012, 577-588.

[86] H. Takeuchi et al., The Serine Phosphatase SerB of *Porphyromonas gingivalis* Suppresses IL-8 Production by Dephosphorylation of NF-kB ReIA/p65, *PLoS Pathogens,* 9, 2013, 1-13.

[87] S. Whitmore, The role of kinases and phosphatases in the pathobiology of *Porphyromonas gingivalis*, Louisville (Kentucky) : *University of Louisville*, 2017.

[88] F. Seghrouchni et al., Design of immunogenic peptides from *Mycobacterium tuberculosis* genes expressed during macrophage infection, *Tuberculosis,* 89, 2009, 210-217.

[89] G.P. Yadav et al., Characterization of *M. tuberculosis* SerB2, an Essential HAD-Family Phosphatase, Reveals Novel Properties, *PLoS ONE,* 9, 2014, 1-24.

[90] S. Shree et al., The *M. tuberculosis* HAD phosphatase (Rv3042c) interacts with host proteins and is inhibited by Clofazimine, *Cellular and Molecular Life Sciences,* 73, 2016, 3401-3417.

[91] A.K. Sharma et al., Bacterial Virulence Factors: Secreted for Survival, *Indian Journal of Microbiology,* 57, 2017, 1-10.

[92] M.E. Glasner et al., Evolution of enzyme superfamilies, *Current Opinion in Chemical Biology,* 10, 2006, 492-497.

[93] A.M. Schnoes et al., Annotation Error in Public Databases: Misannotation of Molecular Function in Enzyme Superfamilies, *PLoS Computational Biology,* 5, 2009, 1-13.

[94] P. Laurino et al., An Ancient Fingerprint Indicates the Common Ancestry of Rossmann-Fold Enzymes Utilizing Different Ribose-Based Cofactors, *PLoS Biology,* 14, 2016, 1-23.

[95] I.S. Ridder and B.W. Dijkstra, Identification of the Mg^{2+}-binding site in the P-type ATPase and phosphatase members of the HAD (haloacid dehalogenase) superfamily by structural similarity to the response regulator protein CheY, *Biochemical Journal,* 339, 1999, 223-226.

[96] A. Seifried et al., Human HAD phosphatases: structure, mechanism, and roles in health and disease, *FEBS Journal,* 280, 2012, 549-571.

[97] Y. Kim et al., Structure- and Function-based Characterization of a New Phosphoglycolate Phosphatase from *Thermoplasma acidophilum*, *Journal of Biological Chemistry,* 2, 2004, 517-526.

[98] E.V. Koonin and R.L. Tatusov, Computer Analysis of Bacterial Haloacid Dehalogenases Defines a Large Superfamily of Hydrolases with Diverse Specificity, *Journal of Molecular Biology,* 244, 1994, 125-132.

[99] W. Wang et al., Structural Characterization of the Reaction Pathway in Phosphoserine Phosphatase: Crystallographic "snapshots" of Intermediate States, *Journal of Molecular Biology,* 319, 2002, 421-431.

[100] Z. Lu et al., HAD Superfamily Phosphotransferase Substrate Diversification: Structure and Function Analysis of HAD Subclass IIB Sugar Phosphatase BT4131, *Biochemistry,* 44, 2005, 8684-8696.

[101] A.J. Stewart et al., Comparative modelling of human PHOSPHO1 reveals a new group of phosphatases within the haloacid dehalogenase superfamily, *Protein Engineering,* 16, 2003, 889-895.

[102] I. Hanukoglu, Proteopedia: Rossmann Fold: A Beta-Alpha-Beta Fold at Dinucleotide Binding Sites, *Biochemistry and Molecular Biology Education,* 10, 2014, 206-209.

[103] J. Abendroth et al., SAD phasing using iodide ions in a high-throughput structural genomics environment, *Journal of Structural and Functional Genomics,* 12, 2011, 83-95.

[104] D.M. Chipman and B. Shaanan, The ACT domain family, *Current Opinion in Structural Biology,* 11, 2001, 694-700.

[105] G. Arora et al., High Throughput Screen Identifies Small Molecule Inhibitors Specific for *Mycobacterium tuberculosis* Phosphoserine Phosphatase, *The Journal of Biological Chemistry,* 289, 2014, 25149-25165.

[106] E. Pierson, Etude de l'inhibition de SerB2, une phosphosérine phosphatase essentielle de *Mycobacterium tuberculosis* : identification et évaluation de nouveaux inhibiteurs potentiels, Namur: *Unamur*, 2018.

[107] J.E. Hawkinson et al., The metabotropic glutamate receptor antagonist L-2-amino-3-phosphonopropionic acid inhibits phosphoserine phosphatase, *European Journal of Pharmacology,* 307, 1996, 219-225.

[108] J.E. Hawkinson et al., Novel phosphoserine phosphatase inhibitors, *European Journal of Pharmacology,* 337, 1997, 315-324.

[109] S-K. Jung et al., Identification of 3-acyl-2-phenylamino-1,4-dihydroquinolin-4-one derivatives as inhibitors of the phosphatase SerB653 in *Porphyromonas gingivalis*, implicated in periodontis, *Bioorganic & Medicinal Chemistry Letters,* 22, 2012, 2084-2088.

[110] T. Yano et al., Reducation of Clofazimine by Mycobacterial Type 2 NADH: Quinone Oxidoreductase, *The Journal Of Biological Chemistry,* 286, 2011, 10276-10287.

[111] P.J. Myler et al., The Seattle Structural Genomics Center for Infectious Disease (SSGCID), *Infectious Disorders Drug Targets,* 9, 2009, 493-506.

[112] R. Stacy et al., Structural genomics of infectious disease drug targets: the SSGCID, *Acta Crystallographica Section F Structural Biology and Crystallization Communications,* F67, 2011, 979-984.

[113] S.N. Hewitt et al., Expression of proteins in *Escherichia coli* as fusions with maltose-binding protein to rescue non-expressed targets in a high-throughput protein-expression and purification pipeline, *Acta Crystallographica Section F Structural Biology and Crystallization Communications,* F67, 2011, 1-4.

[114] A.L. Koch, Turbidity Measurements of Bacterial Cultures in Some Available Commercial Instruments, *Analytical Biochemistry,* 38, 1970, 252-259.

[115] P.R. Baraniak et al., Spatial control of gene expression within a scaffold by localized inducer release, *Biomaterials,* 32, 2011, 3062-3071.

[116] J.A. Bornhorst and J.J. Falke, [16] Purification of Proteins Using Polyhistidine Affinity Tags, *Methods in Enzymology,* 326, 2000, 245-254.

[117] D.S. Waugh, An Overview of enzymatic reagents for the removal of affinity tags, *Protein Expression and Purification,* 80, 2011, 283-293.

[118] R.H. Garrett and C.M. Grisham, Biochemistry - Fourth Edition, Boston (Massachusetts): *Brooks/Cole*, 2010.

[119] W.W. Cleland, Dithiothreitol, a New Protective Reagent for SH Groups, *Biochemistry,* 3, 1964, 480-482.

[120] V. Vagenende et al., Mechanisms of Protein Stabilization and Prevention of Protein Aggregation by Glycerol, *Biochemistry,* 48, 2009, 11084-11096.

[121] K. Itaya and M. Ui, A New Micromethod for the Colorimetric Determination of Inorganic Phosphate, *Clinica Chimica Acta,* 14, 1966, 361-366.

[122] T. Attin et al., Suitability of a malachite green procedure to detect minimal amounts of phosphate dissolved in acidic solutions, *Clinical Oral Investigations,* 9, 2005, 203-207.

[123] N.M. Cuong et al., Donnan Electric Potential Dependence of Intraparticle Diffusion of Malachite Green in Single Cation Exchange Resin Particles: A Laser Trapping-Microspectroscopy Study, *American Journal of Analytical Chemistry,* 3, 2012, 188-194.

[124] B.S. Antharavally et al., Quantitation of proteins using a dye-metal-based colorimetric protein assay, *Analytical Biochemistry,* 385, 2009, 342-345.

[125] A. Cornish-Bowden, Fundamentals of Enzyme Kinetics - 4th Edition, London : *Portland Press*, 2012.

[126] I. Müller, Guidelines for the successful generation of protein-ligand complex crystals, *Acta Crystallographica D Structural Biology,* D73, 2016, 79-92.

[127] A. Wlodawer et al., Protein crystallography for non-crystallographers, or how to get the best (but not more) from published macromolecular structures, *FEBS Journal,* 275, 2008, 1-21.

[128] B.D. Hames (ed.), Gel Electrophoresis of Proteins (Third Edition), Oxford: *Oxford University Press*, 1998.

[129] J.M. Walker (ed.), The Protein Protocols Handbook, Totowa (New Jersey): *Humana Press*, 1996.

[130] Z. Deyl (ed.), Electrophoresis: a survey of techniques and applications (part B: applications), Amsterdam: *Elsevier Scientific Publishing Compagny*, 1983.

[131] Thermo Fisher Scientific. Inc., *User Guide: Pierce 660nm Protein Assay (22660)*, https://www.thermofisher.com/order/catalog/product/22660, accessed 10.01.2018.

[132] C. Arndt et al., Native Polyacrylamide Gels, B.T. Kurien and R.H. Scofield (ed.), Protein Electrophoresis: Methods and Protocols, New York: *Humana Press*, 2012.

[133] M. O'Toole et al., Determination of phosphate using a highly sensitive paired emitter-detector diode photometric flow detector, *Analytica Chimica Acta,* 597, 2007, 290-294.

[134] E. D'angelo et al., Rapid, Sensitive, Microscale Determination of Phosphate in Water and Soil, *Journal of Environmental Quality,* 30, 2001, 2206-2209.

[135] GP. Prism, *GraphPad Software Inc.,* San Diego (California), 2010.

[136] W. Kabsch, XDS, *Acta Crystallographica Section D Biological Crystallography,* D66, 2010, 125-132.

[137] P.D. Adams et al., PHENIX: a comprehensive Python-based system for macromolecular structure solution, *Acta Crystallographica Section D Biological Crystallography,* D66, 2010, 213-221.

[138] P. Emsley et al., Features and development of Coot, *Acta Crystallographica Section D Biological Crystallography,* D66, 2010, 486-501.

[139] F. Corpet, Multiple sequence alignment with hierarchical clustering, *Nucleic Acids Research,* 16, 1988, 10881-10890.

[140] C. Aslanidis and P.J. de Jong, Ligation-independent cloning of PCR products (LIC-PCR), *Nucleic Acids Research,* 18, 1990, 6069-6074.

[141] M. Lewis et al., Crystal Structure of the Lactose Operon Repressor and Its Complexes with DNA and Inducer, *Science,* 271, 1996, 1247-1254.

Annexes

Annex I: Kinetic data

The Michaelis-Menten kinetics of SerB and associated Lineweaver-Burk plot for each harmine derivatives (**88**, **91**, **95** and **124**) are illustrated below.

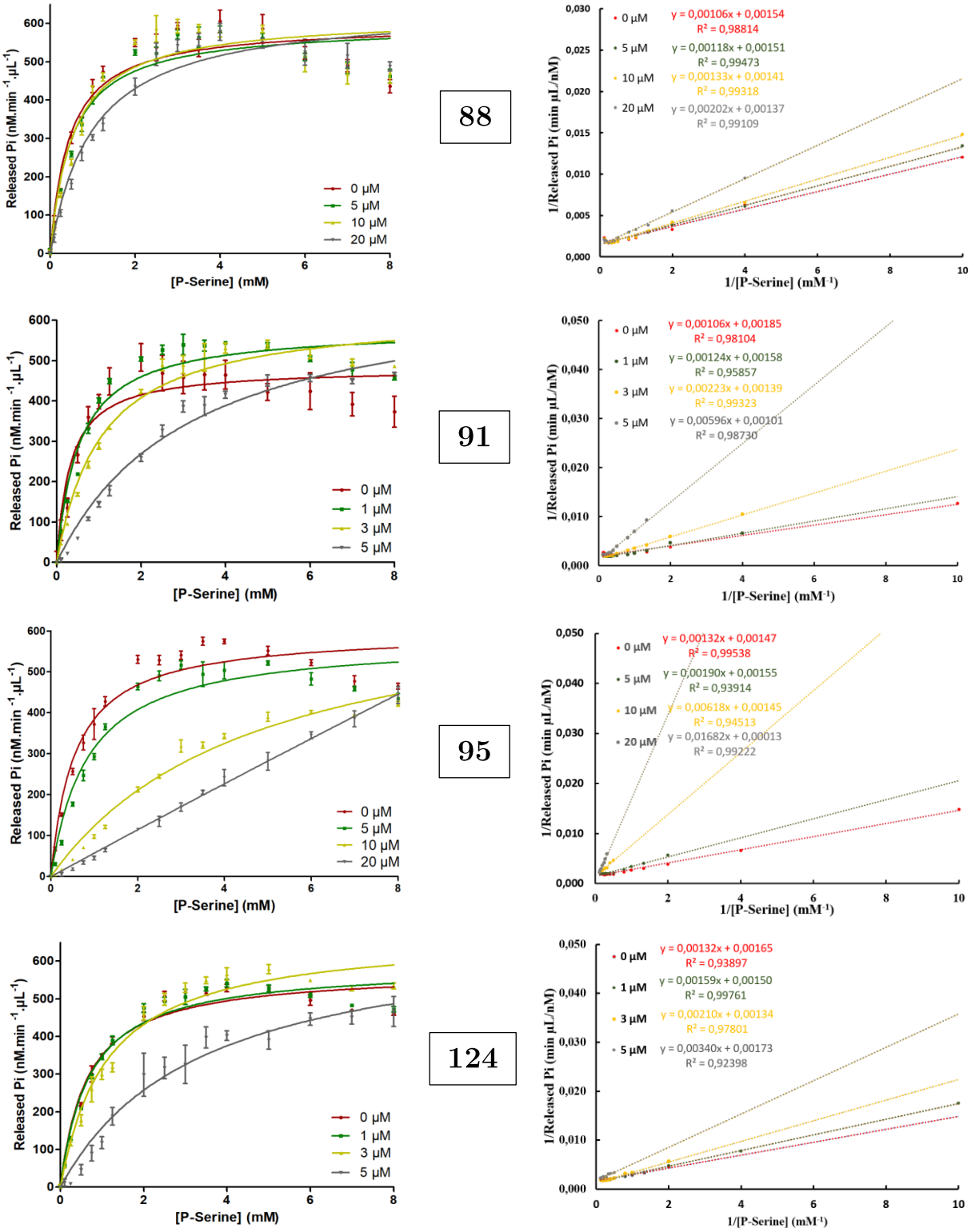

Figure 68 – Michaelis-Menten kinetics of SerB and Lineweaver-Burk plot for each inhibitor.

Annex II: Native polyacrylamide gels

The study of SerB oligomerization states is performed through native polyacrylamide gel analysis. Three incubation times (namely time between solutions preparation and native PAGE analysis) are tested: 10 minutes, 1 hour and 2 days. The associated native gels are shown below:

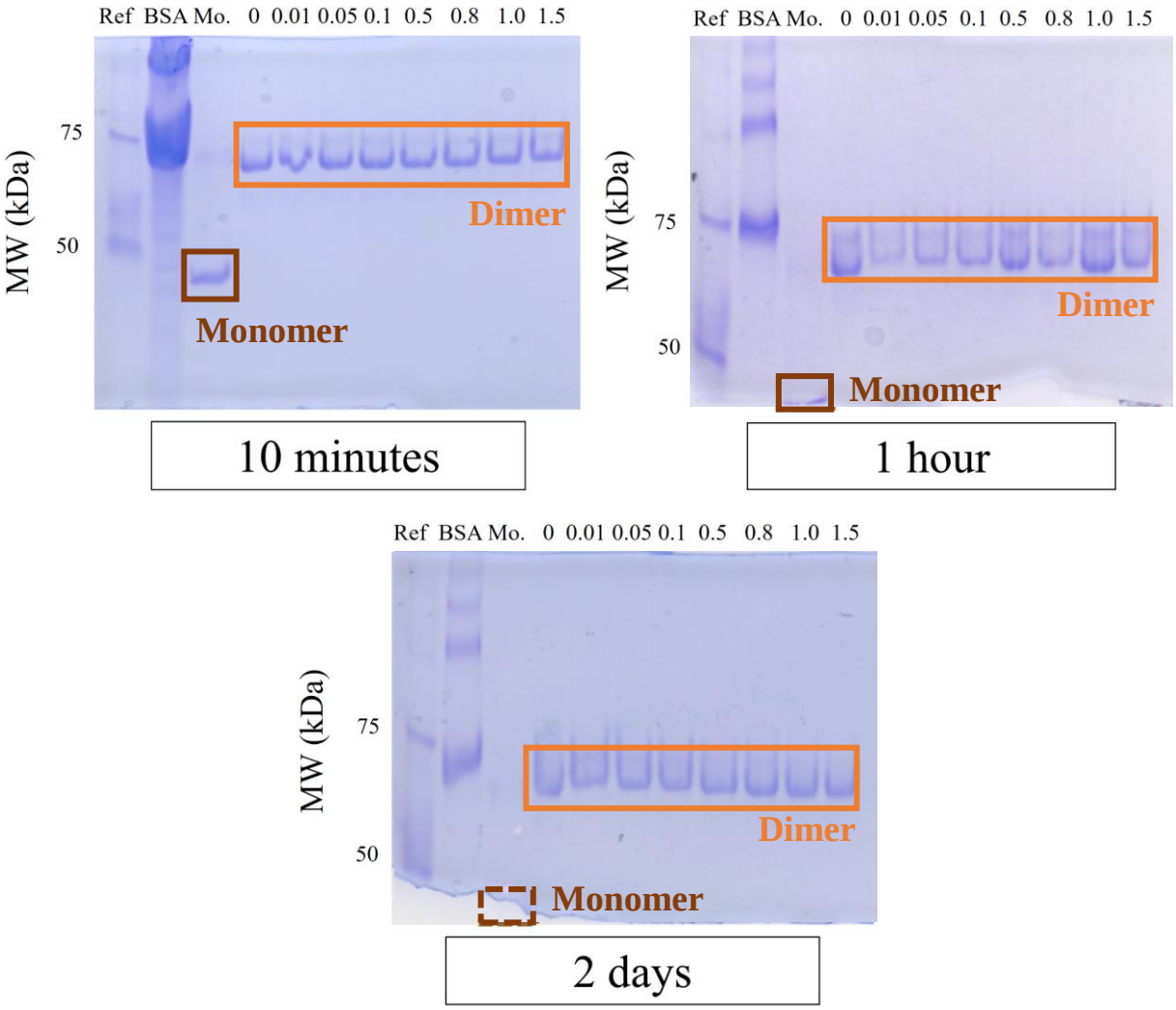

Figure 69 – Native polyacrylamide gel analysis of SerB after 10 minutes, 1 hour and 2 days of incubation, within solution of various L-serine concentrations (0 to 1.5 M). Ref is the molecular weight marker, BSA is used as second reference (MW = 66.5 kDa) and Mo. is the monomeric form of SerB (denatured). Several bands are visible for BSA. This phenomenon has already been described in the literature and could be associated with the presence of contaminant in the BSA commercial solution.

Annex III: Crystallographic data

In order to assess the agreement between observed electron density and proposed structure, several parameters are determined after several refinements. The Table 6 summarizes all of these parameters for the crystallographic structure of SerB.

Table 6 – Experimental values and theoretical interpretation of parameters that define the crystallographic structure of SerB shown in Figure 58. Statistics for the highest-resolution shell are shown in parentheses.

Parameter	Exp. value	Interpretation
Resolution range	42.31 – 2.498 Å (2.588 – 2.498 Å)	Measure of the accuracy of the electron density map.
Space group	I 2 2 2	Symmetry group of molecules configuration in space. *I* means body centered and *222* defines the symmetry elements (rotations).
Unit cell	L: 65.19|109.17|133.96 A: 90|90|90	Unit cell, defined by lengths of edges (L) and angles (A) between them, is the smallest unit with the full symmetry of the crystal.
Completeness	99% (96%)	Coverage of all theoretical possible unique reflections within measured data set.
I/σ	11.37 (1.29)	Signal-to-noise ratio.
Wil. B-factor	63.15 Å^2	B-factor determined through Wilson plot.
R-merge	0.03911 (0.509)	Accuracy of averaged intensities through spread of the individual measurements of equivalent reflections.
R-meas	0.05531 (0.7199)	Redundancy-independent version of R-merge.
$CC_{1/2}$	0.998 (0.663)	Precision of merged data through random half-datasets.
CC*	1 (0.893)	Precision of merged data thanks to $CC_{1/2}$.
Ref. in refine.	16 848 (1 569)	Nb. of reflections used in refinement.
Ref. R-free	843 (78)	Nb. of reflections used for R-free (5% of refine)
R-work	0.2184 (0.4576)	Discrepancy between F_{obs} and F_{calc} (work set).
R-free	0.3046 (0.4653)	R-factor calculated from 5% of randomly selected reflections (test set).
CC_{work}	0.967 (0.632)	Precision of merged data for R-factor.
CC_{free}	0.920 (0.718)	Precision of merged data for R-free.
RMS_{bonds}	0.009	Root-mean-square deviations for bonds.
RMS_{angles}	1.13	Root-mean-square deviations for angles.
Ram. Fav.	94%	Favored residues in Ramachandran plot.
Ram. Allow.	6.1%	Allowed residues in Ramachandran plot.
Ram. Out.	0.0%	Outliers residues in Ramachandran plot.
Rot. Out.	0.3%	Outliers residues in rotamer-library.
Clashscore	15.50	Number of serious clashes per 1000 atoms.
Av. B-factor	67.11 Å^2	Displacement parameter or temperature factor that reflects the average mobility in space.